

UNIVERSITA' DEGLI STUDI DI PADOVA



DEPARTMENT OF INFORMATION ENGINEERING

**BIOMECHANICAL ANALYSIS OF
DIFFERENT RUNNING STYLES
WITH DIFFERENT FOOTWEAR**

Supervisor: Prof. NICOLA PETRONE

Co-supervisors: Dr. LUCA MODENESE

Dr. ANDREW T.M. PHILLIPS

Name: MARTINA BARZAN

Master's Degree in Bioengineering

Academic Year 2013/2014

“So what’s the right way to run?”
“That’s the eternal question”

Christopher McDougall
Born to run

Table of contents

TABLE OF CONTENTS	1
INTRODUCTION	5
CHAPTER 1.....	7
<i>RUNNING BIOMECHANICS.....</i>	<i>7</i>
1.1 <i>Introduction</i>	<i>7</i>
1.2 <i>Walking and running gait cycle.....</i>	<i>7</i>
1.3 <i>Running kinematics</i>	<i>8</i>
1.3.1 <i>Kinematics conventions and joint coordinates.....</i>	<i>9</i>
1.4 <i>Running kinetics.....</i>	<i>14</i>
1.4.1 <i>Ground Reaction Forces.....</i>	<i>14</i>
1.4.2 <i>Sagittal plane joint moments.....</i>	<i>18</i>
1.5 <i>EMG.....</i>	<i>20</i>
1.6 <i>Running styles.....</i>	<i>21</i>
1.7 <i>Running footwear.....</i>	<i>22</i>
CHAPTER 2.....	25
<i>EXPERIMENTAL DATA DESCRIPTION.....</i>	<i>25</i>
2.1 <i>Introduction</i>	<i>25</i>
2.2 <i>Footwear and running styles.....</i>	<i>25</i>
2.3 <i>Experimental setup.....</i>	<i>26</i>
2.4 <i>Marker set.....</i>	<i>27</i>
2.5 <i>Vicon Nexus post-processing</i>	<i>29</i>
2.6 <i>Spatio-temporal parameters.....</i>	<i>32</i>
2.7 <i>Strike patterns.....</i>	<i>33</i>
2.8 <i>Ground reaction forces.....</i>	<i>34</i>
CHAPTER 3.....	47
<i>MUSCULOSKELETAL MODELLING.....</i>	<i>47</i>
3.1 <i>Introduction</i>	<i>47</i>
3.2 <i>OpenSim.....</i>	<i>47</i>
3.3 <i>Model description.....</i>	<i>49</i>
3.3.1 <i>Bone, joint and muscle representation.....</i>	<i>49</i>
3.4 <i>Scale tool.....</i>	<i>53</i>
3.4.1 <i>How to use the scale tool.....</i>	<i>53</i>

CHAPTER 4	61
<i>KINEMATIC AND KINETIC ANALYSIS OF RUNNING</i>	<i>61</i>
4.1 Introduction	61
4.2 Inverse kinematics analysis	62
4.2.1 <i>How inverse kinematics works.....</i>	<i>62</i>
4.2.2 <i>IK adjustments and evaluation of the results.....</i>	<i>64</i>
4.2.3 <i>Joint angles.....</i>	<i>66</i>
4.3 Inverse dynamics analysis.....	73
4.3.1 <i>How inverse dynamics works.....</i>	<i>74</i>
4.3.2 <i>Joint moments.....</i>	<i>75</i>
4.3.3 <i>Joint angular velocity and power.....</i>	<i>78</i>
CHAPTER 5	83
<i>MUSCLE ACTION AND ITS EFFECTS ON THE MECHANICS OF RUNNING.....</i>	<i>83</i>
5.1 Introduction	83
5.2 Load sharing problem.....	83
5.3 Static optimization method.....	84
5.4 Static optimization tool in OpenSim.....	85
5.5 Muscle activations.....	88
5.6 Muscle forces and joint contact forces.....	94
CONCLUSIONS.....	101
REFERENCES	103
AKNOWLEDGMENTS	109

Introduction

Running represents one of the world's most popular sporting and leisure activities and the turnout at running events increases every year. The running boom of the 1970s and 1980s strongly affected running popularity. Nowadays this popularity is increased by the easy accessibility and large health benefits associated with running, such as reduced risk of heart disease, improved cardiovascular functions, weight control and mental alertness (Dorn, 2011). Indeed, the number of U.S. race finishers went up by 224% from 1990 to 2013 (RunningUSA, 2013).

However, the rate of running-related injuries, especially to the lower extremities, remains extremely high. A recent study (van Gent et al., 2007) reported an incidence of lower extremity running injuries ranged from 19.4% to 79.3%. From this study the knee resulted the most common site of lower extremity injuries, with an incidence up to 50% of the total number of running injuries. Some investigations revealed that indirect causes of running injuries may be related to training level, health and lifestyle factors (Satterthwaite et al., 1999, Macera et al., 1989). Nevertheless, a complete analysis of the musculoskeletal biomechanics of running is fundamental to identify the direct causes of injuries.

Scott and Winter (1990) were among the first researchers to highlight the importance of placing side by side external loads (i.e. ground contact forces) with internal loads (muscle and joint contact forces) when evaluating the importance of skeletal loading to injuries. Indeed, several studies investigated the biomechanics of running (De Wit et al., 2000, Divert et al., 2005, Novacheck, 1998) without considering the effects of internal loads. Generally, internal loads responsible for the damage of biological tissues have much larger magnitude than external loads. However, the only way to experimentally measure internal loads is by using invasive methods like instrumented prostheses implants, so only a low number of dataset of this kind is available in literature. A feasible approach to obtain non-invasive estimations of internal load values is to use musculoskeletal models. Indeed, in the last years musculoskeletal modelling has been widely adopted to estimate internal loading of the musculoskeletal system, to analyze

athletic performance, to identify the causes of pathological movements and to provide a scientific treatment planning (Delp et al., 2007). One of the most common musculoskeletal modelling software system is OpenSim (Delp et al., 2007), which enables the inspection of musculoskeletal models, the visualization of their motion and the extraction of useful information by using specific tools (Seth et al., 2011).

The aim of this study was to present an investigation into the differences between running adopting different running styles and wearing different footwear based on the kinematics, kinetics and internal loading computed by a musculoskeletal model. An attempt of yielding insight on injury mechanisms that may derive from different running conditions was then sought. Experimental data were collected at St. Mary's University (Twickenham, London) in 2012 from a young male subject while running barefoot, "minimalist" and with "thick wedged" shoes adopting different strike patterns. Data were then post-processed and used for further musculoskeletal modelling analyses.

A general overview of running biomechanics, with a specific focus on the comparison of kinematics and kinetics between running and walking will be provided in Chapter 1. Experimental data description and data post-processing will be described in Chapter 2. Chapter 3 will introduce musculoskeletal modelling with its potentialities and the scaling tool. Kinematic and kinetic analysis of running will be then presented in Chapter 4. Finally, chapter 5 will evaluate muscle action and its effect on the mechanics of running.

CHAPTER 1

Running biomechanics

1.1 Introduction

Running analysis has been a topic of interest since the time of the ancient Greeks (Novacheck, 1998). Nowadays, the fact that running characterizes one of the most common recreational activity, has prompted an explosion of interest in research and assessment. Hence, a precise and accurate knowledge of the biomechanics of running represents a fundamental tool to appropriately evaluate the running motor action.

The following chapter will give an overall biomechanical evaluation of running which will enable to properly interpret and compare the final results of the present study. Firstly, a comparison between running and walking gait cycle will be provided to generally see how running differentiates from walking. Secondly, running kinematics and kinetics will be presented. Timing activation of the most commonly documented muscles involved in running will be then depicted. Finally, a description of the two independent variables of the study, in other words running styles and footwear, will be introduced.

1.2 Walking and running gait cycle

In gait analysis, the gait cycle represents a fundamental unit of measurement (Gage, 1990). A gait cycle is defined as the period which elapses from the instant when one foot comes in contact with the ground and the instant when the same foot contacts the ground again. Each gait cycle can be subdivided into two phases: *stance* and *swing* (Figure 1.1). The stance phase describes the period when the foot is in contact with the ground and it begins with the initial contact. This phase corresponds to the 62% of the gait cycle during walking and to the 39% of the gait cycle during running (Novacheck,

1998). On the other hand, the swing phase refers to the time when the foot is lifted up to move forward the lower limb and it is initially defined by the toe off (Perry, 1992). It corresponds to the 38% of the gait cycle during walking and to the 61% of the gait cycle during running.

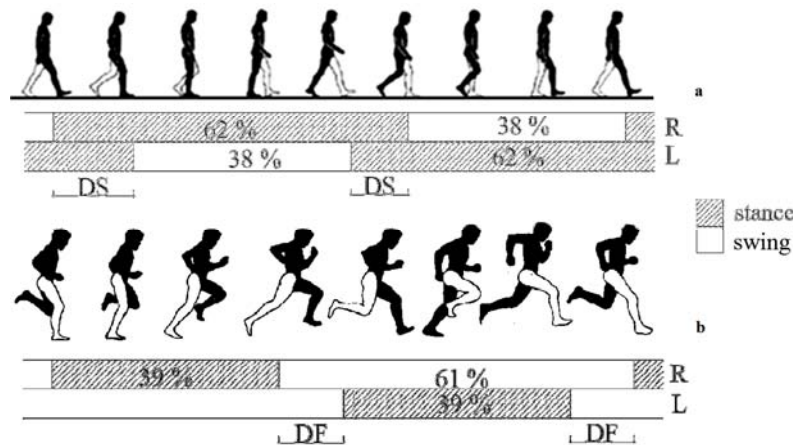


Figure 1.1. Walking (a) and running (b) gait cycle. Two double support (DS) periods and two double float (DF) periods occur during walking and running respectively. Percentages of the swing and stance phase with respect to the gait cycle are shown, considering a running speed of 3.2 m/s. Information for these graphs comes from data collected at the Motion Analysis Lab at Gillette Children's Speciality Healthcare.

In walking, three intervals within the stance phase are identifiable. They refer to an initial double stance, a single limb support and a terminal double stance interval. In fact, because in this activity the stance phase is longer than 50% of the gait cycle, two intervals when both feet are touching the ground (double support) can be recognized.

The appearance of two periods when neither foot is on the ground (double float) and the related disappearance of double support depicts the difference between walking and running. In fact, occurring the toe off before 50% of the gait cycle, two periods of double float, one at the beginning and one at the end of the swing, are recognizable during running (Figure 1.1).

1.3 Running kinematics

The term *kinematics* refers to the description of the movement itself, without considering internal and external forces that enable the body to execute that movement (Novacheck, 1998, Winter, 2009).

The terminology adopted to describe anatomical movements will be briefly introduced in the following section, followed by a description of the lower limb joint coordinates, focused on the comparison between walking and running.

1.3.1 Kinematics conventions and joint coordinates

To completely and accurately describe a movement, a clear anatomical terminology has been established.

Firstly, two terms which need to be kept in mind while speaking about anatomical conventions are *proximal* and *distal*. The term proximal refers to the part of the considered limb closest to the heart. On the other hand, the term distal is related to the part of the considered limb furthest to the heart (Mosby, 2009).

Furthermore, three anatomical planes, *transverse*, *frontal* and *sagittal* plane, have been defined. Each anatomical plane will be presented together with the description of the lower limb joint coordinates associated to it. The *transverse* plane (Figure 1.2) lies parallel to the horizon and it divides the body in a upper and a lower part (Root et al., 1999).

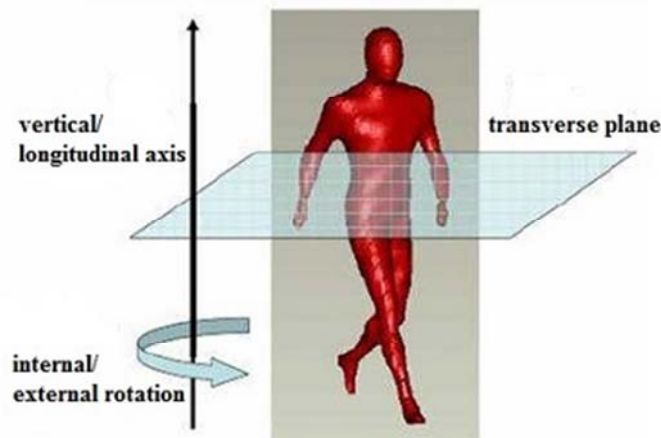


Figure 1.2. Transverse plane and definition of internal/external rotation along the vertical axis. The figure has been taken from Pizzutilo (2012).

Internal and external rotation movements are executed along the vertical axis, which is perpendicular to the transverse plane. Internal rotation occurs when the limb moves toward the midline of the body while external rotation occurs when the limb moves away from the midline of the body (Swartz, 2010).

Pelvic and hip rotations and their corresponding coordinates during the gait cycle in walking and running are shown in Figure 1.3. Motion in the transverse plane is sharply small in magnitude. Pelvic rotation plays a different role in walking and in running. During walking, pelvic rotation contributes to lengthen the stride. In fact, to execute a longer step, the pelvis is amply rotated forward in correspondence with the initial contact, decreasing consequently the horizontal velocity (Novacheck, 1998). In contrast, maximum internal pelvic rotation appears in midswing during running to lengthen the stride. At initial contact the pelvis displays an external rotation. In this way the horizontal propulsion force is maximized and the potential loss of speed is avoided.

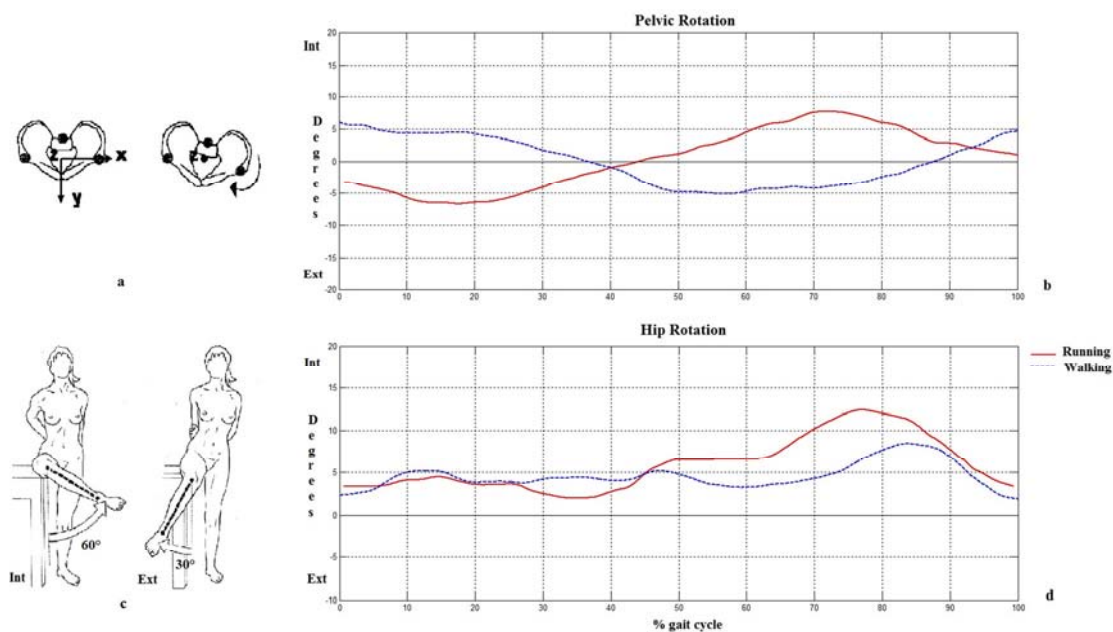


Figure 1.3. Transverse plane movements (a, c) and corresponding joint coordinates (b, d). Movement figures have been taken from the American Academy of Orthotists & Prosthetists (a) and from Kapandji, I.A. (1987) (c). A comparison between joint coordinates in walking (dashed blue line) and running (solid red line) at a running speed of 3.2 m/s is shown. These graphs derive from data collected at the Motion Analysis Lab at Gillette Children's Specialty Healthcare.

The *frontal* plane (Figure 1.4) divides the body into an anterior and a posterior part (Root et al., 1999).

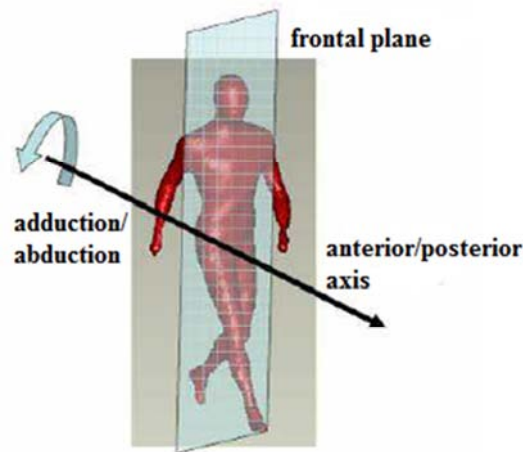


Figure 1.4. Frontal plane and definition of adduction/abduction movements along the anterior/posterior axis. The figure has been taken from Pizzutilo (2012).

Abduction and adduction movements are carried out in the frontal plane about the anterior/posterior axis. Abduction is defined as the movement away from the midline of the body, while adduction points toward the midline of the body (Perry, 1992).

In the frontal plane, collateral ligaments limit the motion of the hip and the ankle. On the other hand, substantial motion occurs at the hip. The relatively stationary trend of the pelvis while the limb is loaded can be easily seen in Figure 1.5. The hip adducts accordingly to the pelvis, promoting an impact shock absorbing mechanism. During the stance phase, the pelvis drops until the beginning of double float. However, in the swing phase an inversion of the motion is apparent, consequently to the raising of the pelvis to obtain foot clearance (Novacheck, 1998). It is possible to conclude that, both in walking and in running, the hip is adducted during limb loading in stance phase and it is abducted in correspondence to swing. The specular behavior of the pelvis and the hip contributes to the minimization of the upper body movement.

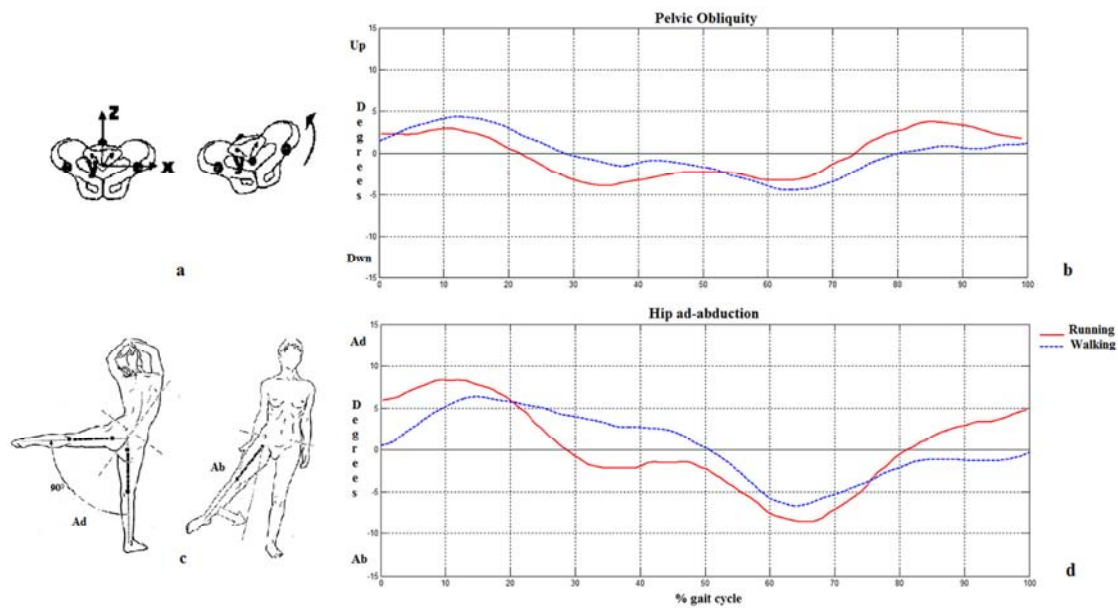


Figure 1.5. Frontal plane movements (a,c) and corresponding joint coordinates (b,d). Movement figures have been taken from the American Academy of Orthotists & Prosthetists (a) and from Kapandji, I.A. (1987) (c). A comparison between joint coordinates in walking (dashed blue line) and running (solid red line) at a running speed of 3.2 m/s is shown. These graphs derive from data collected at the Motion Analysis Lab at Gillette Children's Specialty Healthcare.

Finally, the *sagittal* plane (Figure 1.6) divides the body into a right and a left part (Root et al., 1999).

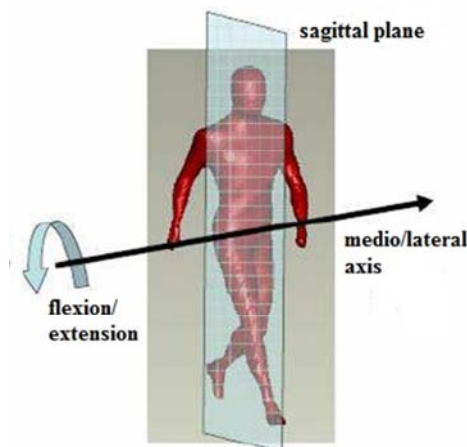


Figure 1.6. Sagittal plane and definition of flexion/extension movements along the medio/lateral axis. The figure has been taken from Pizzutilo (2012).

Flexion and extension movements are executed along the sagittal plane. Flexion corresponds to bending the joint, allowing the distal segment to rotate towards the

proximal segment, whereas extension is defined as the straightening of the limb in which the bones comprising the joint move to a more parallel alignment (Perry, 1992). Pelvic tilt, hip and knee flexion/extension, dorsi/plantar flexion and their corresponding coordinates during the gait cycle in walking and running are shown in Figure 1.7.

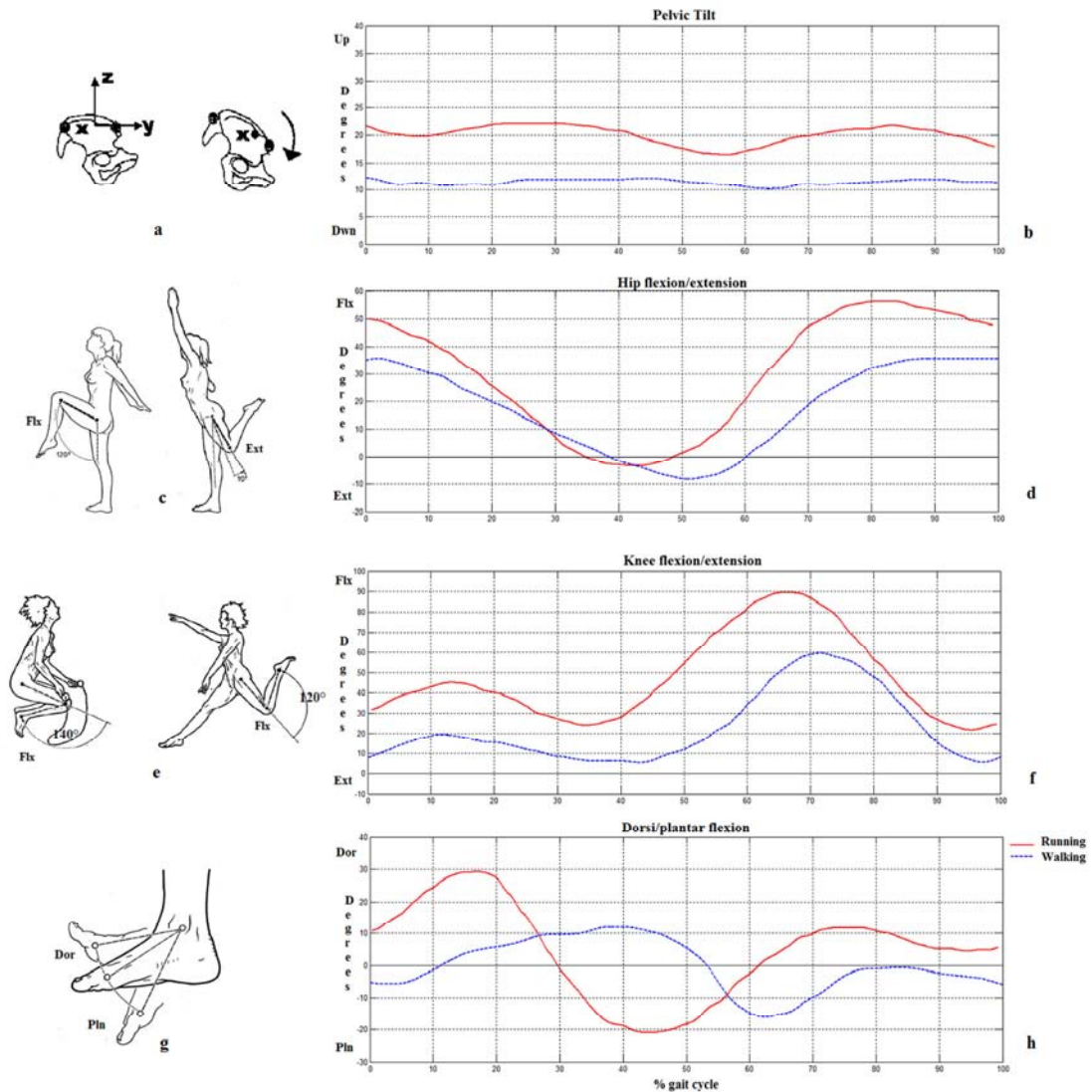


Figure 1.7. Sagittal plane movements (a, c, e, g) and corresponding joint coordinates (b, d, f, h). Movement figures have been taken from the American Academy of Orthotists & Prosthetists (a) and from Kapandji, I.A. (1987) (c). A comparison between joint coordinates in walking (dashed blue line) and running (solid red line) at a running speed of 3.2 m/s is shown. These graphs derive from data collected at the Motion Analysis Lab at Gillette Children's Specialty Healthcare.

In the sagittal plane, the trend of the tilt of the pelvis changes slightly from walking to running, as pelvic motion needs to be minimized to conserve energy and maintain efficiency. In fact, previous studies (Burnet et al., 2009) demonstrated a high correlation

(Pearson's $R=0.939$) between changes in maximum pelvic motion and oxygen consumption, concluding therefore that an increased pelvic motion during running results in metabolic inefficiency and performance reduction. Nevertheless, the pelvis tilts slightly further forward during running, probably because of a reduced hip extension (approximately 2° in running and 8° in walking) (Schache et al., 2000).

Maximum hip extension occurs slightly later in walking (50% of the gait cycle versus 40% of the gait cycle during running). Differently from walking, larger hip flexion during the second half of the running swing phase can be noticed in preparation for initial contact. In correspondence with this event in fact, an excessive deceleration of the body that would occur if the foot were too far ahead of the body center of mass needs to be avoided.

Despite the similarity between the trend of knee motion in walking and running, the extremes of motion are considerably different. For example, maximum knee flexion during swing is much lower during walking (60°) than during running (90°).

During walking, because of the position of the tibia, heel strike occurs with the ankle in plantar flexion. In contrast, larger ankle dorsiflexion is necessary to achieve initial heel contact during running.

1.4 Running kinetics

Kinetics is the study of the forces which cause the movements considered in the kinematic analysis and the resultant energetics (Winter, 2009). Basically, kinetic analysis gives an explanation of the “how and why” the movements occur (Novacheck, 1998).

1.4.1 Ground Reaction Forces

Ground reaction force (GRF) is defined (Kwon, 1998) as the reaction to the force the body exerts on the ground. This is related to Newton's second and third laws of motion. In fact the body, while in contact with the ground, decelerates during impact and accelerates during propulsion, exerting a force against the ground (2nd law) which provides an opposite action (3rd law) (Richards, 2008). The GRF, along with the weight, represents a significant external force and it is normally measured by a force plate.

A force plate can consist of four piezoelectric triaxial transducers that measure the force acting between the foot and the ground into the vertical (Z), antero-posterior (Y) and medio-lateral (X) directions (Figure 1.8). The point of application of the vertical force component on the force plate is called *center of pressure* (COP) (Kwon, 1998). Being null the horizontal moments with respect to the COP, the force platform provides the force F applied to the COP and the so-called free moment M_z , which has only the vertical (Z) component.

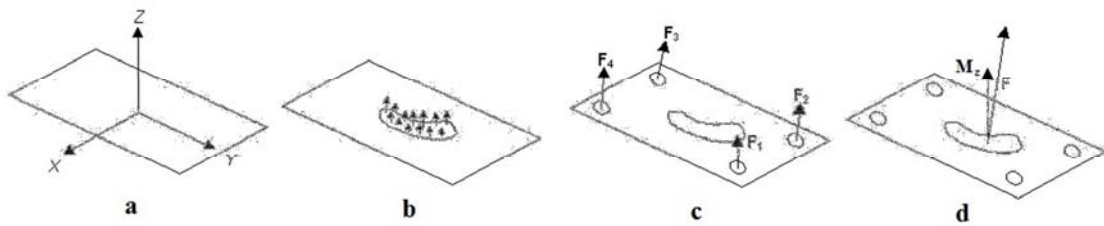


Figure 1.8. Ground Reaction Force. Reference frame of the force-plate (a), interaction between the foot and the ground (b), four reaction force vectors measured by the transducers (c), single ground reaction force F ($F_1 + F_2 + F_3 + F_4$) and free moment M_z (d). The figure has been taken from Kwon (1998).

The *vertical* force pattern during running is slightly similar to the walking one (Figure 1.9a). Typical trends such as impact peak, trough and propulsive peak can be recognized in both styles but their function is considerably different.

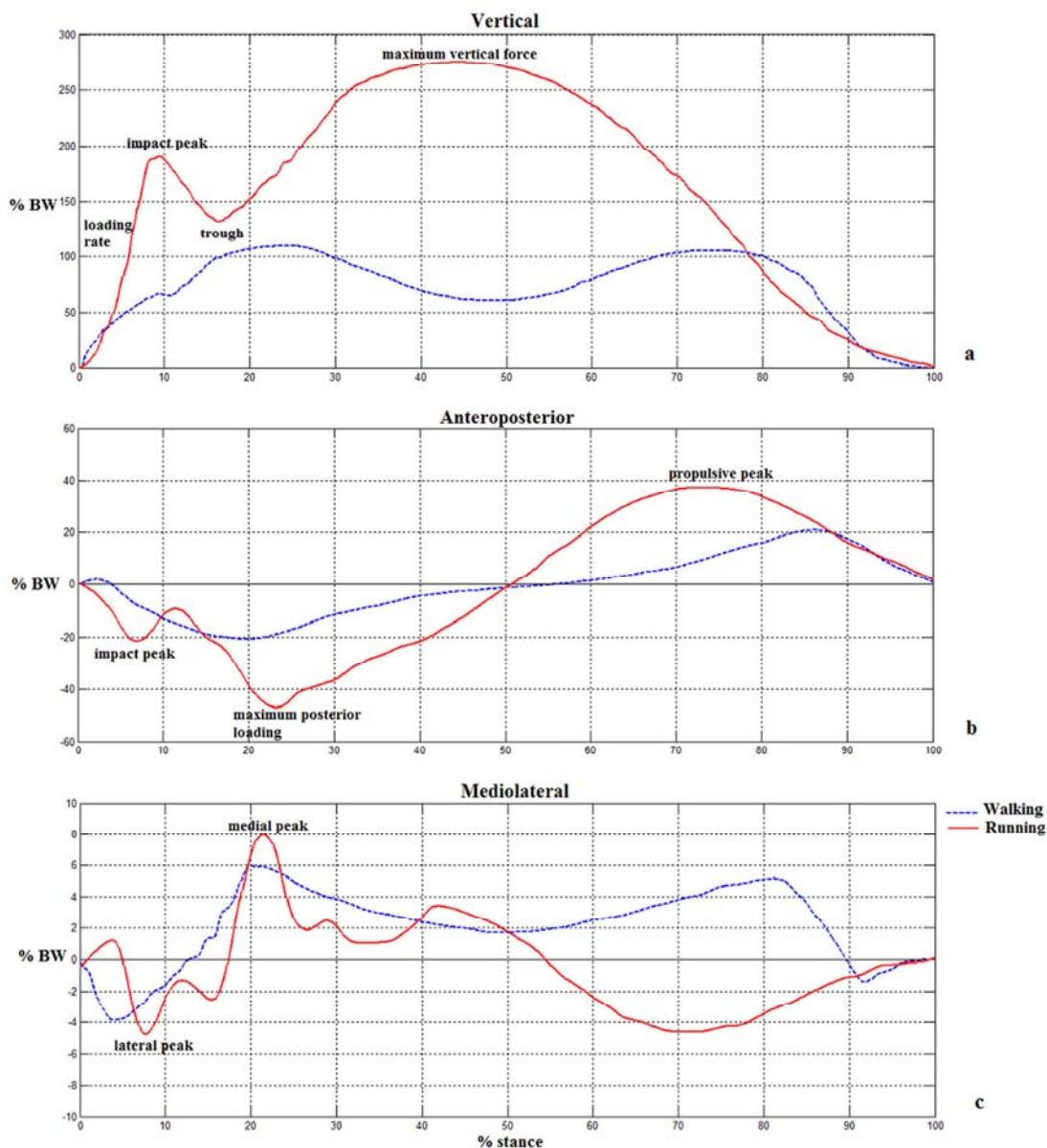


Figure 1.9. Vertical (a), anteroposterior (b), mediolateral (c) Ground Reaction Forces. Comparison between walking (dashed blue line) and running (solid red line) at a running speed of 4 m/s. Data for walking and running derive from Richards (2008) and Hamill (1983) respectively.

How the shock is absorbed from initial contact is shown by the vertical loading rate (Richards, 2008). This value corresponds to the ratio between the change in force during the initial loading (usually computed between the 20 and the 80% of the instant peak force) and the time taken for that change and it is generally measured as body weight (BW) per stance duration. The higher the loading rate, the poorer the shock absorption, which is related to poor function of the ankle and knee joint and eventually to poor

shock absorbency of the shoes being worn. Differently from walking, no correspondence can be seen between the trough and the zero crossing in the anterior-posterior force. Nevertheless, the trough reveals a reduction in force after the initial impact, which relates to the rapid movement of the ankle into plantarflexion to the foot flat position. The deceleration of the body downward is highlighted by the maximum vertical force. The control of the knee on the vertical deceleration of the body in the loading phase leads to a growth in force. This contributes to produce a stretching effect on the knee extensors. In this lengthening phase the muscles are acting eccentrically, followed by a shortening (concentric) action (Komi, 2000). Therefore, this combination of eccentric and concentric actions initiates a stretch shorting cycle that aids propulsion in this specific phase, since elastic energy has been shown to be stored during the eccentric contractions of running (Saunders). In fact, this propulsion effect can be seen slightly after the maximum vertical peak as the knee starts to extend to move the body forward (Richards, 2008). However, it has to be kept in mind that maxima and minima depend on velocity (Novacheck, 1998).

The *anteroposterior* force during running is substantially similar to that for walking (Figure 1.9b) and the whole pattern can be divided into a loading and a propulsion period. The magnitude of the posterior impact peak together with the one of the vertical impact peak provide a measurement of the strength of the ground impact. It depends on the nature of initial contact and the footwear. The maximum posterior force occurs when the body decelerates at impact, during the loading or breaking. After this instant, the force reduces to zero in correspondence with the midstance point, which normally occurs shortly before half the stance time during running. On the other hand, the maximum anterior force appears during propulsion as the body accelerates forward (Richards, 2008). The forward movement of the center of pressure during the propulsion phase moves the force away from the ankle joint, maximizing the ankle moment and the power production. These factors contribute to drive the person forwards. Another relevant measurement while studying running is represented by the breaking and thrusting impulse. This impulse corresponds to the area under the anteroposterior force curve and, in detail, breaking impulse is negative whereas thrusting impulse is positive. The two impulses should have the same magnitude. They

provide a measurement of the body acceleration or deceleration during the stance phase (Richards, 2008).

The *mediolateral* force (Figure 1.9c) is strictly correlated to the amount of pronation/supination during stance phase. The presence either of a medial or a lateral peak depend on the position of the foot and on which part of the foot contacts the ground. Similarly to walking, the mediolateral force can significantly affect the loading and stability of the ankle and knee joints in the frontal plane (Richards, 2008).

1.4.2 Sagittal plane joint moments

The larger and functionally most important moments act in the sagittal plane (Figure 1.10).

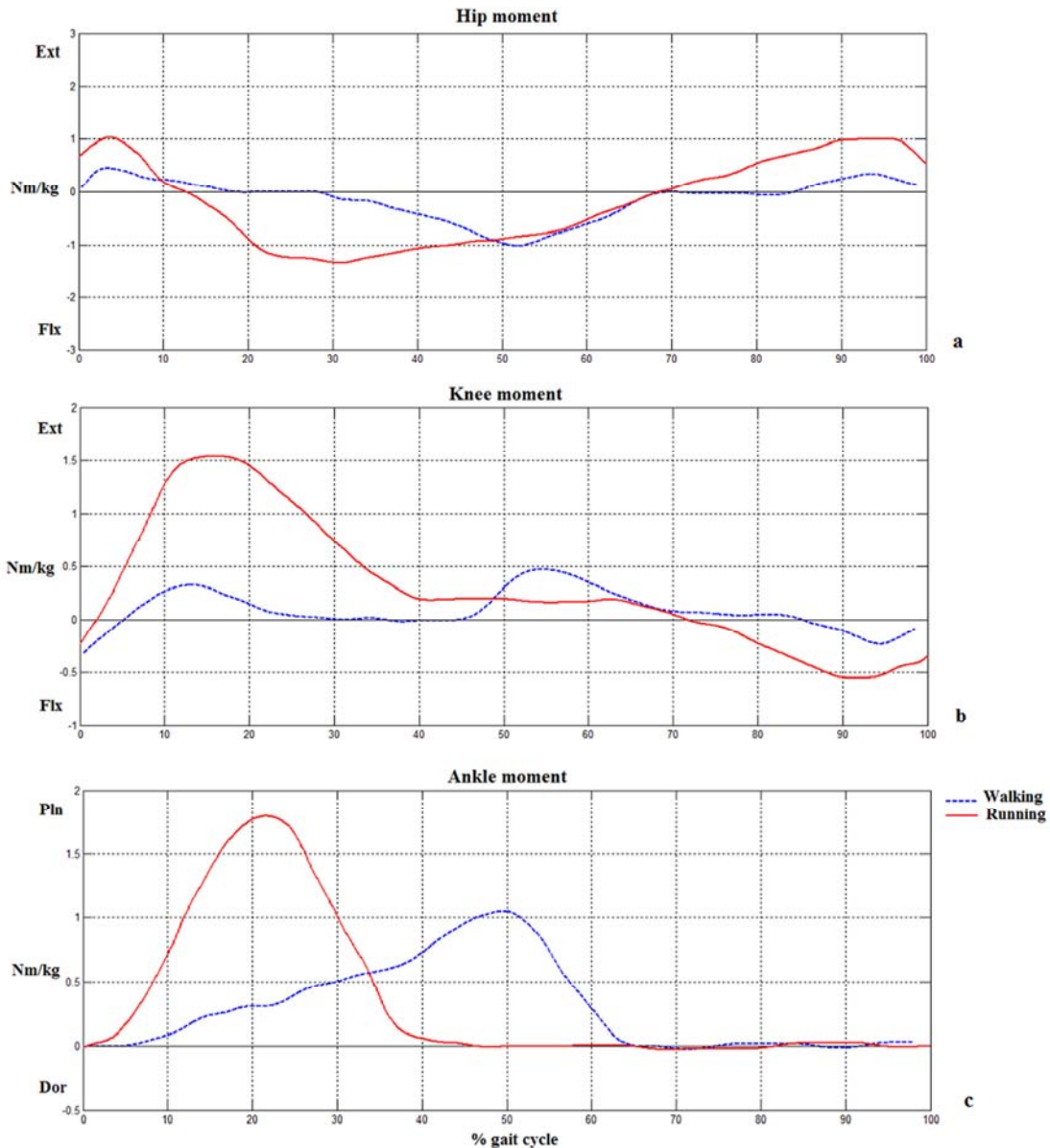


Figure 1.10. Sagittal plane moments. Hip flexion/extension (a), knee flexion/extension (b) and dorsi/plantar flexion moments during a complete gait cycle. Walking is represented by a dashed blue line while running at a speed of 3.2 m/s by the solid red line.

Similarities in the *hip* moment pattern in walking and running can be recognized but the magnitude is considerably different (Figure 1.10a). The hip extensors are dominant just before and after initial contact (Novacheck, 1998). During the first part of the stance phase, they stabilize the posture of the trunk. In this way, the extensor moment avoids the trunk to flex forward. On the other hand, the hip flexor moment which occurs in the second half of stance stabilizes the trunk posture by preventing it from flexing backward (Winter, 2009).

The amplitude of the *knee* extensor moment is significantly larger in running than in walking (Figure 1.10b). In the first part of the stance phase in fact, the extensor moment is produced by the quadriceps. In the second half of swing phase the hamstrings become dominant to prepare for the ground contact producing a knee flexor moment which controls rapid knee extension (Novacheck, 1998). The *ankle* moment shows a similar pattern in walking and in running (Figure 1.10c) but the magnitude is substantially different also in this case. At initial contact in running, the eccentric contraction of the tibialis anterior lowers the forefoot to the ground. The beginning of the plantarflexion moment occurs at 5-10% of the running gait cycle (Novacheck, 1998).

1.5 EMG

This section will focus on the electromyographic (EMG) activity of the most commonly documented lower limb muscles involved in running (Figure 1.11).

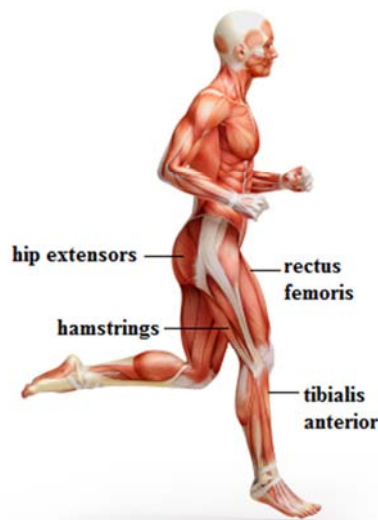


Figure 1.2. Principal muscles involved during running. Figure has been taken from Spencer, A. (2012).

Typical EMG activity of hamstrings, hip extensors, rectus femoris and tibialis anterior during walking and running is represented in (Figure 1.12).

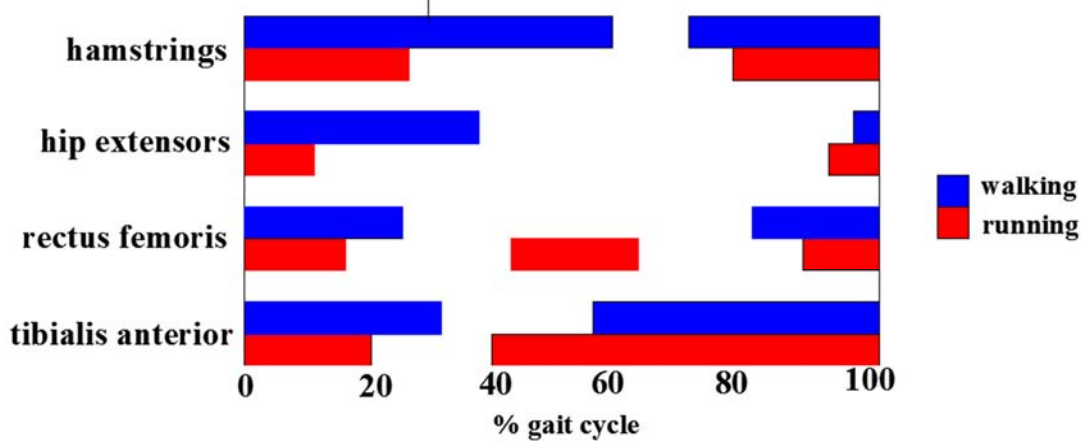


Figure 1.32. Muscle timing activation in the complete gait cycle. EMG activity is represented by the solid bar in walking (blue) and running (red). Data for walking derive from Benedetti et al. (2012) , Nene et al. (2004) and data for running derive from Novacheck (2008).

The largest muscle activation can be generally seen in anticipation of and just after the initial contact (0 and 100% of the gait cycle). Rectus femoris timing activation is considerably shorter in running than in walking. In running, it is active from late swing to heel strike to support the contact with the ground and to absorb the shock deriving from the initial contact (Novacheck, 1998). The hamstrings and the hip extensors timing activations are significantly smaller in running than in walking. During the second half of swing and the first part of stance these muscles extend the hip. Furthermore, the hamstrings are responsible of the deceleration of the momentum of the tibia as the knee extends before initial contact. Tibialis anterior becomes active earlier during swing in running in comparison to walking. Its function is plantar dorsiflexion to allow the initial contact with the hindfoot and to control the lowering of the forefoot to the ground at the beginning of the stance phase.

1.6 Running styles

Based on how a runner's foot strikes the ground, three different running styles can be identified and used to group runners into *rearfoot*, *midfoot* and *forefoot* strike pattern runners (Lieberman et al., 2010c). Rearfoot strike occurs when the heel lands first, followed by the lowering of the forefoot towards the ground (Figure 1.13a). Midfoot strike occurs when the heel and the ball of the foot land simultaneously (Figure 1.13b). Finally, forefoot strike occurs when the ball of the foot (generally below the 4th and the

5th metatarsal) lands first, followed by the lowering of the heel towards the ground (Figure 1.13c).

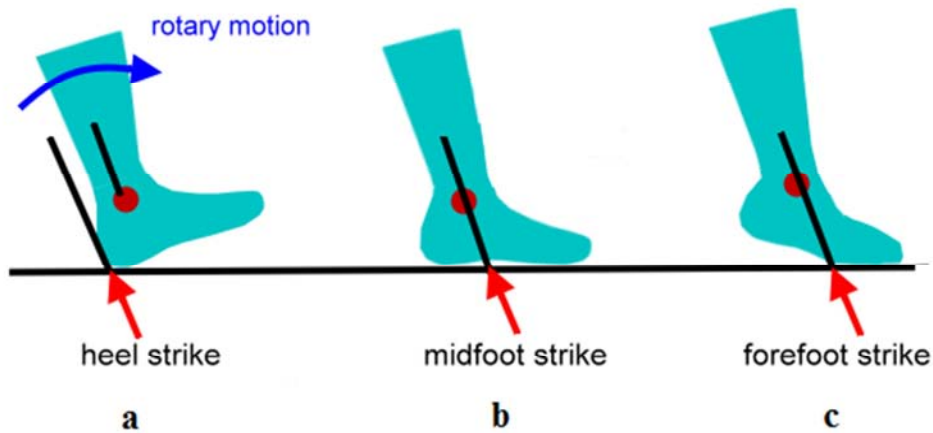


Figure 1.43. Rearfoot (a), midfoot (b) and forefoot (c) strike pattern. The figure has been taken from Chai, H.M. (2003).

1.7 Running footwear

Generally, it is quite natural to affirm that the perfect running shoe has to allow the foot to behave as it would if bare, providing in the meanwhile maximum protection from the environment (Saxby, 2011).

As running has been shown to be a quite injurious sport, with injuries occurring especially when the foot collides the ground (Lieberman et al., 2010c), specific design features need to be taken into account while designing running shoes.

According to Winter and Bishop (1992), a traditional running shoe has to:

- limit joint cartilage damage and control shock absorption in correspondence to heel contact reducing the initial peak of ground reaction force (Cavanagh and Lafortune, 1980);
- protect against the harsh ground surface during the stance phase;
- align the forefoot to obtain a uniform force distribution at the most common injury sites.

Consequently, both shock absorption and stabilization of the foot have to be guaranteed. Recently, to closely simulate barefoot running conditions, a new kind of footwear has been introduced in the running shoes market. These shoes are technically called *minimalist* and they are defined (Lieberman et al., 2010a) as “any footwear that lacks high cushioned heels, stiff soles and arch support”. One of the main advantages of

running with minimalist shoes is that it may require less energy. In fact, being this kind of shoes lighter than traditional running shoes, less mass need to be accelerated at the end of the runner's leg. Furthermore, the feeling of running like in barefoot conditions may be very comfortable since feet have a lot of sensory nerves (Lieberman, 2010). However, the thick sole may not provide an adequate protection from the environment. A comparison between traditional and minimalist running shoes will be presented in the following chapters, based on the effects that each kind of shoe has on running kinematics, kinetics and internal loads.

CHAPTER 2

Experimental data description

2.1 Introduction

Experimental data were collected at St Mary's University (Twickenham, London, UK) in 2012, during a collaboration with Structural Biomechanics Group at Imperial College London. The St Mary's University is one of the most comprehensive Performance and Rehabilitation Centre in the UK and it is specialized in gait and ultimate running analysis (StMary'sUniversity, 2013).

The purpose of this chapter is to provide an overall description of data collection procedures and instruments. Furthermore, data post-processing pipeline necessary to provide useful inputs for further analyses will be discussed. In addition, some features of interest, such as spatio-temporal parameters and the identification of strike patterns in executing the trials with different footwear will be reported as first achievements derived from data processing. Finally, a detailed section concerning the comparison of ground reaction forces will be included. This final paragraph will highlight the first relevant differences between the different running styles and footwear.

2.2 Footwear and running styles

The study involved a single 24-year-old experienced runner (height 1.79 m, mass 87.2 kg) without any history of joint articular pain. Barefoot running and running with two different kinds of footwear, a minimalist and a traditional running shoe, were performed. It is important to mention that the involved subject suffered a stress fracture in the fibula when moving from traditional shod running to minimalist running (Sheikh-Warak, 2012). However, he was fully recovered by the time of the data collection.

The subject was asked to perform from eight to ten running trials for each running style. The chosen minimalist shoe was a Vivobarefoot Aqua lite (Figure 2.1a). This shoe is characterized by a 3mm zero-drop sole, a considerably wide toe-box and an extremely

flexible sole. The tiny thickness of the sole does not provide a great shock absorption but it allows maximum proprioception ensuring some protection at the same time (Sheikh-Warak, 2012).



Figure 2.1. Minimalist (a) and traditional (b) running shoes used in the study.

On the other hand, the utilized traditional running shoe was a Nike Impax (Figure 2.1b). This shoe is endowed with a 45mm shock absorbing heel and a 20 mm thickness forefoot. During the data collection the subject was encouraged to adopt a rearfoot strike while wearing the traditional shoe (Sheikh-Warak, 2012). No running speed was imposed.

2.3 Experimental setup

Data collection was performed at the gait analysis laboratory at the St Mary's University (Twickenham, London, UK). Motion data were collected by a stereophotogrammetric system (Vicon Motion Systems Ltd., Oxford, UK) . This optoelectronic system is based on eight infrared cameras coaxial with infrared illuminators and passive reflective markers (Figure 2.2). Even if motion capture is uniquely possible in a limited volume and in a reconstructed environment, it represents the most common technology because it provides high accuracy and high frequency acquisition (Petrone, 2013). However, it has to be kept in mind that an optoelectronic system offers an estimation, not a direct measurement, of the kinematic variables (Pizzutilo, 2012).

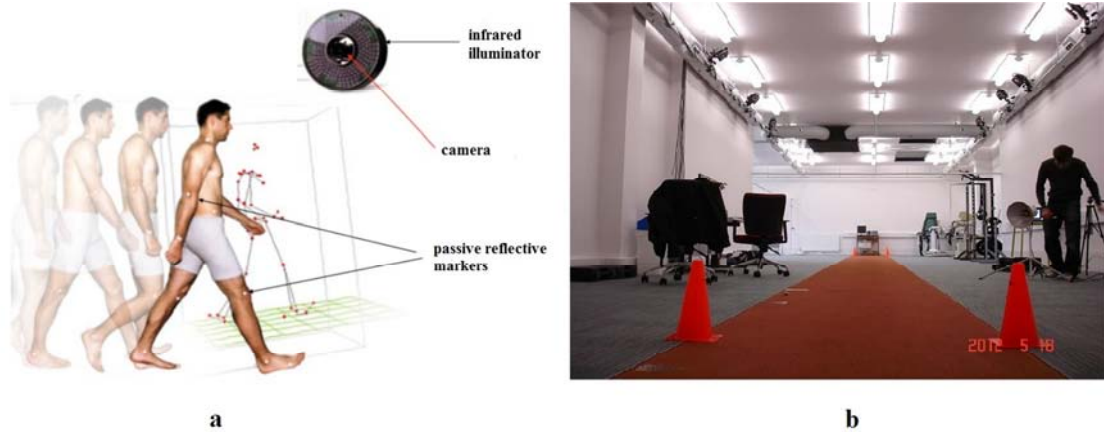


Figure 2.2. Typical stereophotogrammetric system components (a) and gait lab in St Mary's University (b).

Furthermore, a 200 fps high speed video camera and a Kistler force plate recorded kinematic and kinetic data during the trials. In particular, the high speed camera was useful to carefully analyze the foot contact with the ground.

Regarding the execution of the trial, a noteworthy observation can be done. In fact, the subject was observed to hit perfectly the force plate during barefoot and minimalist running, whereas he missed the force plate or he landed on the wrong foot while wearing traditional shoes. This may derive from the intentional attempt to heel striking but also from a reduced awareness of the subject with the ground during traditional running. Moreover, the involved runner mentioned having to think less about absorbing the initial impact during traditional running since the shoes were providing it.

Finally, cones were used to define the run path (18.92 m). This distance was settled to allow the runner to accelerate, maintain pace, hit correctly the force plate with the right foot, maintain pace till the end of the path and decelerate.

The subject started each trial with the same leg, to ensure consistency between the experimental trials. Consistency was also guaranteed by using a metronome to pace the running gait and a stop watch to assure a similar running speed between the trials (Sheikh-Warak, 2012).

2.4 Marker set

Passive reflective markers are plastic supports covered in a reflective film. Their roundness (25 mm diameter) guarantees the best reflection of infrared rays (Pizzutilo, 2012).

The definition of the marker set is defined as a *protocol*. The efficiency of a protocol is evaluated (Pizzutilo, 2012) based on:

- tridimensionality (there should be at least 3 markers per segment);
- visibility of the markers;
- reliability of the definition of the anatomical planes, to guarantee an objective physiological and clinical interpretation;
- simplicity on markers application;
- simplicity of bony landmarks identification;
- accuracy;
- velocity in preparing the subject.

Trying to satisfy all these features, a 49-marker protocol was defined and it is shown in Figure 2.3.

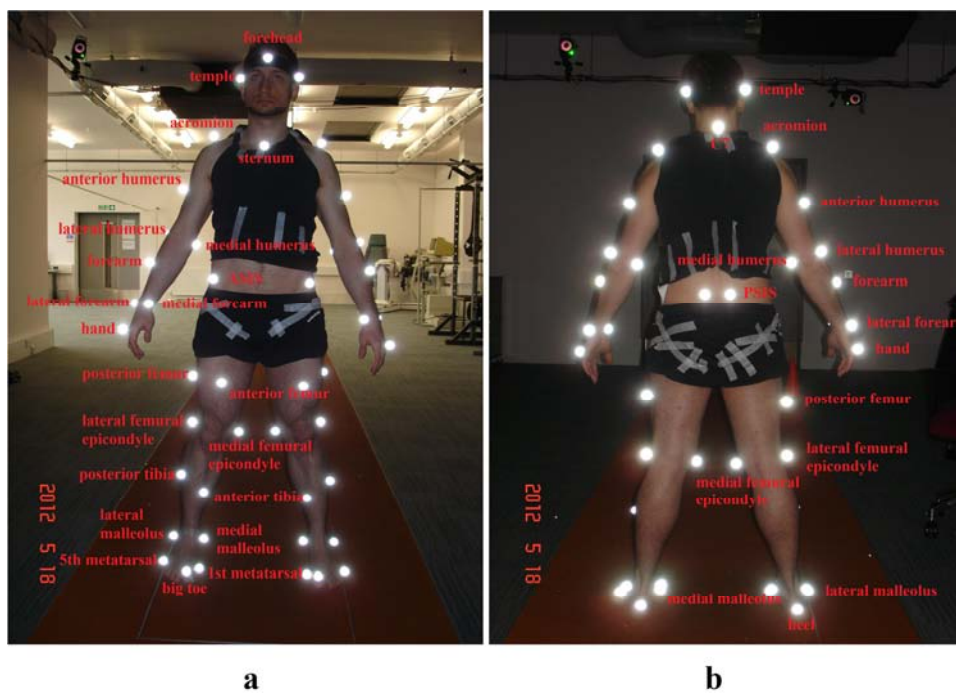


Figure 2.3. Marker set. Anterior (a) and posterior (b) view. For clarity, only the markers on the right side are labeled.

Both anatomical and technical markers have been included in the protocol. Anatomical markers were placed in correspondence to anatomical landmarks, such as bone processes or corners that are exposed superficially and minimize the skin movements. On the other hand, technical markers were applied on the segments as auxiliary markers to guarantee the tridimensionality of the protocol.

Marker plates were fixed on the skin using a double sided sticky tape. Two pieces of micro porous tape in parallel fastened then opposite sides of the marker plate (Sheikh-Warak, 2012).

2.5 Vicon Nexus post-processing

After being collected by Vicon cameras in the gait laboratory, raw data were available in a C3D (Coordinate 3D) format, which provides an efficient way of storing 3D coordinates, analog data and associated parameters (Motion Lab Systems, 2008). Data were processed using Vicon Nexus Software (Vicon Motion Systems Ltd., Oxford, UK) before being used in other applications.

Vicon Nexus Software allows to build a customized template which represents the subject's motion in a simplified but distinct way. All the markers were manually labeled as defined in Figure 2.3 and grouped into 13 bodies representing respectively:

- head
- trunk
- pelvis
- arm (left and right)
- forearm (left and right)
- thigh (left and right)
- shank (left and right)
- foot (left and right)

The described template was built firstly in a static trial (Figure 2.4) and later applied to all the dynamic trials.

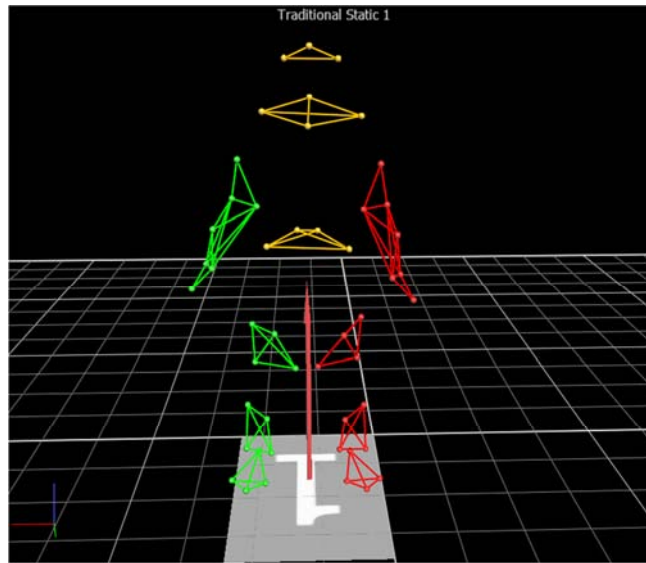


Figure 2.4. Model template definition in a static trial.

Gait events as heel strike and toe off were detected by an automatic pipeline for the right foot (the one hitting the force platform) and selected manually for the left foot. For each trial all the marker trajectories and labeling were checked individually to avoid wrong marker identifications, a common issue when the markers are quite close each other. Each trial was therefore restricted from the left toe off to the left heel strike to achieve the same running gait interval.

Sometimes, cameras lost track of a particular marker and therefore, there were missing data within the trial. Gap filling operations were therefore necessary to interpolate missing frames for a specific marker. There are two general gap filling approaches: *spline fill* and *pattern fill* algorithms. The spline fill algorithm is an automatic method, that extrapolates the missing trajectory based on the last known and first reappearing set of coordinates. This method should be adopted in presence of small gaps, generally smaller than 60 frames (Livingstone, 2008). Obviously, the larger the gap, the more likely the spline method will provide a wrong result. Furthermore, the spline fill method is considerably susceptible to the erratic marker trajectory occurring in the last frames before the gap. In fact, the extrapolation is based on where the marker was going before it disappeared and often a marker disappears due to a wrong motion. On the other hand, the pattern fill algorithm is used when large gaps occur. In this method, another marker with a similar motion to the missing marker has to be chosen. The software then generates a trajectory based on the selected marker, recognizing that the missing and the

chosen markers are attached to the same body. This algorithm works best when dealing with body symmetric markers. Figure 2.5 shows an example of the two gap filling algorithms.

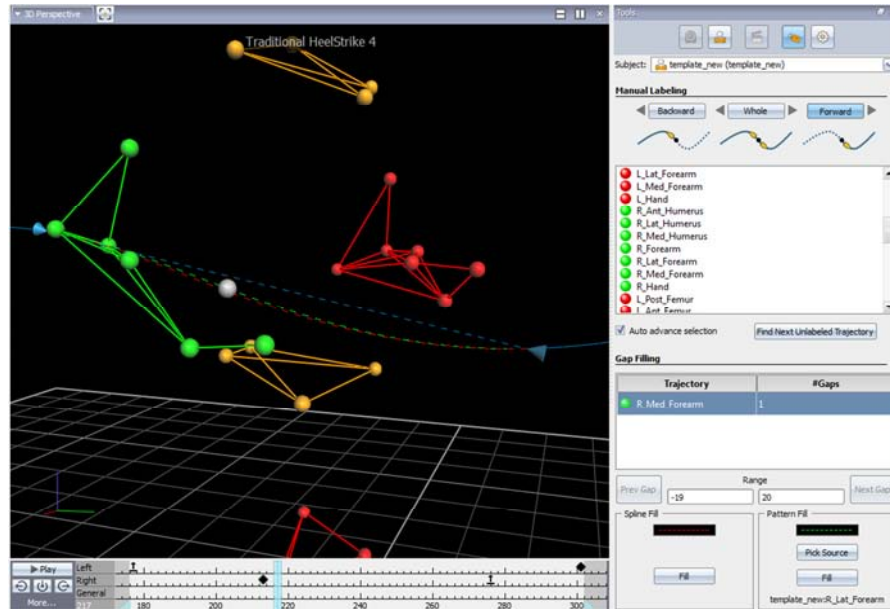


Figure 2.5. An example of gap filling. Spline fill (dashed red line) and pattern fill (dashed green line) trajectory reconstructions.

After filling the gaps, the continuity of the trajectory of each marker was checked. Marker trajectories were then filtered applying a fourth order Butterworth filter with a 6 Hz cut-off frequency (Winter et al., 1974). At the very end of the pipeline, unlabeled trajectories were deleted. This last step was necessary to avoid the presence of ghost markers which may appear due to poor calibration results or reconstruction parameters (ViconMotionSystems). An example of an unprocessed and a processed trial is shown in Figure 2.6.

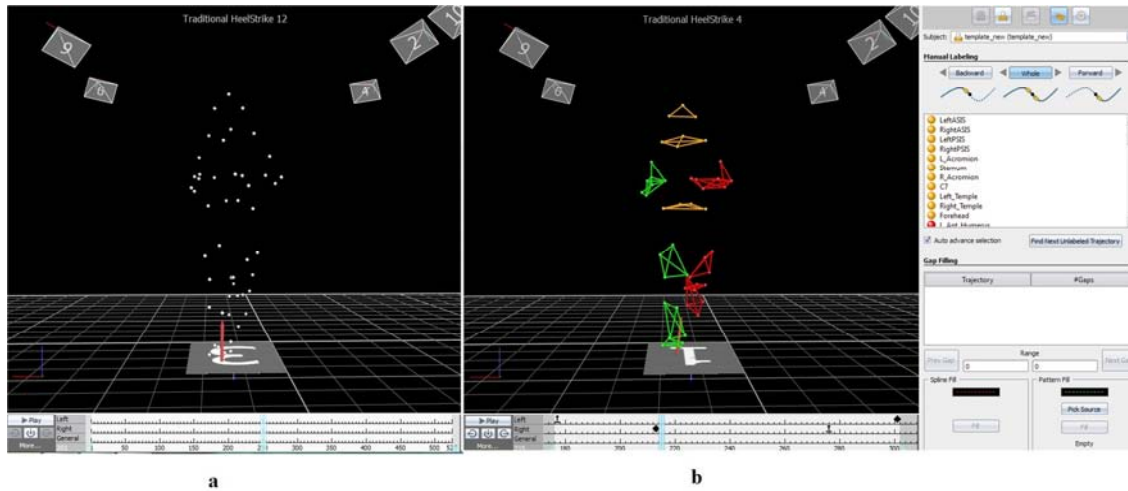


Figure 2.6. Unprocessed (a) and processed (b) trials. Marker names and gait events (arrow for toe off and rhombus for heel strike) are visible on the right and at the bottom boxes respectively.

2.6 Spatio-temporal parameters

Generally, spatio-temporal parameters are reported in detail to describe motion features. Therefore, for the three different running styles these parameters were computed (Table 2.1) using BTK (Biomechanical ToolKit) 0.3 (Barre and Armand, 2014), an open-source and cross-platform library for biomechanical analysis. BTK can read acquisition file (c3d format) and modify them using Matlab functions.

Table 2.1. Comparison of spatio-temporal parameters for the three running styles.

	Barefoot	Minimalist	Traditional
Step time (ST) [s]	0.36 (0.01)	0.34 (0.01)	0.36 (0.01)
Step length (SL) [m]	1.12 (0.05)	1.15 (0.05)	1.22 (0.12)
Speed (v) [m/s]	3.17 (0.18)	3.35 (0.17)	3.41 (0.36)
Cadence (C) [step/min]	166	177	167

Step time (ST) was calculated as the difference between the time at which the left and the right heel strikes took place respectively. As the step length (SL) is defined (Perry, 1992) as the distance between the sequential points of initial contact by the two feet, it was obtained as the difference in the frontal direction between the position of the marker on the left heel during the left foot heel strike and the marker on the right heel during the right foot heel strike. The running speed (v) was computed as the displacement of the marker located on the Sternum during the step time. This marker

was chosen to describe as reliably as possible the movement of the body. The cadence (C) corresponds to the step rate per minute (Perry, 1992).

The obtained values highlight an increase in step length and running speed from barefoot to shod running. A smaller step length value during barefoot running may be related to a forefoot strike pattern (Altman and Davis, 2012). Despite the above-mentioned values being in accordance with previous studies (De Wit et al., 2000, Squadrone and Gallozzi, 2009a), the similar step time and, consequently, the similar cadence between barefoot and shod running do not agree with literature, that proved cadence to be higher in barefoot than in shod conditions.

2.7 Strike patterns

Although the subject was encouraged to adopt a rearfoot strike pattern during traditional running, a rigorous method was chosen to identify the adopted strike pattern. The chosen procedure consists on the expression of the location of the initial contact point of the right foot with respect to the position of the marker placed on the right heel as a percentage of the foot length (Rooney and Derrick, 2013). A heel strike index (HSI) has consequently been calculated considering the initial contact point as the average of the first five locations of the center of pressure. The distance between the initial contact point defined in this way and the right heel resulted in 0.214 ± 0.012 m in barefoot, 0.173 ± 0.061 m in minimalist and 0.086 ± 0.014 m in traditional shod running. The foot length has been calculated after Winter (2009) as 15.2% of the subject height.

Rearfoot strike is defined (Cavanagh and LaFortune, 1980) as the situation when the foot strike is located in the posterior third of the foot, while midfoot and forefoot strikes derive from a foot strike in the middle and in the anterior third respectively. Based on this definition, it is possible to conclude that the subject was adopting forefoot strike pattern during barefoot running (average HSI = 78.8, larger than 66.6% of the foot length), midfoot strike pattern (average HIS = 63.6, between 33% and 66% of the foot length) wearing minimalist shoes and rearfoot strike pattern (average HSI = 31.8, lower than 33.3% of the foot length) wearing traditional shoes (Figure 2.7).

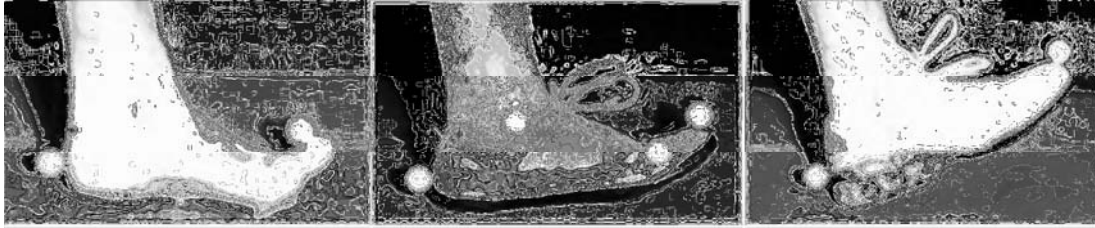


Figure 2.7. Strike pattern comparison.

However, the obtained values agree with literature since barefoot running encourages a forefoot strike pattern (Altman and Davis, 2012). Comfort and thickness of the sole below the heel may represent potential explanations of the rearfoot strike pattern while wearing traditional running shoes (Lieberman, 2010).

The standard deviation (SD) of the distance between the location of the initial contact and the marker on the right heel gives an idea of the repeatability of the trials during the same session. Minimalist session has the largest SD, consequently it is possible to affirm that the subject had the lowest repeatability.

2.8 Ground reaction forces

This section will seek to examine the differences between the vertical, anteroposterior and mediolateral force components in the three running styles.

The interaction of the three force components may be shown with a Pedotti (or butterfly) diagram. This diagram represents the magnitude and the direction of the resultant ground reaction force (GRF). An example of Pedotti diagram obtained using Mokka 0.6.2 (Barre and Armand, 2014), an open source application for 3D motion files visualization, is shown in Figure 2.8.

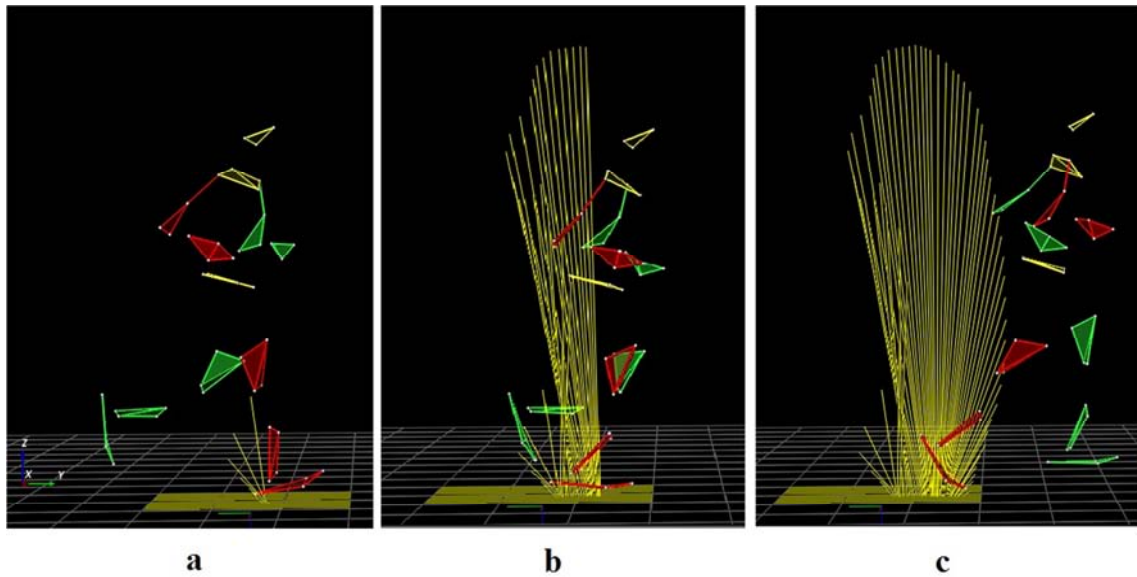


Figure 2.8. Mokka visualization of Pedotti diagram at heel strike (a), midstance (b) and toe-off (c).

From Figure 2.8 it is clearly visible that the GRF is pointing posteriorly in the first part of the stance (a) since it is a deceleration phase, corresponding to the loading response. On the other hand, after midstance (c) the force is pointing in an anterior direction, corresponding the propulsion phase to an acceleration phase. Overall, the Pedotti diagram represents a good way of visualizing the interaction of the forces in the different directions but it is better to examine each force component singularly to study the magnitude and function of the GRF (Richards, 2008).

The average GRFs normalized by the percentage of the stance phase and the body weight (BW) are reported in Figures 2.9, 2.10 and 2.11 for barefoot, minimalist and traditional running respectively.

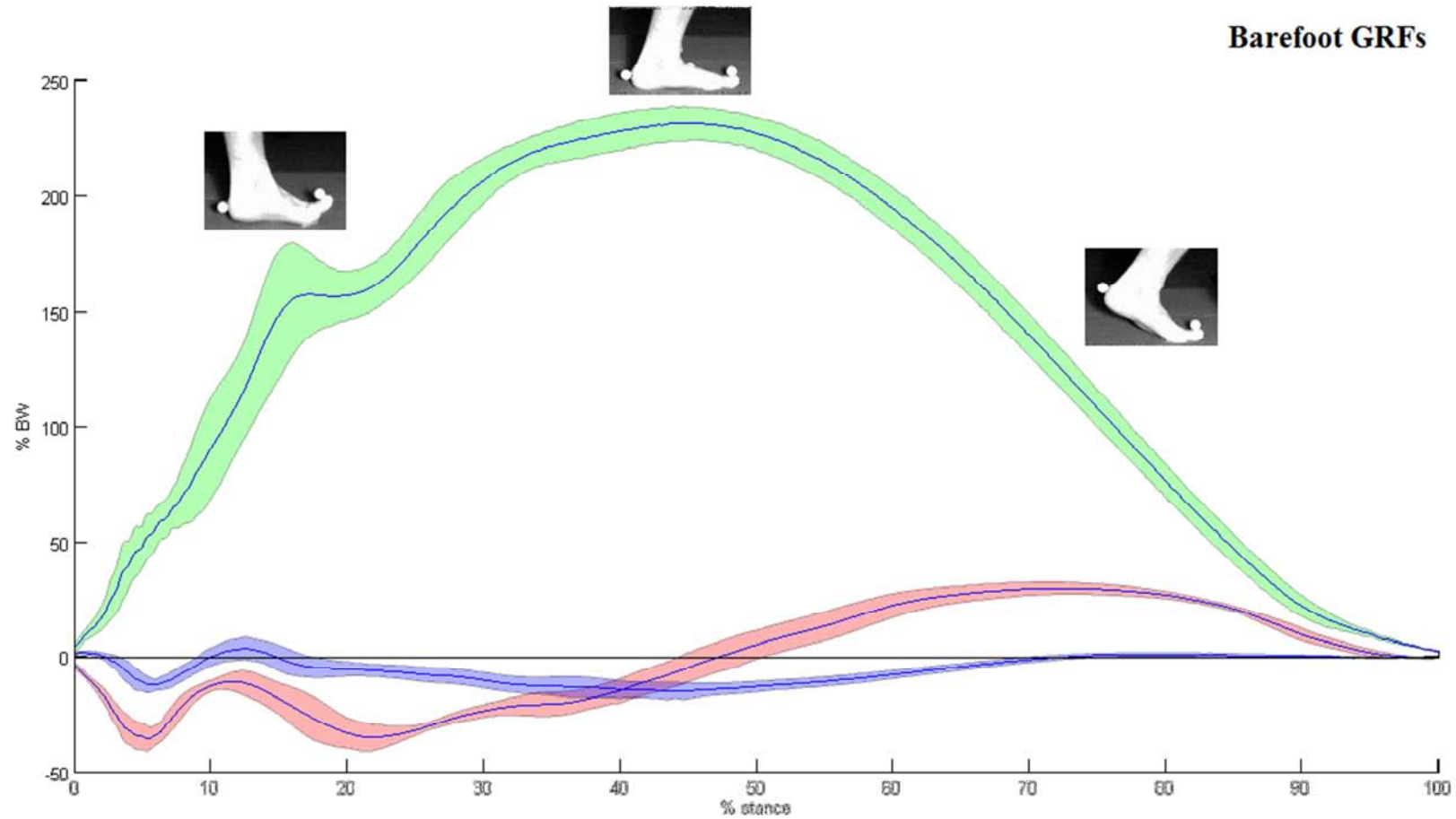


Figure 2.9. GRFs during barefoot running. Average and SD for the vertical (green), anteroposterior (pink) and mediolateral (blue) reaction forces have been plotted, normalized by the percentage of the stance phase and the body weight (BW). Gait event images were extracted from high speed camera videos.

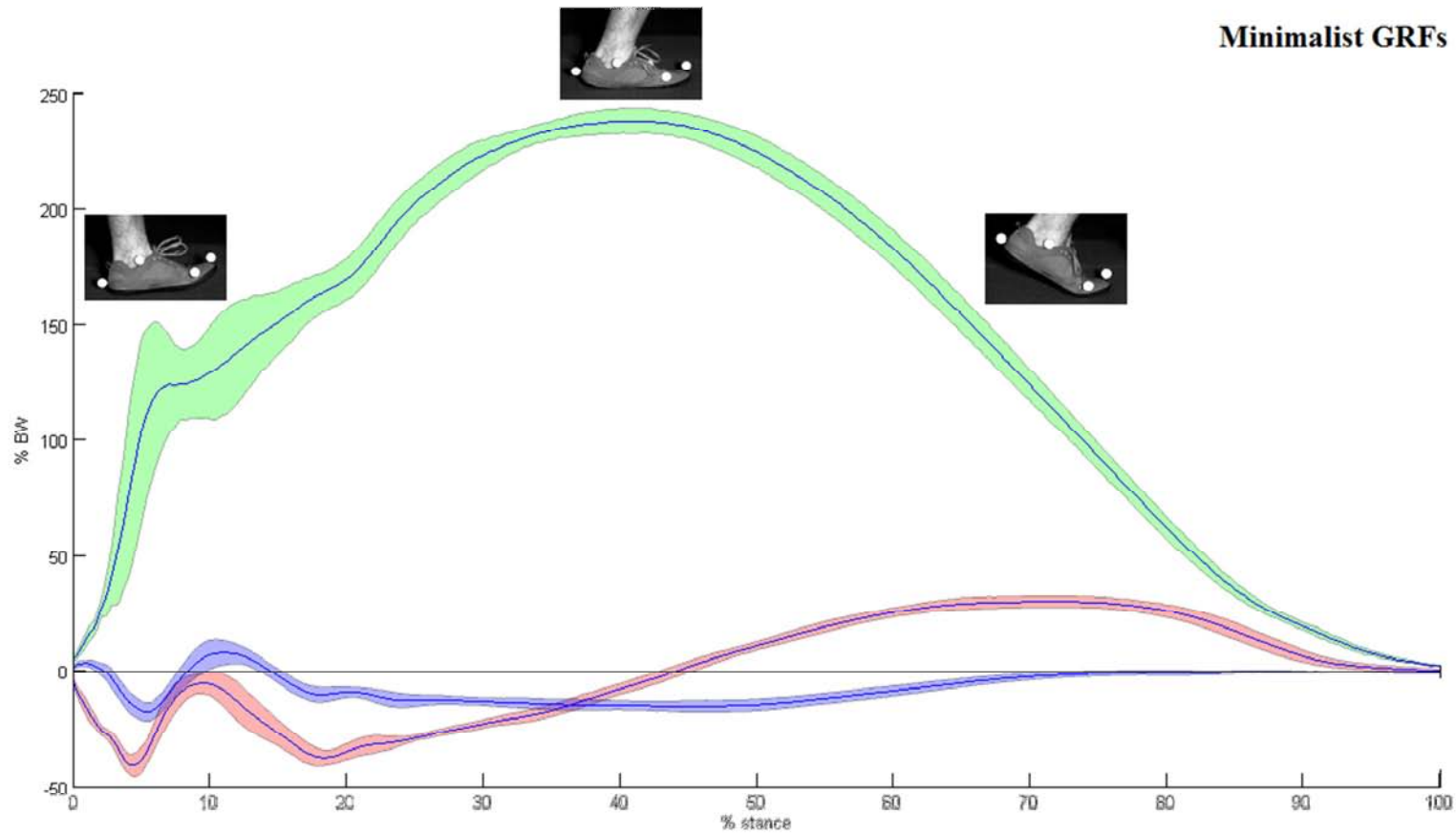


Figure 2.10. GRFs during minimalist running. Average and SD for the vertical (green), anteroposterior (pink) and mediolateral (blue) reaction forces have been plotted, normalized by the percentage of the stance phase and the body weight (BW). Gait event images were extracted from high speed camera videos

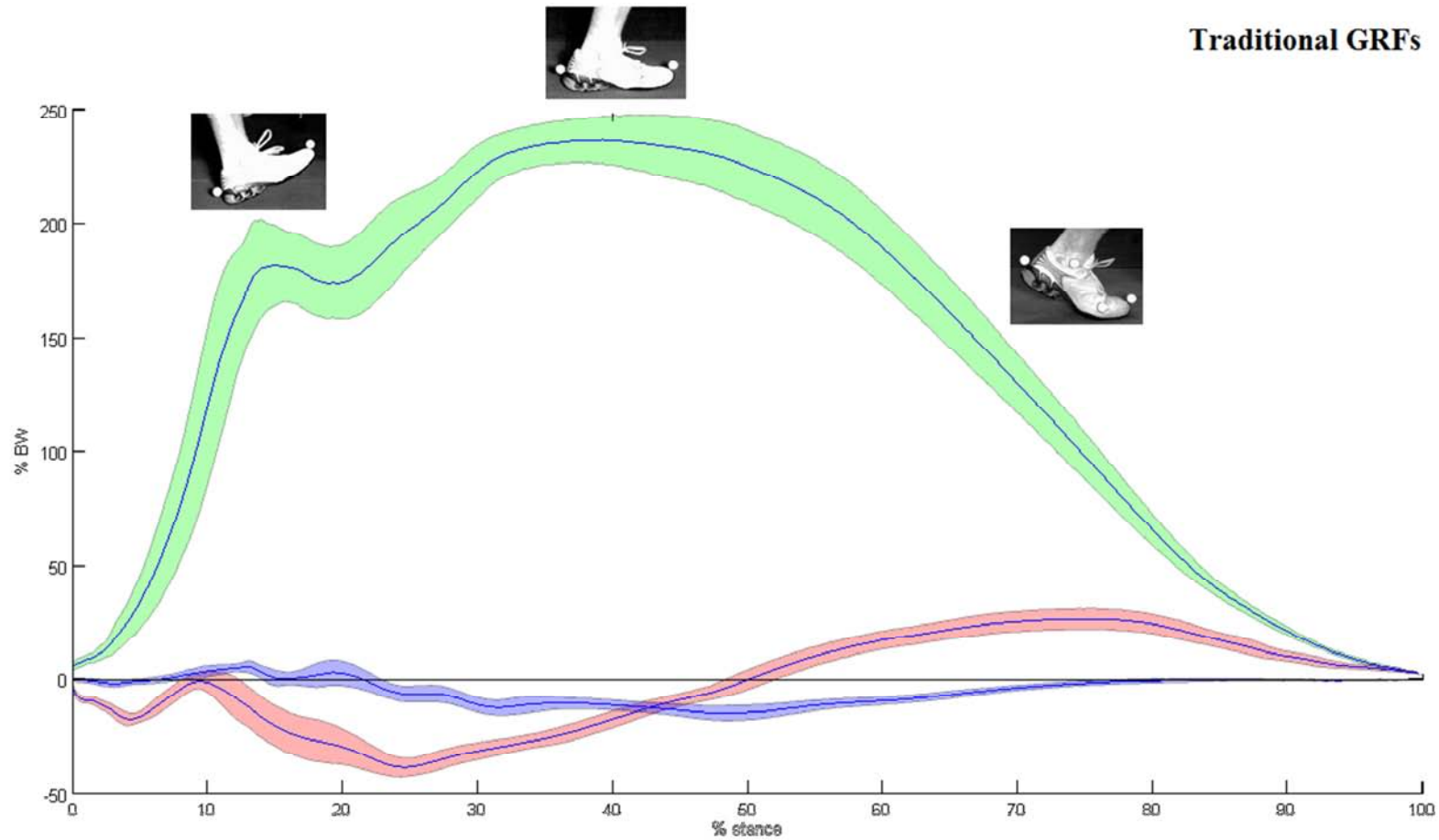


Figure 2.11. GRFs during traditional running. Average and SD for the vertical (green), anteroposterior (pink) and mediolateral (blue) reaction forces have been plotted, normalized by the percentage of the stance phase and the body weight (BW). Gait event images were extracted from high speed camera videos

After importing the content of c3d files in Matlab using BTK, GRFs were defined when the vertical component was above 20N to avoid the inclusion of erroneous peaks due to noisy data before the real contact of the foot on the platform. Each force component will be analyzed in detail in the following paragraphs.

Vertical GRF will be taken into account firstly as it is the largest in magnitude and it is normally the most used to evaluate the characteristics of the running style. A clearer and qualitative comparison between the vertical force in the three different running styles can be visualized in Figure 2.12.

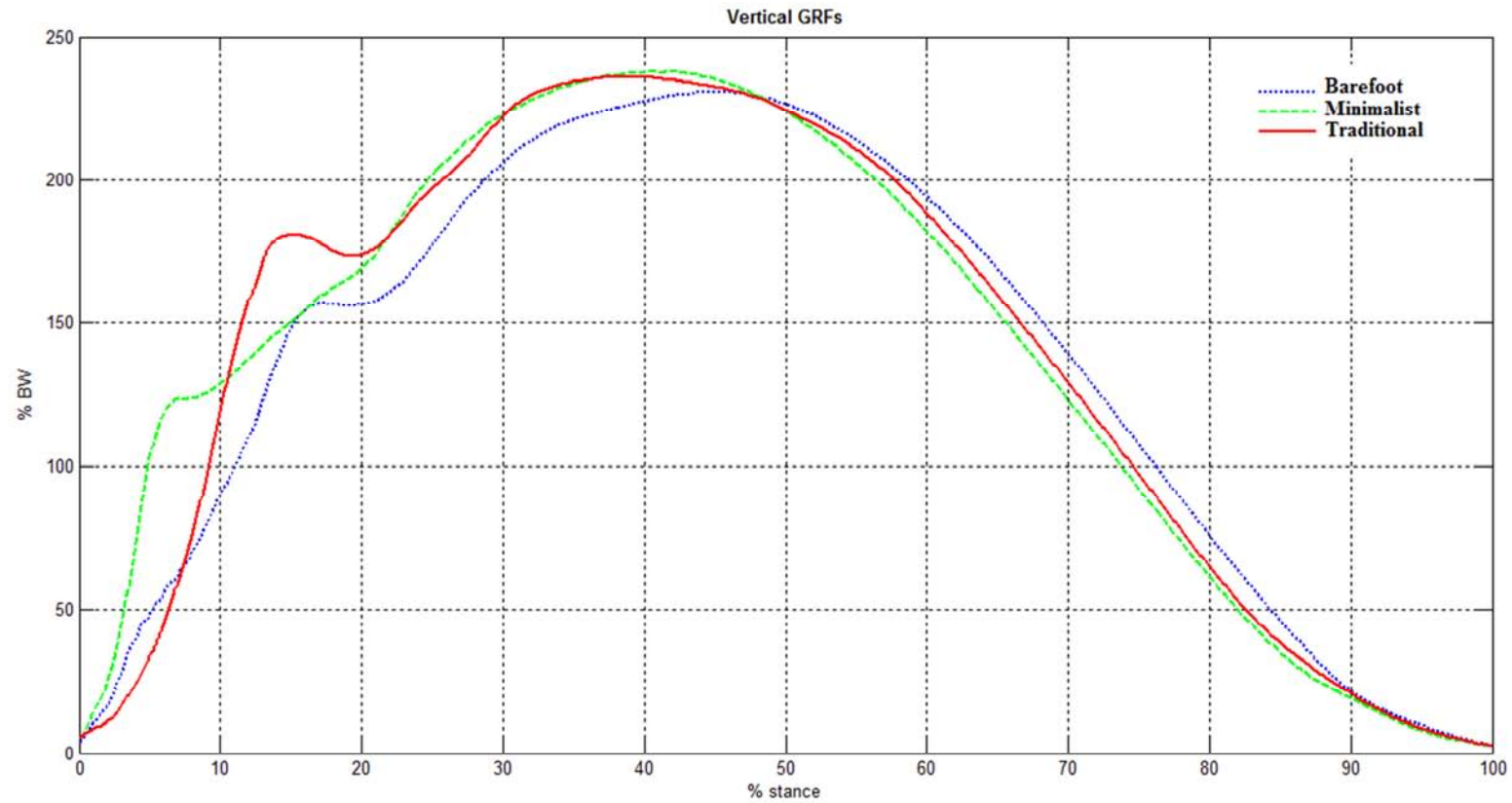


Figure 2.12. Average vertical GRFs for barefoot (dotted blue line), minimalist (dashed green line) and traditional (solid red line) running styles. Data are shown as percentage of the stance phase and of the body weight (BW).

To quantitatively compare the different running styles, some features of interest related to the vertical force component have been calculated and reported in Table 2.2.

Table 2.2. Comparison of parameters related to the vertical GRF for the three running styles.

	Barefoot	Minimalist	Traditional
Impact peak [%BW]	156.5	138.7	184.7
Time to impact peak [% stance]	16.1	6.7	14.8
Active peak [% BW]	232.6	237.7	236.1
Time to active peak [% stance]	43.8	41.8	39.2
Vertical loading rate [BW/stance]	9.3	20.6	15.5

Despite several studies concerning GRFs being available, just few of them can be taken into consideration when making a comparison with the obtained data since maximum and minimum values are velocity dependent (Novacheck, 1998).

As previously mentioned (section 1.4.1), the vertical loading rate provides a measure of how the shock is absorbed from initial contact. Minimalist running shows the highest vertical loading rate (20.6 BW/stance), highlighting the fact that it is the running style with the poorest shock absorption. This may derive from a combination of poor shoes shock absorbency and poor function of the ankle/knee joints (Richards, 2008). On the other hand, barefoot running seems to have the greatest shock absorption (vertical loading rate of 9.3 BW/stance), proving a complete function of the ankle and knee joints and attenuating the risk of plantar fasciitis (Tam et al., 2014). The low vertical loading rate value is therefore related to the forefoot strike pattern and it is in accordance with Richards (2008) who depicted an increase of vertical loading rate from forefoot strike to rearfoot strike runners.

Also the impact peak relates to shock absorbency characteristics (section 1.4.1). Previous studies (Cavanagh and Lafortune, 1980, Richards, 2008, Novacheck, 1998) reported an increase of the impact peak values from forefoot to rearfoot strike runners. In particular, forefoot strike runners were generally characterized by a not discernable or very small impact peak value while rearfoot strike runners showed the largest and most discernable peak. This feature can be confirmed in the present study since the impact peaks are slightly recognizable in barefoot and minimalist running but clearly

discernable in traditional running (Figure 2.12). In addition, traditional running reports the highest peak value (184.7 %BW), potentially increasing the risk of stress fractures of the tibia and the occurrence of patellofemoral pain (Tam et al., 2014). The obtained data agree also with De Wit et al. (2000), which reported smaller impact peak values for barefoot runners in comparison to shod runners. In detail, impact peak magnitudes from De Wit et al. (2000) and the present study generally agree for a similar running speed (3.5 m/s). Shod and barefoot running were in fact characterized by an impact peak of 190 %BW (184.7 %BW in the current study) and 180 %BW (156.5 %BW in the current study) respectively. Minimalist running shows an anomalous behavior, having the lowest impact peak value (138.7 %BW) and the shortest time to peak (6.7 %stance). The low peak value highlights the fact that the runner was not hitting harshly the ground and it is clearly related to the strike pattern. The short impact time may be related to a stiff-legged run (Tongen and Wunderlich, 2010). In addition, the poor repeatability in maintaining the same strike pattern found in section 2.6 for this running style can be confirmed looking at GRFs plot. In the region corresponding to the minimalist foot strike (5-10 % of the stance phase) the SD is quite large (maximum value of 30.5% BW) in comparison to the other styles (maximum values of 24.6% and 21.7% BW for barefoot and traditional running respectively in their foot strike region).

Furthermore, impact peak and step length were shown to be related (Mercer et al., 2001, Altman and Davis, 2012). Longer stride lengths is correlated to an impact peak growth and, consequently, to an increase of the risk of running injuries (Schubert et al., 2013). This evidence can be confirmed in this study since a longer step length in traditional running ($1.22 \pm 0.12\text{m}$) in comparison to barefoot ($1.12 \pm 0.05\text{ m}$) and minimalist ($1.15 \pm 0.05\text{m}$) running is related to a higher peak impact force (184.7 %BW).

The trough after the impact peak is barely noticeable in barefoot and minimalist running as a consequence of the ankle dorsiflexion movement instead of plantarflexion which derives from a forefoot strike pattern (Richards, 2008).

Concerning the magnitude of the active peak, no significant differences are discernible between the three running styles (p values > 0.05). However, barefoot running has the lowest active peak (232.6 %BW), in accordance with Cavanagh (1980) and De Wit (2000). This proves that the deceleration of the body downward is smaller during barefoot running.

The obtained values are slightly lower than those found in literature (De Wit et al., 2000, Cavanagh and Lafortune, 1980) but this may depend on a small difference in the running speed (3.5 m/s in literature, average of 3.3 m/s in the current study) since the active peak considerably depends on running speed (Richards, 2008).

Figure 2.12 shows a qualitative comparison of the anteroposterior ground reaction force for the three running styles. From Figure 2.13 it is clearly visible that minimalist running reports the largest posterior impact peak. This is conflicting with the literature (Richards, 2008) since the largest peak is expected to derive from rearfoot strikers, having these runners the highest vertical impact peak.

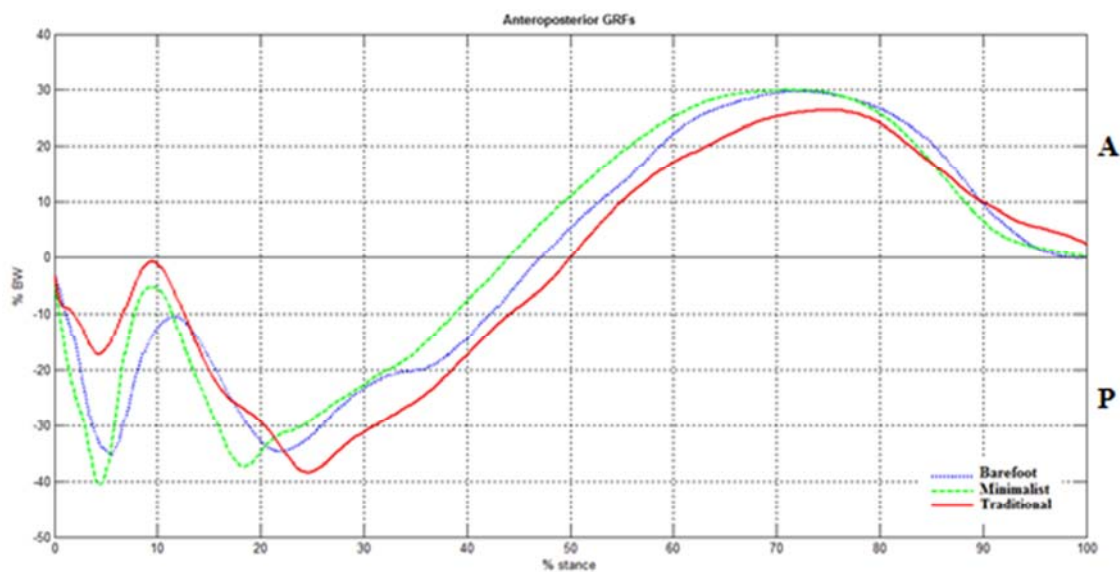


Figure 2.13. Average anteroposterior GRFs for barefoot (dotted blue line), minimalist (dashed green line) and traditional (solid red line) running styles. Data are shown as percentage of the stance phase and of the body weight (BW).

According to Richards (2008), no relevant differences are perceptible in the amplitude of the maximum posterior braking force (between 34 and 40 %BW) and the maximum anterior thrusting force (31-32 %BW) between the different running styles.

The point when the force reduces to zero, which corresponds to midstance, occurs for all the styles slightly before half the stance time (from 44 to 49 %stance).

Braking and thrusting impulses have been computed calculating the area under the anteroposterior force graph. The net impulse is negative for barefoot (-20.1) and traditional (-161.7) running, showing that the person was slowing down. On the other

hand, net impulse is positive in minimalist running proving that the subject was speeding up (Richards, 2008).

In Figure 2.14 the average values of the mediolateral ground reaction force are reported for the three running styles.

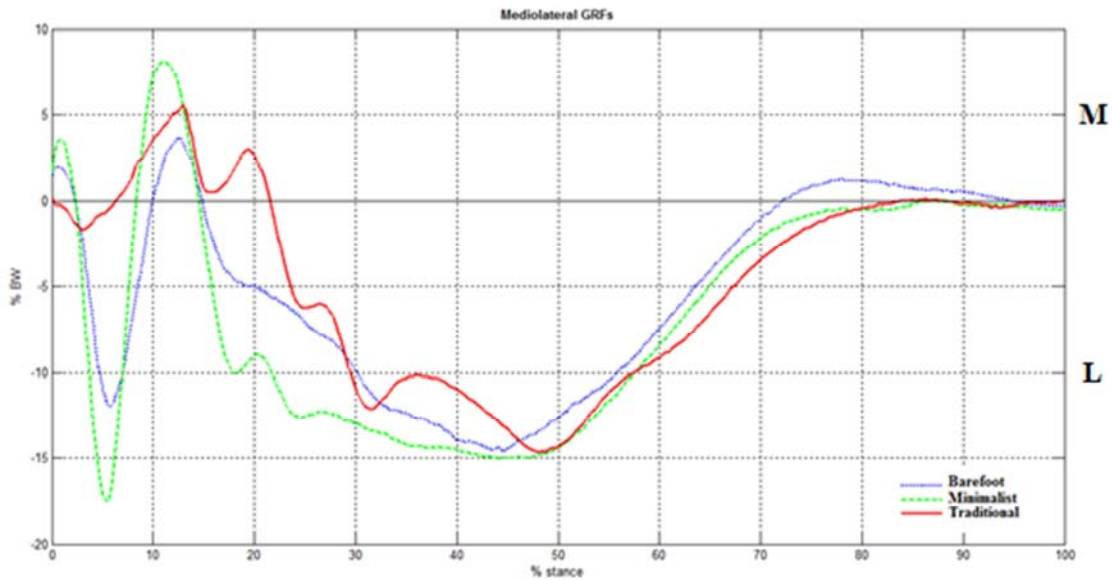


Figure 2.14. Average mediolateral GRFs for barefoot (dotted blue line), minimalist (dashed green line) and traditional (solid red line) running styles. Data are shown as percentage of the stance phase and of the body weight (BW).

The most notable difference is the magnitude of the lateral impact force in minimalist running (17.2%BW), considerably higher than the other running styles (10.8%BW for barefoot and 1.41% for traditional running). This leads to the observation that the subject was supinating during the initial impact while wearing minimalist shoes. Being also the medial peak highest in minimalist running (8.07%BW, towards 3.13%BW for barefoot and 5.6%BW for traditional running), it is possible to affirm that minimalist shoes allows the subject to more freely supinate or pronate during stance. All these findings, which highlight an abnormal behavior during minimalist running, lead to the hypothesis that the subject was not able to run properly while wearing minimalist shoes. This hypothesis may provide an explanation to the fibula stress fracture reported by the subject when he moved to minimalist running (Sheikh-Warak, 2012). The current hypothesis will be analyzed in the following chapters.

CHAPTER 3

Musculoskeletal modelling

3.1 Introduction

Movement science is driven by empirical observation. However, observation alone cannot completely clarify movement dynamics. First of all, some relevant variables, such as the forces generated by muscles, are generally not measurable in a non invasive way. Secondly, it is difficult to elucidate cause-effect relationships in complex systems considering experimental data alone. Recently, the introduction of musculoskeletal modelling and simulation, together with experiments, enabled researchers to uncover the principles that drive the muscle coordination, to establish the influence of neuromuscular impairments on abnormal movements and to predict the functional consequences of treatments (Delp et al., 2007). Moreover, musculoskeletal modelling provides scalable, reusable, transferable and reproducible models (Seth et al., 2011), allowing the biomechanical community to exchange, analyze and improve simulations.

A brief description of the software used in the current study for the development of musculoskeletal model (OpenSim) and its main functionalities will be introduced in this chapter. After that, the adopted model will be described, with particular focus on bone, joint and muscle representation. The first step in the biomechanical analysis, that is scaling, will then be presented. Scaling functionalities and the choice of the required parameters will be discussed, followed by the description of some adopted adjustments. Finally, a section concerning the evaluation of the scaling results will be included.

3.2 OpenSim

In the early 1990s, Delp worked on computer-assisted surgery (Delp et al., 1990) to evaluate the muscle length in children affected by cerebral palsy and to make physicians aware of the consequences of some treatment choices. The idea of building a musculoskeletal model in a software environment was born exactly from this

experience. Then, this idea evolved in a commercial software (Delp and Loan, 1995) and almost twenty years later OpenSim was released (Delp et al., 2007). The first OpenSim version was introduced at the American Society of Biomechanics Conference in 2007. OpenSim is an open-source platform which allow to build musculoskeletal models, simulate movement and analyze resulting behaviors (Seth et al., 2011, Delp et al., 2007). Furthermore, the biomechanics community can build on the platform a library of simulations which can be exchanged, tested, analyzed and improved through external collaborations. The OpenSim libraries are written in C++ and they are accessible through an object-oriented API.

An end-user graphical interface (GUI) provides access to the main functionalities (Figure 3.1).

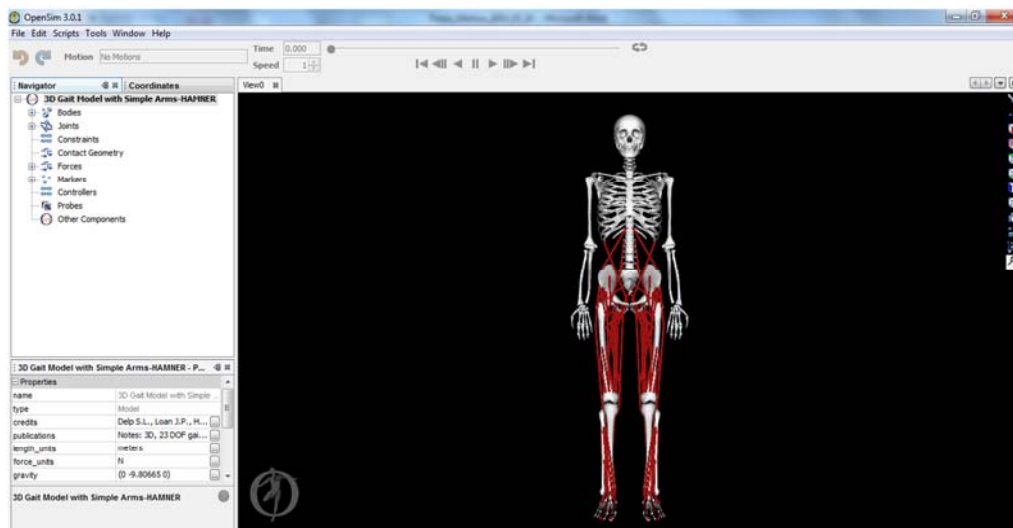


Figure 3.1. Screenshot from OpenSim 3.0. Whole body 23-degree-of -freedom musculoskeletal model (Hamner, 2010). Muscles are shown as red lines.

As previously mentioned, OpenSim enables to perform advanced biomechanical analyses, in particular:

1. Scaling;
2. Inverse kinematics;
3. Inverse dynamics analysis;
4. Static optimization;
5. Computed Muscle Control;
6. Forward dynamics analysis.

However, only the first four tools will be taken into account in the present study.

The scaling tool adjusts the anthropometry of a model to match patient-specific measurements. The inverse kinematics (IK) tool solves joint coordinates from available spatial marker positions which correspond to specific body landmarks. The inverse dynamics (ID) analysis determines the set of generalized forces (for example torques and net forces) associated with each movement. Finally, *static optimization* tool decomposes net generalized forces amongst individual muscle forces at each time instant. Each tool will be introduced and explained in detail in the following sections.

3.3 Model description

The model adopted in the current study is a full-body OpenSim model used by Hamner et al. (2010) to create a muscle-actuated simulation of running. Muscle geometries from Delp et al. (1990) are included in the lower extremity model while idealized torque actuators at each degree of freedom (DOF) describe the upper-extremity (SimTK, 2011). However, some adjustments were applied to adapt the preexisting model to the present case study. The adjusted model has 29 degrees of freedom.

3.3.1 Bone, joint and muscle representation

Several elements with a specific representation compose OpenSim models. These components are mainly *bones*, *joints* and *muscles*.

The utilized model presents bones that are represented as twenty rigid bodies, as shown in Figure 3.2.

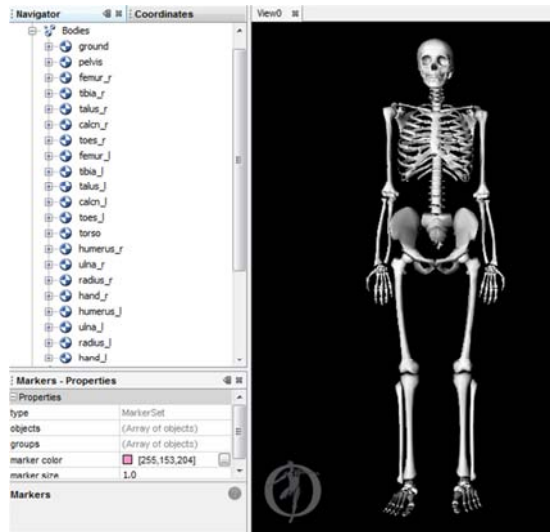


Figure 3.2. Bones representation in the OpenSim model. The list of the bodies is visible in the Navigator panel (left).

The lower extremity has been modeled as six rigid-body segments: pelvis, femur, tibia, talus, calcaneus and toes. Each segment has its own fixed reference frame and a joint reference system (Seth et al., 2010).

After defining rigid bodies, the relationship between those bodies needs to be defined. A joint establishes the kinematic relationship between two frames each attached to a rigid body, called respectively the parent body (P) and the child body (B) (Figure3.3).

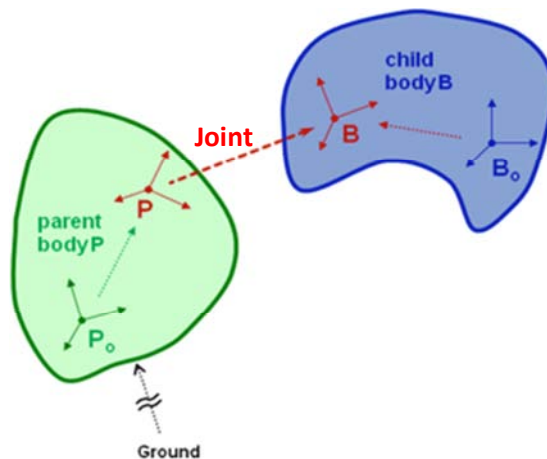


Figure 3.3. Joint definition in OpenSim. The joint (red dashed line) defines the kinematic relationship between two frames (B and P) each affixed to a rigid-body (the child B and the parent P). Figure adapted from Seth et al. (2010).

Each arm has five degrees of freedom. In fact, the shoulder is modeled as a ball-and-socket joint with three degrees of freedom while the elbow and the forearm are each

modeled with a revolute joint with one degree of freedom (Holzbaur et al., 2005). However, being the biomechanical analysis of running the aim of this study, only the lower extremity joints will be introduced in detail.

The lumbar motion is represented as a ball-and-socket joint, while the pelvis has three degrees of freedom with respect to ground: pelvic tilt, obliquity and rotation (Anderson and Pandy, 1999). Each lower limb consists of five degrees of freedom; being the hip designed as a ball-and-socket joint it presents three degrees of freedom: flexion/extension (ROM: 120° flex; -120° ext), adduction/abduction (ROM: 120° add; -120° abd) and internal/external rotation (ROM: 120° int; -120° ext). The knee and the ankle are modeled as hinge joints (Figure 3.4) have only one degree of freedom each: flexion/extension movements (ROM: -120° flex; 10° ext) and dorsi/plantar flexion movements (ROM: 90° dorsiflex; -90° plantarflex) respectively.

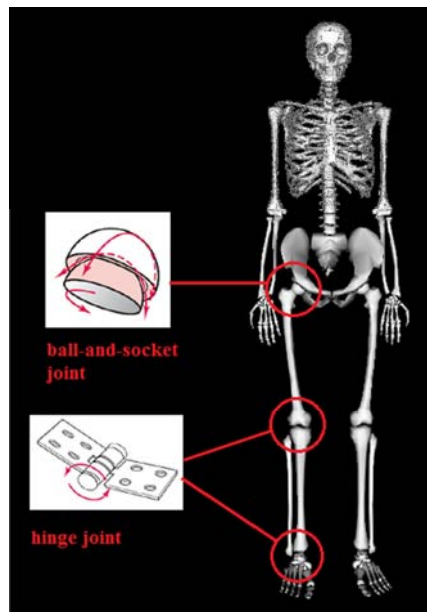


Figure 3.4. Hip, knee and ankle joints representation in the adopted OpenSim model.

In details, the knee is modeled as a one degree of freedom custom joint. The knee in fact does not operate as a simple pin, because of the rolling and sliding of the ellipsoidal femoral condyles on the tibia plateau (Yamaguchi and Zajac, 1989). The modeled tibia has one rotational degree of freedom (θ) but it translates in the plane of rotation (x, y) with respect to the femur (Figure 3.5) . This translation is a function of the knee flexion angle.

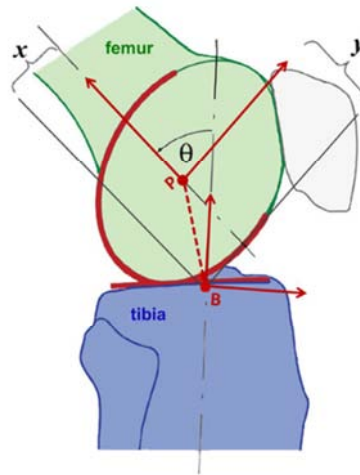


Figure 3.5. Schematic of the knee joint (Seth et al. 2010). The femur represents the parent body (P) and the tibia the child body (B). The tibia has one rotational degree of freedom (θ) but it translates in the (x, y) plane with respect to the femur.

On the other hand, the ankle joint is modeled as a one degree of freedom frictionless revolute (Delp et al., 1990).

Finally, the model includes 92 musculoskeletal actuators of the lower limbs and torso. Muscle lines of action are represented by a straight line approach (Figure 3.1). For the purposes of this investigation, the following muscle parameters were considered:

- Muscle isometric force (F_{ISO})
- Optimal length of the muscle (L_0)

PCSA is defined (Klein Horsman et al., 2007) as the ratio between the muscular volume and the fibre length:

$$PCSA = \frac{Vol}{L_{FIB}} \quad (3.1)$$

Being the maximum muscle tensile stress:

$$\sigma_{MAX} = \left(\frac{F_{ISO}}{PCSA} \right)_{L_{OPT}} \quad (3.2)$$

and

$$F_{ISO} = \sigma_{MAX} \left(\frac{Vol}{L_{FIB}} \right) \quad (3.3)$$

the maximum isometric force for the current model has been calculated from measured PCSA (Wickiewicz et al., 1983, Friederich and Brand, 1990) and from a specific maximum tensile stress of 61 N/cm² (simtk-confluence.stanford.edu) for all muscles. The latter value was slightly increased from magnetic resonance results (11-47 N/cm²) (Fukunaga et al., 1996) to compensate for age-related muscle atrophy.

3.4 Scale tool

Scaling a generic musculoskeletal model allows to modify the anthropometry of the generic model so that it matches the anthropometry of a specific subject. Scaling represents a preliminary step to solving inverse kinematics and inverse dynamics problems because these solutions are considerably sensitive to the accuracy of scaling (Scheys et al., 2011). Furthermore, previous investigations (Scheys et al., 2008, Arnold et al., 2006, Duda et al., 1996) showed that parameters related to musculoskeletal geometry, such as muscle-tendon and moment-arm lengths, and to muscle-tendon dynamics, such as muscular force, are significantly affected by individual musculoskeletal geometry. Subject-specific models are therefore essential to obtain reliable simulations.

The scale tool consists of two fundamental steps: scaling and marker placement. The scaling step scales both the mass properties and the dimensions of the body segments, geometrically adapting the generic model to the subject-specific model. On the other hand, the marker placement step defines which of the markers are representative of the referential pose of the model. During this step, an inverse kinematics algorithm is applied to place the scaled model in the referential pose and then all the markers are rearranged. The latter step is particularly useful in the presence of clusters of markers.

3.4.1 How to use the scale tool

The required inputs and outputs for the scaling tool are shown in Figure 3.6. Both experimental data, OpenSim and setting files are necessary. All the mentioned files were generated either using the OpenSim GUI or the free source code editor Notepad++. Each file will be briefly described in the following paragraphs.

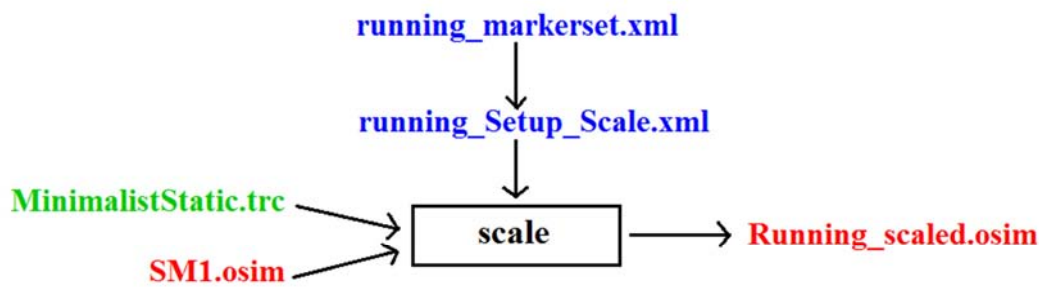


Figure 3.6. Inputs and Outputs of the Scale Tool. Experimental data are shown in green; OpenSim files in red and settings files in blue.

The `running_markerset.xml` file contains the list of the 46 markers used in the study. The three markers located on the head were discarded since a specific body for the head was not defined and the torso can be more accurately defined from the markers placed on the sternum, C7 and on the acromia. In addition, the file displays also the location of each marker and the body on which it resides.

The `running_Setup_Scale.xml` file contains the mass of the subject which was precisely computed using btk functions in Matlab from a static trial, while the subject was standing on the platform. Knowing the subject mass is fundamental since the scaled model will match that value. Furthermore, the definition of the scale method is required in this file. Scaling can be in fact performed using two methods:

- *measurement-based scaling*, which compares distance measurements between specific landmarks on the model (virtual markers) and the corresponding experimental marker position;
- *manual scaling*, which is normally adopted when suitable marker data are not available and allows to scale a segment based on some factors calculated outside OpenSim.

In the current study measurement-based scaling method was chosen. Experimental marker positions provided in a static `.trc` file were used to determine scale factors. A single scale factor was computed using one or more marker pairs. The marker pairs for each measurement (shown in Figure 3.7) were chosen aiming to capture as reliably as possible the subject's anthropometry.

Body Name	Measurement(s) Used	Applied Scale Factor(s)
ground	Unassigned	1.0
pelvis	pelvis	1.182990
femur_r	thigh	1.015194
tibia_r	shank	1.038094
talus_r	foot	1.147655
calc_r	foot	1.147655
toes_r	foot	1.147655
femur_l	thigh	1.015194
tibia_l	shank	1.038094
talus_l	foot	1.147655
calc_l	foot	1.147655
toes_l	foot	1.147655
torso	torso	0.994561
humerus_r	arm	1.088956
ulna_r	forearm	1.054132
radius_r	forearm	1.054132
hand_r	Unassigned	1.0
humerus_l	arm	1.088956
ulna_l	forearm	1.054132
radius_l	forearm	1.054132
hand_l	Unassigned	1.0

Figure 3.7. Scale factors for each body segment deriving from the measurement-based scaling.

For example, consider the two marker pairs used to define the thigh segment: the first pair is composed by RightASIS and R_Lat_Fem_Epic and the second pair by LeftASIS and L_Lat_Fem_Epic (Figure 3.8).

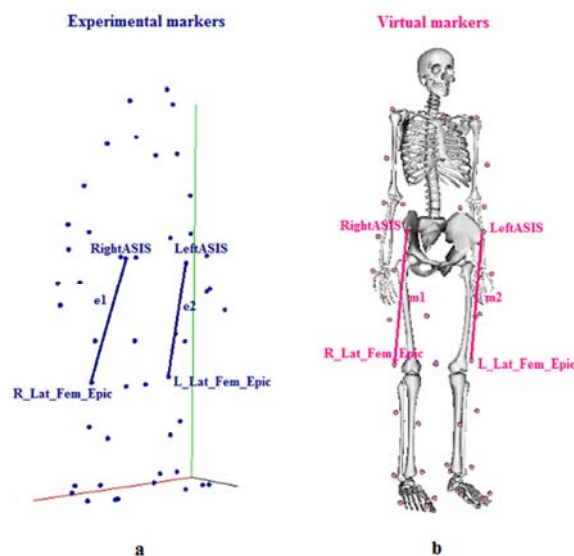


Figure 3.8. Experimental markers (blue) detected using motion capture. Virtual markers (pink) placed on the model in anatomical correspondence. Distances between experimental markers (e_i) relative to the distances between corresponding virtual markers (m_i) were used to obtain scale factors.

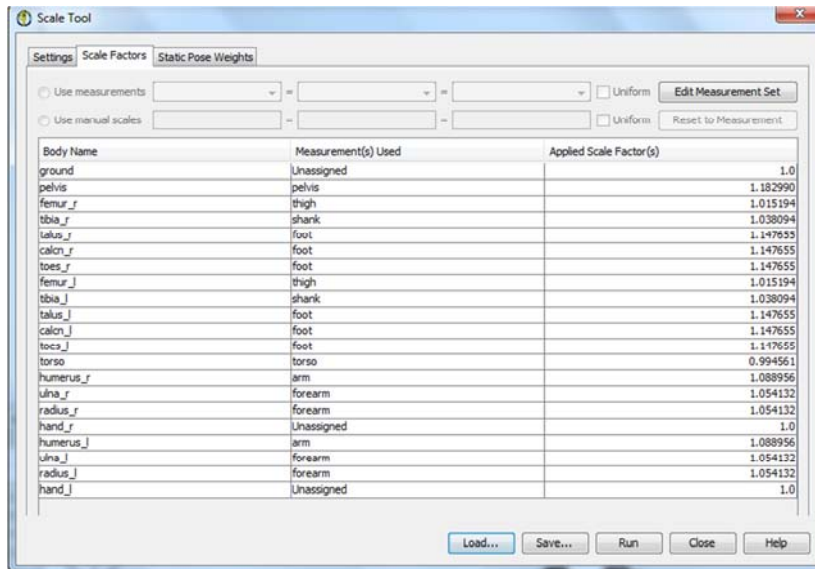
The scale factor (s_1) deriving from the first pair was computed as the ratio between the distance e_1 of the experimental markers position (Figure 3.8a) and the distance m_1 between the corresponding markers in the model (Figure 3.8b), resulting in:

$$s_1 = e_1/m_1 \quad (3.4)$$

Having more than one pair of markers, the overall scale factor (s) was computed as the average of the scale factors calculated for both of the pairs:

$$s = (s_1 + s_2)/2 \quad (3.5)$$

where s_2 was the scale factor due to the second pair. The scale factor was therefore used to scale the size of the body segments and, at the same time, the masses of the segments were adjusted to match the specified subject mass. The scale factors for each body segment resulting from the measurement-based scaling are shown in Figure 3.9.



Body Name	Measurement(s) Used	Applied Scale Factor(s)
ground	Unassigned	1.0
pelvis	pelvis	1.182990
femur_r	thigh	1.015194
tibia_r	shank	1.038094
talus_r	foot	1.147655
calcan_r	foot	1.147655
toes_r	foot	1.147655
femur_l	thigh	1.015194
tibia_l	shank	1.038094
talus_l	foot	1.147655
calcan_l	foot	1.147655
toes_l	foot	1.147655
torso	torso	0.994561
humerus_r	arm	1.088956
ulna_r	forearm	1.054132
radius_r	forearm	1.054132
hand_r	Unassigned	1.0
humerus_l	arm	1.088956
ulna_l	forearm	1.054132
radius_l	forearm	1.054132
hand_l	Unassigned	1.0

Figure 3.9. Scale factors for each body segment deriving from the measurement-based scaling.

The running_Setup_Scale.xml file also includes a section regarding marker placement where parameters for placing markers on the scaled model are specified. Virtual markers were moved to match experimental marker position for the generalized coordinate values calculated in a static pose with the average marker positions. Marker and coordinate weights establish how strongly the algorithm should try to match them (simtk-confluence.stanford.edu). This represents an inverse kinematics (IK) algorithm and it is based on the solution of the weighted least square problem defined as:

$$\min_q \left[\sum_{i \in \text{markers}} w_i \|x_i^{exp} - x_i(q)\|^2 \right] \quad (3.6)$$

where q is the vector of generalized coordinates, x_i^{exp} is the experimental position of the i^{th} marker and $x_i(q)$ is the position of the corresponding marker on the model, dependent on the coordinate values (Lu and O'Connor, 1999). Marker's weight w_i is normally high if associated with a marker placed in a reliable position with negligible skin movement, whereas it has a low value otherwise. A simple analogy can describe the effect of marker weights on IK. It is possible to think that the subject involved in the experimental trials had some springs attached between the virtual and the experimental markers. The stiffness of the spring specifies the weight that has to be assigned to the cost function (3.6). The higher the stiffness (weight), the lower the marker displacement, and viceversa, the lower the stiffness, the higher the marker displacement. Following these guidelines, markers located on the pelvis (ASIS and PSIS) display the highest weight (100) because they need to be the most accurate ones, since the model is a kinematic chain which originates from the pelvis. The pelvis represents the mean of connection between the model and the global reference system (gait lab). Also, higher weight was attributed to markers located on the lateral portion of the body with respect to those located on the medial portion. In fact, empirical observations and previous investigations (Lu and O'Connor, 1999, Cappozzo et al., 1996) showed that markers placed on the lateral side of the body are supposed to exhibit smaller artefact movements with respect to those attached to the medial side. Secondly, technical markers, which are the ones not placed in correspondence of bony landmarks, need to be discarded. In fact, the weight of some technical markers (Ant_Humerus, Forearm, Hand, Post_Femur, Ant_Femur, Post_Tibia, Ant_Tibia, BigToe) was fixed equal to zero. These markers will be automatically replaced after the inverse kinematics step. However, it has to be kept in mind that the number of the markers specified in the IK step need to be at least equal to the number of degrees of freedom of the body where the markers are attached with respect to the parent body. The adopted marker weights are reported in Table 3.1:

Table 3.1. Weight assigned to each marker.

marker	weight	marker	weight
R_Acromion	30	L_Ant_Femur	0
L_Acromion	30	L_Med_Fem_Epic	25
C7	0	L_Lat_Fem_Epic	30
Sternum	20	R_Post_Femur	0
R_Ant_Humerus	0	R_Ant_Femur	0
R_Med_Humerus	20	R_Med_Fem_Epic	30
R_Lat_Humerus	36	R_Lat_Fem_Epic	32
R_Forearm	0	L_Post_Tibia	0
R_Med_Forearm	25	L_Ant_Tibia	0
R_Lat_Forearm	30	R_Post_Tibia	0
R_Hand	0	R_Ant_Tibia	0
L_Ant_Humerus	0	L_Med_Malleolus	20
L_Med_Humerus	24	L_Lat_Malleolus	44
L_Lat_Humerus	30	R_Med_Malleolus	20
L_Forearm	0	R_Lat_Malleolus	30
L_Med_Forearm	20	L_Heel	38
L_Lat_Forearm	30	L_5thMetatarsal	10
L_Hand	0	L_1stMetatarsal	20
RightASIS	100	L_BigToe	0
LeftASIS	100	R_Heel	30
RightPSIS	100	R_5thMetatarsal	10
LeftPSIS	100	R_1stMetatarsal	10
L_Post_Femur	0	R_BigToe	0

The scaling step is an iterative process and it requires some adjustments to obtain admissible results. As previously mentioned (section 3.4), the accuracy of the scaling procedure is fundamental to perform reliable inverse kinematics and inverse dynamics operations. At the end of the scaling procedure, the messages window displays two error values: the maximum error for bony landmarks and the root mean square (RMS) error of the inverse kinematics step performed. According to the OpenSim best practices (simtk-confluence.stanford.edu) results deriving from scaling are considered meaningful if the maximum error for bony landmarks and RMS error are less than approximately 2 cm and 1 cm respectively.

Apart from assigning different weights to the markers, other expedients were adopted to achieve considerably low error values. For example, the position of some markers in the model was slightly changed to match more accurately the real configuration. Especially, because of the subject's particularly muscular thigh, the most relevant changes in the marker positions were made in correspondence to the medial femoral epicondyle. Moreover, another reason to slightly adapt the position of the markers in the model is that the dimension of the markers adopted in the experimental trials was larger (25mm diameter) (Sheikh-Warak, 2012) than the size of the markers normally adopted in gait analysis (14mm) (Kirtley, 2006). Despite the fact that having larger markers provides

more reliability during motion capture (Page et al., 2006), it leads to some inaccuracies during scaling.

Additionally, since the maximum error occurred steadily in correspondence to the markers located on the forearm or on the hand, the wrist deviation degree of freedom was locked. In this way, the number of degrees of freedom of the hand with respect to the forearm was reduced and the error slightly decreased. Furthermore, the maximum value of the pronation of the forearm was increased from 90° to 180° to allow a free movement of the forearm, without any constraints. Consequently, markers placed on the hand acquired a more accurate position. Moreover, the subtalar and metatarsophalangeal joints were locked having assigned a prescribed value of 0° to them.

After adopting all these expedients, the final errors resulted in:

- Max error = 2.4 cm (L_Lat_Malleolus);
- RMS error = 1.9 cm.

The obtained results are slightly higher than the recommended values. This can be due to the fact that an high number of markers were used in the current study, therefore the minimization of the error results more difficult.

CHAPTER 4

Kinematic and kinetic analysis of running

4.1 Introduction

A common methodology for analyzing a movement is to evaluate its kinematics and kinetics. As previously detailed, kinematics describes the considered movement without considering the causing forces. On the other hand, kinetics studies the forces responsible for that movement. To achieve this aim, OpenSim provides two different analyses: the Inverse Kinematics (IK) tool and Inverse Dynamics (ID) analysis. Using a properly scaled model, it is possible to compute joint angles through IK that best reproduce the subject's motion. ID then uses kinematic measures together with measured external forces (e.g. GRFs) to compute net joint moments. An overview of the IK and ID problems is represented in Figure 4.1.

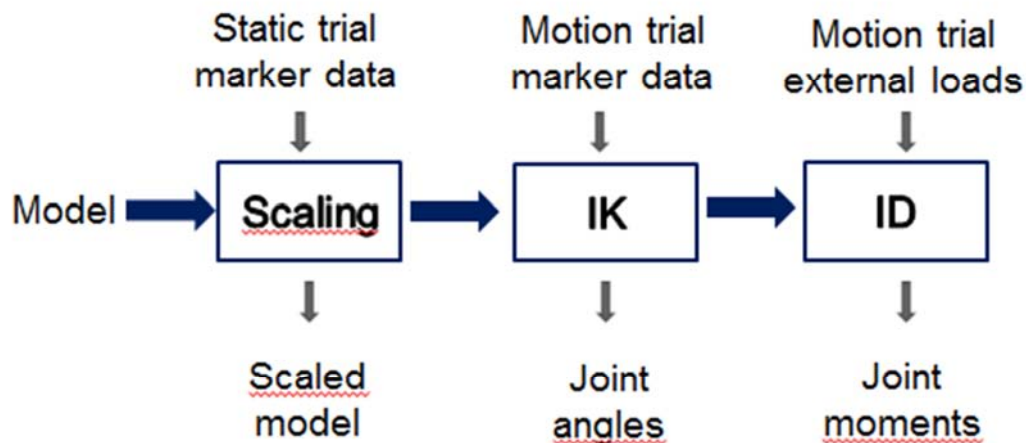


Figure 4.1. Schematic of the IK and ID analysis.

IK and ID algorithms will be individually described in this chapter. Furthermore, a comparison between joint angles, joint moments, joint angular velocity and joint power in the three different running styles will be provided.

4.2 Inverse kinematics analysis

It has been shown (Lu and O'Connor, 1999) that traditional methods used to describe the body kinematics do not produce reliable results, especially in evaluating frontal and transverse plane components, due to marker skin movement artefacts. In fact, in the traditional methods joints are misplaced since each body segment is considered individually without any joint constraints.

In OpenSim, an inverse kinematics (IK) tool based on a global optimization method is adopted. Effectively, the determination of the poses (position and orientation) of the body segments is based on the minimization of the total error (sum of distances) between measured and model-determined marker positions. Furthermore, joint constraints are imposed by the model. However, the introduced IK tool assumes that a good model which describes the kinematic system is available. Therefore, the importance of having a model appropriately scaled is highlighted again. In this way, the model is maintained constant and only the coordinates are moved.

4.2.1 How inverse kinematics works

IK tool analyses each frame of experimental data and arranges the model in a pose that best matches experimental marker and coordinate data for that instant (Lund and Hicks, 2014). The variation of the joint angles, described by the generalized coordinates, during the motion allows the model markers to match the experimental markers (Figure 4.2) .

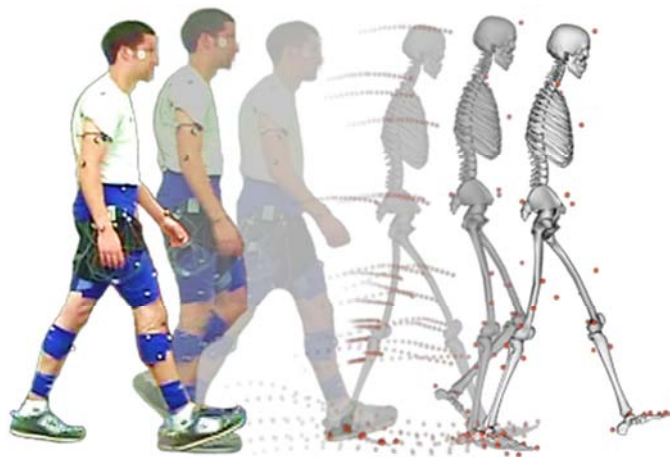


Figure 4.2. IK tool overview. Experimental skin marker (white ones on the left) are matched by model markers (pink ones on the right) by varying the joint angles during the motion. Figure from simtk-confluence.stanford.edu.

Mathematically speaking, the solution which best matches experimental markers is expressed by a weighted least squares problem (which has been briefly introduced in section 3.4.1). This problem can be formulated as follows (Hicks and Dembia, 2013):

$$\min_q \left[\sum_{i \in \text{markers}} w_i \|x_i^{\text{exp}} - x_i(q)\|^2 \right] \quad (4.1)$$

where q represents the vector of generalized coordinates, x_i^{exp} is the experimental position of the i^{th} marker, $x_i(q)$ indicates the position of the corresponding marker on the model and q_j^{exp} is the experimental value for the j^{th} coordinate.

The required inputs and outputs for the IK tool are shown in Figure 4.3. Both experimental data, OpenSim and setting files are necessary. All the mentioned files were generated either using the OpenSim GUI or Notepad++. Each file will be briefly described in the following paragraphs.

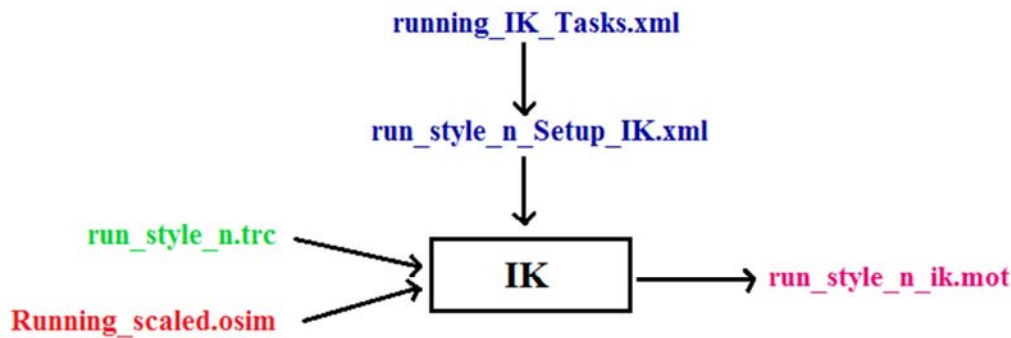


Figure 4.3. Inputs and Outputs of the IK Analysis. Experimental data are shown in green, OpenSim files in red and settings files in blue. The output is a motion file (fuchsia).

The `running_IK_Tasks.xml` file contains the marker weightings to be used in the analysis. The weights of the markers held steady with respect to those defined during scaling procedure. However, all the technical markers which were not considered during scaling because of their not fundamental role in computing the static pose were introduced. A low weight equal to five was assigned to each of them (Ant_Humerus, Forearm, Hand, Post_Femur, Ant_Femur, Post_Tibia, Ant_Tibia, BigToe). The `run_style_n_Setup_IK.xml` file contains the model to which the IK solver is applied and the specific trial, expressed as a `.trc` file, to be used by the solver. Moreover, a time range was defined. This time interval should correspond to the duration of the selected part of the trial (from left toe off to left heel strike), hence a time range of 6 seconds was defined as upper limit. The constraint weight was increased from 20 to Infinity to

strictly enforce the constraints. In addition, the accuracy of the solution was settled to $1e^{-9}$. The last two expedients were adopted to obtain smooth and few noisy results. Nevertheless, these choices have the disadvantage of making the simulations slower.

4.2.2 IK adjustments and evaluation of the results

As well as the scaling step, also the IK step needed some adjustments to obtain admissible results. In this case, the accuracy of inverse kinematics results is essential for using static optimization.

IK activity records were written into .log files using a LogReader.m file provided by Luca Modenese. This MatLab file enabled to read the IK logs and extract information otherwise just printed on the messages window. This code was particularly useful to display the maximum error obtained while computing IK and the marker to which it was associated. Using this file, the accuracy of the c3d post-processing procedure was checked. Moreover, having several trials, this file allowed to easily compute average error values, for example within the same running style and, therefore, to evaluate the results.

While running IK it was noticed that the maximum error, representing the maximum distance (meters) between an experimental marker and its correspondent model marker at a specific instant, always occurred at the marker placed on the big toe, either left or right. The error was considerably larger during barefoot session (0.080 ± 0.007 m) than during minimalist (0.059 ± 0.007 m) and traditional (0.054 ± 0.007 m) sessions. The reported values are not surprising since the big toe is expected to move freely while running barefoot, whereas it is constrained by the shoes during shod running, while the model had a single-segment foot.

Results deriving from IK are considered meaningful if the maximum marker error and the RMS error are less than 2-4 cm and 2 cm respectively. Therefore, by only comparing the obtained maximum marker errors with the recommended ones the results were not satisfactory. Trying to obtain admissible errors, two possible solutions were adopted and compared. The first one consisted in discarding the marker located on the big toe, imposing a weighting factor equals to zero. In effect, the big toe was not necessary in the definition of the movement of the foot, since other three markers were

placed on it. However, the limitation of this choice is that, during simulations, the foot was seen to penetrate the ground, but simulations were not affected.

The second option consisted in adding a degree of freedom to the model unlocking the metatarsophalangeal joint. In this case the flexion/extension movement of the toes was allowed. The model marker positioned on the big toe was therefore expected to match more closely the correspondent experimental marker because of the more realistic movement of the foot.

The errors obtained from the three approaches are shown in Table 4.1.

Table 4.1. Comparison between the errors obtained from three different IK analyses for barefoot, minimalist and traditional sessions.

Barefoot				
	Max error	Mean error range	SD range	RMS range
Original model	0.080	0.054-0.057	0.005-0.009	0.020-0.024
Imposing weight of the big toes = 0	0.052	0.040-0.042	0.005-0.006	0.018-0.022
Including mtp joint	0.080	0.054-0.057	0.005-0.009	0.019-0.024
Minimalist				
	Max error	Mean error range	SD range	RMS range
Original model	0.059	0.041-0.043	0.006-0.008	0.017-0.022
Imposing weight of the big toes = 0	0.054	0.040-0.042	0.006-0.008	0.017-0.020
Including mtp joint	0.059	0.041-0.043	0.006-0.008	0.017-0.022
Traditional				
	Max error	Mean error range	SD range	RMS range
Original model	0.054	0.038-0.041	0.006-0.008	0.017-0.023
Imposing weight of the big toes = 0	0.054	0.038-0.041	0.006-0.008	0.017-0.023
Including mtp joint	0.054	0.038-0.041	0.006-0.008	0.017-0.023

From the reported values, it is possible to notice that the inclusion of the metatarsophalangeal joint does not cause any differences with respect to the original model. On the other hand, the exclusion of the markers located on the big toes generally leads to smaller errors. An appreciable reduction of the maximum error can be highlighted especially in the Barefoot session, where the big toes could move without shoes constraint. Even if the maximum marker error obtained for all the three sessions (0.052m for Barefoot, 0.054m for Minimalist and Traditional) resulted being slightly larger than the recommended upper limit (0.04m), the values of the mean error range (0.040-0.042m for Barefoot and Minimalist, 0.038-0-041m for Traditional) and the RMS error (0.018-0.022m for Barefoot, 0.017-0.020m for Minimalist and 0.017-0.023m

for Traditional) are satisfactory. For these reasons, the approach that excluded the markers positioned on the big toes will be used in the further analyses.

In addition, the investigation of the location of the maximum error in the different trials led to a systematic pattern. In fact, the maximum error tended to appear always in correspondence to the markers positioned on the anterior or lateral femur. In particular, during the first frames of the trial the error corresponded to the right femur and then it switched to the left femur. After analyzing the frame at which the switch usually took place, it was possible to affirm that the maximum error was related to the swing phase. This was probably due to the fact that, during this phase, the muscles were more susceptible to oscillations.

Another way of visualizing the accuracy of the results is to load in OpenSim the IK motion file and synchronize it with the correspondent experimental data, as shown in Figure 4.4. The distance between the model markers (pink) and the experimental markers (blue) can give a qualitative idea of the accuracy of the inverse kinematics step.

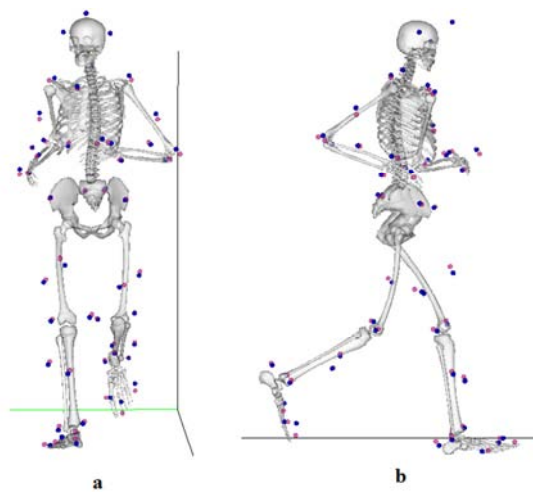


Figure 4.4. IK motion file (pink markers) and experimental data (blue markers) for a chosen Barefoot trial at the heel strike instant. Frontal (a) and lateral (b) views.

4.2.3 Joint angles

After achieving admissible results from the inverse kinematics tool, joint angles in the three anatomical planes were plotted. In the following paragraphs a brief comparison of the joint coordinates for the three different running styles will be introduced, with a particular focus on their behavior during initial contact. Since the aim was to compare

the average trend of the joint coordinates in the three running styles, it was not possible to identify a specific time corresponding to initial contact during the considered running gait cycle (defined from left toe off to left heel strike). It is important to notice that the considered running cycle was defined from left toe off (0% of the considered interval) to left heel strike (100% of the considered interval), since the idea was to investigate the behavior of the right leg while hitting the force platform during running. A time interval within which the initial contact for all the trials occurred was detected and it corresponded to 23-25% of the considered running cycle. The time range corresponding to the initial contact was considered interesting since it was expected to reveal the most significant differences between the running styles due to the different adopted strike patterns. First of all, joint coordinates in the transverse plane are shown in Figure 4.5.

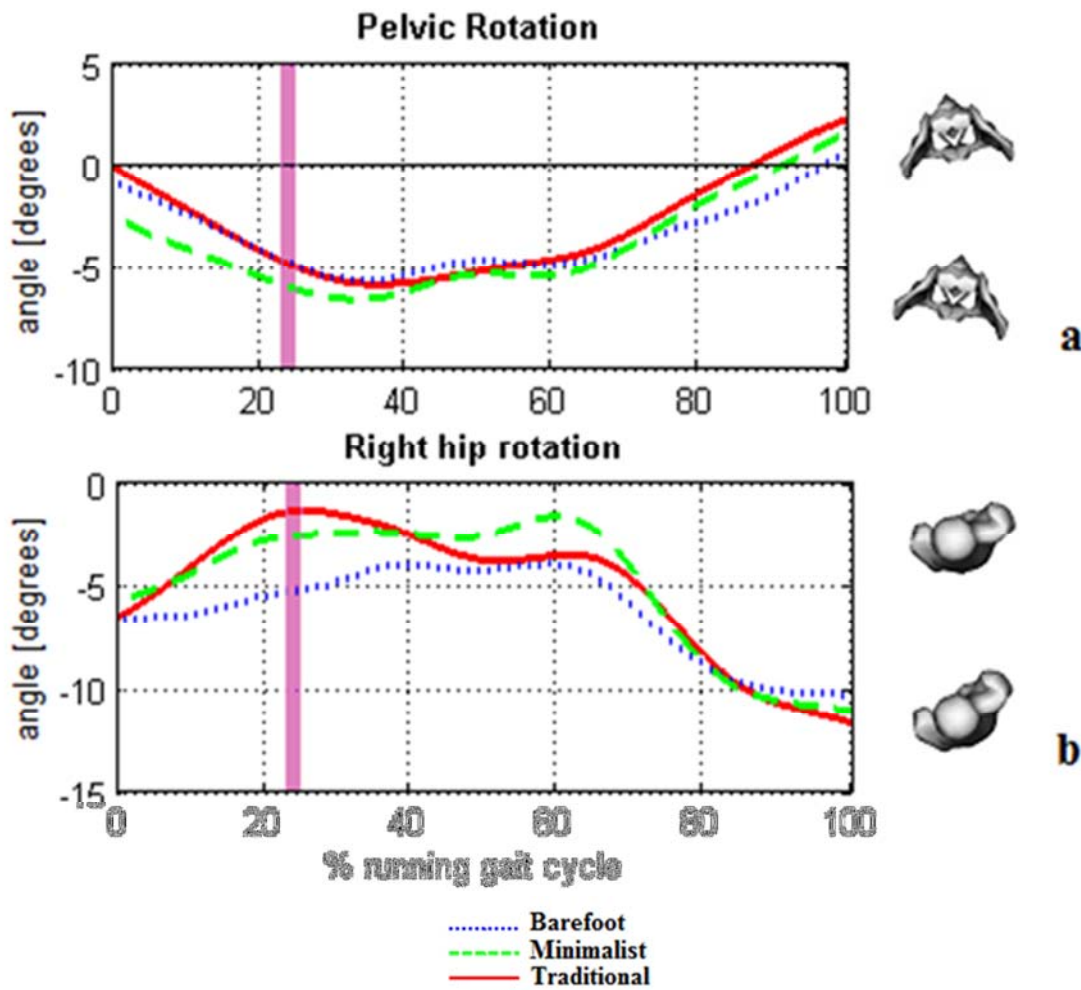


Figure 4.5. Comparison between transverse plane joint coordinates for the three running styles. Barefoot running is represented as dotted blue line, Minimalist running as green dashed line while Traditional running as red solid line. Figures from the OpenSim model represent pelvic rotation (a) and right hip rotation (b). Joint angles are shown as a percentage of the considered running gait cycle (from left toe off to left heel strike). The pink band identifies initial contact instant (23-25% of the considered running gait cycle).

As mentioned in section 1.3.1, motion in the transverse plane is considerably small in magnitude. Consequently, significant differences were not expected to be recognizable between the different running styles. However, minimalist condition shows the largest external pelvic rotation at initial contact (6.2 ± 1.2 degrees). The external pelvic rotation is responsible of maximizing the horizontal propulsion force and avoiding the potential loss of speed (Novacheck, 1998). This is in agreement with what found in section 2.8, where only during minimalist running the subject was speeding up, being the net

impulse positive. Moreover, traditional running displays both the lowest pelvic (5.0 ± 1.8 degrees) and hip (1.3 ± 1.5 degrees) external rotation.

Joint coordinates in the frontal plane are now introduced. As previously mentioned in section 2.8, the hip abducts according to the pelvis (Novacheck, 1998). In fact, from Figure 4.6 it is possible to notice a specular behavior between the trend of pelvic obliquity and that of hip ab/adduction. Traditional running displays the most positive pelvic obliquity and the least conspicuous hip abduction, whereas minimalist running shows the most negative pelvic obliquity and the most pronounced hip abduction. In particular, at initial contact traditional running displays the most positive pelvic obliquity (1.8 ± 0.6 degrees), followed by barefoot running (1.4 ± 0.6 degrees) and minimalist running (0.6 ± 0.5 degrees), confirming what previously stated. Nevertheless, at the same instant minimalist condition shows the highest hip abduction (4.6 ± 0.8 degrees), followed by traditional (3.6 ± 1.3 degrees) and barefoot (2.6 ± 0.7 degrees) conditions.

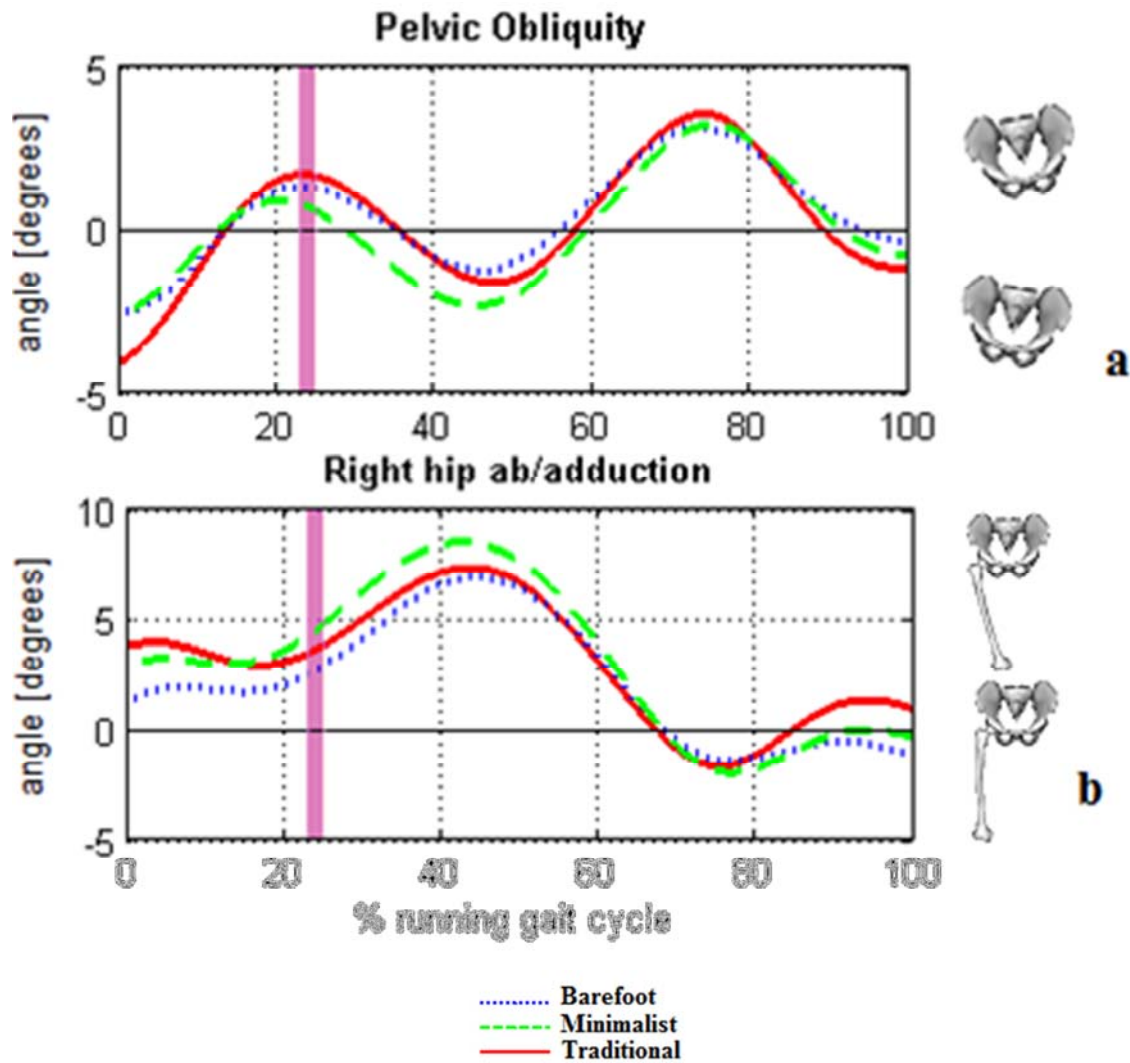


Figure 4.6. Comparison between frontal plane joint coordinates for the three running styles. Barefoot running is represented as dotted blue line, Minimalist running as green dashed line while Traditional running as red solid line. Figures from the OpenSim model represent pelvic obliquity (a) and right hip ab/adduction (b). Joint angles are shown as a percentage of the considered running gait cycle (from left toe off to left heel strike). The pink band identifies initial contact instant (23-25% of the considered running gait cycle).

Finally, joint coordinates in the sagittal plane will be described. Overall, the trend which represents lumbar extension/flexion movement remains the same in the three running styles (Figure 4.7), with a common lumbar flexion while loading response (25-27 % of the considered running gait cycle) and a transition to lumbar extension after midstance (44-48 % of the considered running gait cycle). However, while running with traditional shoes, the subject was used to flex more the lumbar spine in comparison with the other two running styles.

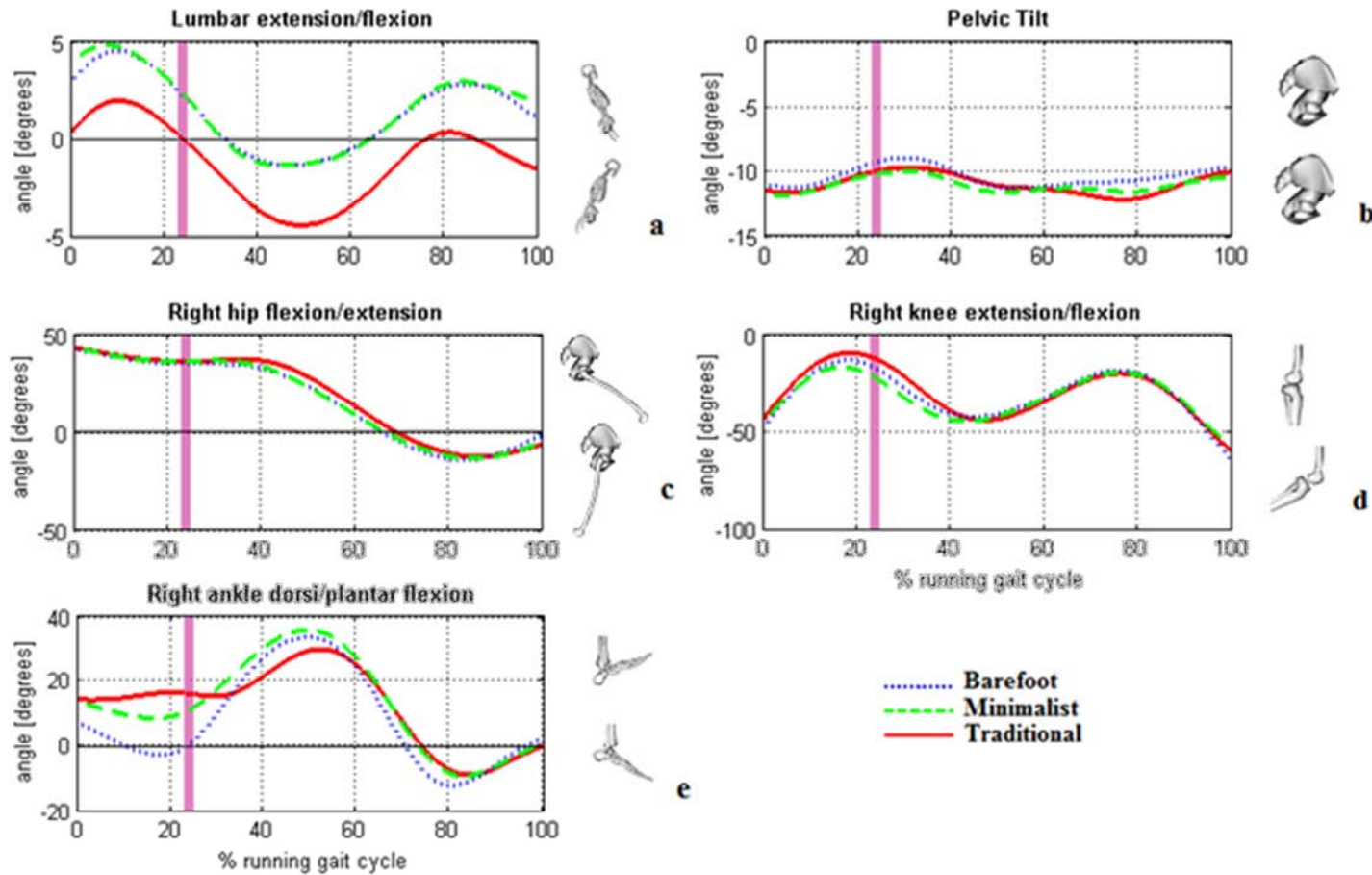


Figure 4.7. Comparison between sagittal plane joint coordinates for the three running styles. Barefoot running is represented as dotted blue line, Minimalist running as green dashed line while Traditional running as red solid line. Figures from the OpenSim model represent lumbar extension/flexion (a), pelvic tilt (b), right hip flexion/extension (c), right knee extension/flexion (d) and right ankle dorsi/plantar flexion (e). Joint angles are shown as a percentage of the considered running gait cycle (from left toe off to left heel strike). The pink band identifies initial contact instant (23-25% of the considered running gait cycle).

Lumbar flexion/extension and anterior/posterior pelvic tilt resulted in high correlation (Schache et al., 2002). As anterior tilt increases before right toe off (77-80 % of the considered running gait cycle), extension of the lumbar spine increases. This combined behavior was hypothesized (Slocum and James, 1968) to raise the extension range of motion of the lower limb.

Moreover, anterior pelvic tilt and peak hip extension during running were found to have a significant correlation (Schache et al., 2000). In particular, runners who displayed reduced peak hip extension before toe off were expected to show an increased anterior pelvic tilt. This evidence is slightly appreciable in the current study, since the differences between the running styles are quite low. Nevertheless, traditional running displayed the highest anterior pelvic tilt (12.4 ± 0.9 degrees) and the lowest peak hip extension (9.9 ± 1.8 degrees) during toe off.

More relevant differences between the running styles were found in correspondence with the distal joints. At initial contact the knee was flexed and then it continued to flex up to nearly 50° to absorb the impact shock (Richards, 2008). First of all, the highest knee flexion in minimalist running during the swing phase does not support that the short impact time found in this style (section 2.6) may be related to a stiff-legged running (Altman and Davis, 2012). Secondly, according to (Lieberman et al., 2010c, Schütte et al., 2011), more knee flexion at impact was observed in forefoot strike runners than in rearfoot strike runners. However, in the current investigation minimalist conditions showed the highest knee flexion at foot contact (23.3 ± 6.2 degrees) while, in previous studies (Schütte et al., 2011), knee flexion for minimalist running at foot strike (16.14 ± 2.76 degrees, running speed of 3.6 m/s) was found to be lower than in barefoot running (18.79 ± 3.02 degrees) and higher than in shod running (11.05 ± 3.18 degrees). Therefore, these evidences might represent a further proof of the fact that the subject was not running properly while wearing minimalist shoes.

At foot impact, ankle and knee flexion were found to be coordinated to absorb the vertical landing forces on the body (Richards, 2008). The orientation of the foot was considerably more horizontal in barefoot than in shod running (Figure 4.8). This evidence resulted from a more vertical position of the shank while barefoot running, since no difference was found in thigh orientation between forefoot and shod running at

initial contact. The foot placement was prepared well before initial contact for all the three styles.

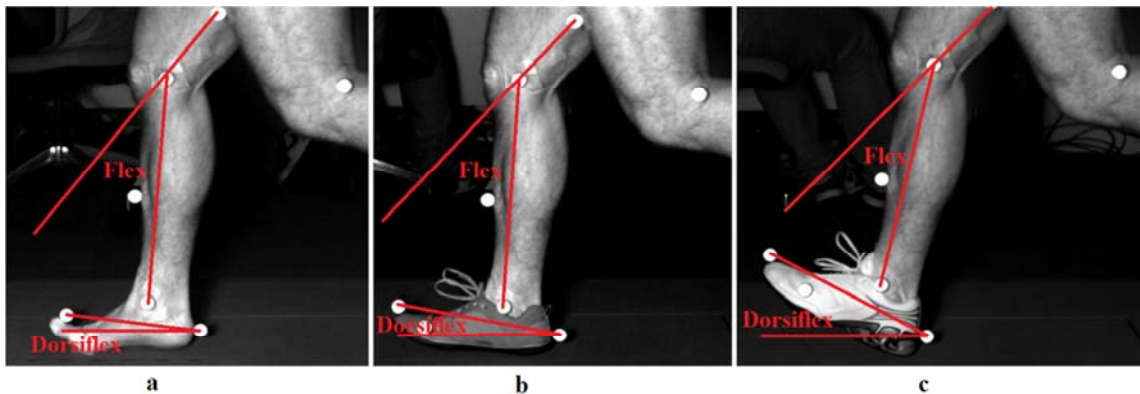


Figure 4.8. Knee and ankle angles comparison at initial contact in barefoot (a), minimalist (b) and traditional (c) running.

Furthermore, according to previous investigations (Squadrone and Gallozzi, 2009b, Schütte et al., 2011, Altman and Davis, 2012), the highest plantarflexion at foot strike was noticed while running barefoot (0.14 ± 4.1 degrees) and it acted to reduce the force on the foot by increasing the plantar contact area (Stockton and Dyson, 1998, De Wit et al., 2000). On the other hand, foot position at initial contact in minimalist and traditional running was dorsiflexed, with dorsiflexion angles of 11.3 ± 3.7 degrees and 15.7 ± 1.2 degrees respectively. Therefore, minimalist running was characterized by lower dorsiflexion than traditional running at foot strike, confirming results reported by Squadrone and Gallozzi (2009b) and Schütte et al. (2011). This is probably due to the different strike pattern adopted in each style. Based on these results, traditional running seems to increase the risk of Achilles tendinopathy, having the largest ankle dorsiflexion at impact (Tam et al., 2014).

4.3 Inverse dynamics analysis

The aim of the inverse dynamics (ID) analysis is to determine the joint torques and joint forces (generalized forces) during the movement. To achieve this aim, ID takes the kinematics measures and it combines them with external forces (ground reaction forces) and subject's anthropometrics (Winter, 2009). The mass-dependent relationship between force and acceleration, expressed by Newton's second law $F = ma$, is mathematically formulated with equations of motion. ID solves these equations, in an

inverse dynamics sense, to determine the set of generalized forces necessary to match estimated accelerations (Seth et al., 2011).

4.3.1 How inverse dynamics works

The classical equations of motion can be written as follows:

$$M(q)\ddot{q} + C(q, \dot{q}) + G(q) = \tau \quad (4.3)$$

where

$$q, \dot{q}, \ddot{q} \in R^N \quad \text{are the vectors of generalized positions, velocities, accelerations} \quad (4.4)$$

$$M(q) \in R^{N \times N} \quad \text{is the system mass matrix} \quad (4.5)$$

$$C(q, \dot{q}) \in R^N \quad \text{is the vector of Coriolis and centrifugal forces} \quad (4.6)$$

$$G(q) \in R^N \quad \text{is the vector of gravitational forces} \quad (4.7)$$

$$\tau \in R^N \quad \text{is the vector of generalized forces} \quad (4.8)$$

The kinematic measures are represented by the generalized positions, velocities and accelerations (eq 4.4). Therefore, all the terms on the left-hand side of the equation of motions (4.3) are known, while the term on the right-hand side of the equation is unknown. During ID analysis the known motion of the model is used to solve the equations of motion for the unknown generalized forces.

The required inputs and outputs for the IK tool are shown in Figure 4.9. Both experimental data, OpenSim and setting files are necessary. All the mentioned files were generated either using the OpenSim GUI, Notepad++ or Matlab. Each file will be briefly described in the following paragraphs.

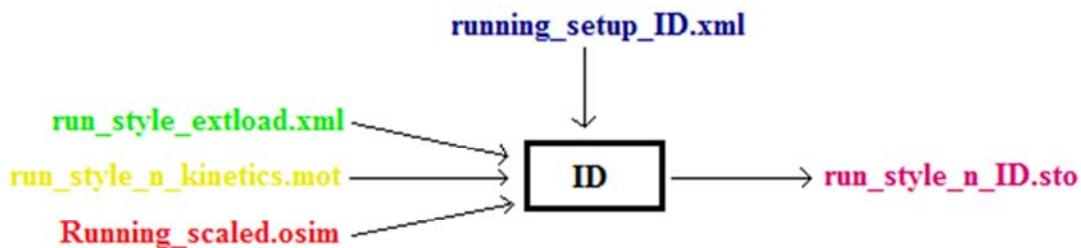


Figure 4.9. Inputs and Outputs of the ID Analysis. Experimental data are shown in green, OpenSim files in red and settings files in blue. Files generated by the workflow are shown in yellow (input) and fuchsia (output).

The running_setup_ID.xml file contains the time range over which the ID is solved and it corresponds to the duration of the examined trial. Furthermore, it specifies that

muscles and coordinate actuators were ignored and replaced with idealized motors providing joint torque to equilibrate the system at each time frame. The external loads applied to the model and the coordinate data files were also specified. A low-pass cut-off frequency of 6 Hz (Winter et al., 1974) was chosen for filtering the coordinate data, since noise is amplified by differentiation.

The external loads were defined in the `run_style_extload.xml` file. The vertical ground reaction force was applied to the right calcaneus and it was expressed with respect to the ground. Ground force and torque were therefore applied.

Motion files (`run_style_n_kinetics.mot`) were generated from acquisition files (`c3d`) using the Matlab function `TransformC3DToMotFilesRunning.m` provided by Luca Modenese. This function extracted and filtered GRFs from `c3d` files and saved them into OpenSim format, respecting the conventions for the definition of the reference system defined by the International Society of Biomechanics (ISB) (Wu and Cavanagh, 1995). The function then generated a motion file containing the GRFs. The parameters that needed to be settled were the orientation of the desired reference system (moving and upwards directions as defined in Vicon), features related to the filter (cut-off frequency and filter order) and the initial and final events specifying the data to be extracted. According to the reference system defined in Nexus, moving and upwards directions were assigned to y and z axes respectively. According to Hamner et al. (2010), ground reaction forces were low-pass filtered at a cut-off frequency of 20 Hz. Initial and final events were defined as left foot off and left heel strike respectively.

The ID output is a storage file (`run_style_n_ID.sto`) which contains the net joint torques and forces acting along the coordinate axes that provide accelerations estimated from experimental motion and applied external forces.

4.3.2 Joint moments

Trunk, pelvis, hip, knee and ankle moments in the three anatomical planes during the considered running gait cycle are shown in **Errore. L'origine riferimento non è stata trovata.** 4.10. Some relevant differences between the different running styles will be highlighted in the following paragraphs.

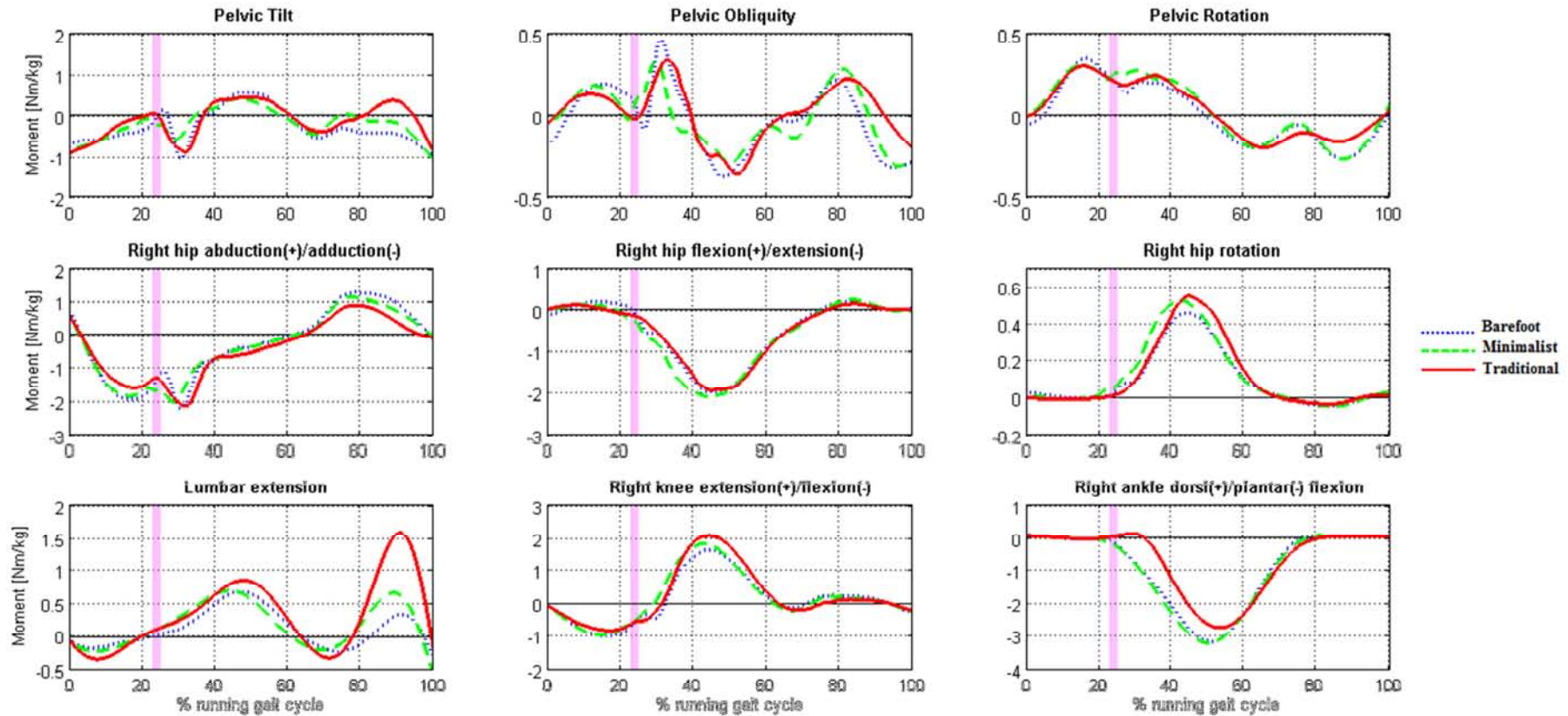


Figure 4.10. Comparison between joint moments in the three anatomical planes for the three running styles. Barefoot running is represented as a dotted blue line, minimalist running as green dashed line while traditional running as a red solid line. Joint moments are shown as a percentage of the considered running gait cycle (from left toe off to left heel strike). The pink band identifies initial contact instant (23-25% of the considered running gait cycle).

Firstly, a considerably higher peak hip internal rotation moment at midstance while wearing traditional running shoes (0.56 ± 0.04 Nm/kg) in comparison with barefoot conditions (0.46 ± 0.03 Nm/kg) was noticed. Previous clinical investigations (Kerrigan et al., 2009) suggested that an increase in hip internal rotation moment might increase the risk of hip osteoarthritis (OA). According to this evidence, shod running could have a role in the development of this degenerative joint disease. Furthermore, according to Kerrigan et al. (2009), results deriving from the analysis of the knee moment showed a reduced peak knee extension moment at midstance during barefoot running (1.62 ± 0.24 Nm/kg) compared to shod conditions (2.08 ± 0.1 Nm/kg). However, findings for peak knee extension moment in minimalist running (1.85 ± 0.03 Nm/kg) do not agree with previous studies (Bonacci et al., 2013) where this value was slightly higher than the correspondent in traditional running. Bonacci et al. (2013) suggested that a higher knee extension moment during shod running may have implications for knee injury and pain. Generally, a slight and almost indiscernible ankle dorsiflexion moment at initial contact took place for all the three running styles, changing in a larger plantarflexion moment at midstance. The magnitude and the time of occurrence of the small initial dorsiflexion moment were shown to depend on heel height (Reinschmidt and Nigg, 1995). In the current study, the higher the heel wedging in the shoe, the higher the magnitude (0.18 ± 0.01 Nm/kg for traditional running, 0.06 ± 0.01 Nm/kg for minimalist and barefoot running) and the later the time of occurrence (29%, 21% and 19% of the running cycle for traditional, minimalist and barefoot running respectively) of peak dorsiflexion moment. During the first half of the stance phase in minimalist and barefoot running the ankle plantarflexion moment increased in comparison with traditional running. This evidence may depend on the different strike pattern, since forefoot runners were found to contract their plantarflexor muscles with greater force than rearfoot runners (Rooney and Derrick, 2013). Furthermore, according to previous investigations (Perl et al., 2012, Reinschmidt and Nigg, 1995, Bonacci et al., 2013), considerably higher peak ankle plantarflexion moment was found at midstance in barefoot running (3.16 ± 0.1 Nm/kg) compared to shod running (2.7 ± 0.2 Nm/kg). Since ankle plantarflexion moment is normally identified as an indicator of Achilles tendon loading (Reinschmidt and Nigg, 1995), heel lifting or heel wedging in running shoes may represent a solution to contribute to prevention and treatment of Achilles tendinitis.

4.3.3 Joint angular velocity and power

Joint angular velocity corresponds to the rate of movement of a joint and it is related to the dynamics of muscle activation and force generation during running. Hip, knee and ankle angular velocities ω were obtained by computing in Matlab the first derivative of each joint angle φ from IK with respect to time:

$$\omega = \frac{d\varphi}{dt} \quad (4.9)$$

In particular, it has been shown (Heidenfelder et al., 2008, De Wit et al., 2000) that knee and ankle angular velocities are used to adapt to different shoe conditions. For example, a higher knee flexion velocity (Figure 4.11) at impact during barefoot running (267.8 ± 28.7 °/s) compared to traditional running (212.3 ± 53.7 °/s) may represent a strategy to reduce impact loading by reducing the effective mass (i.e. every portion of the body that comes to a dead stop along with the impact point of the foot (Lieberman, 2010)) of the contacting leg (De Wit et al., 2000).

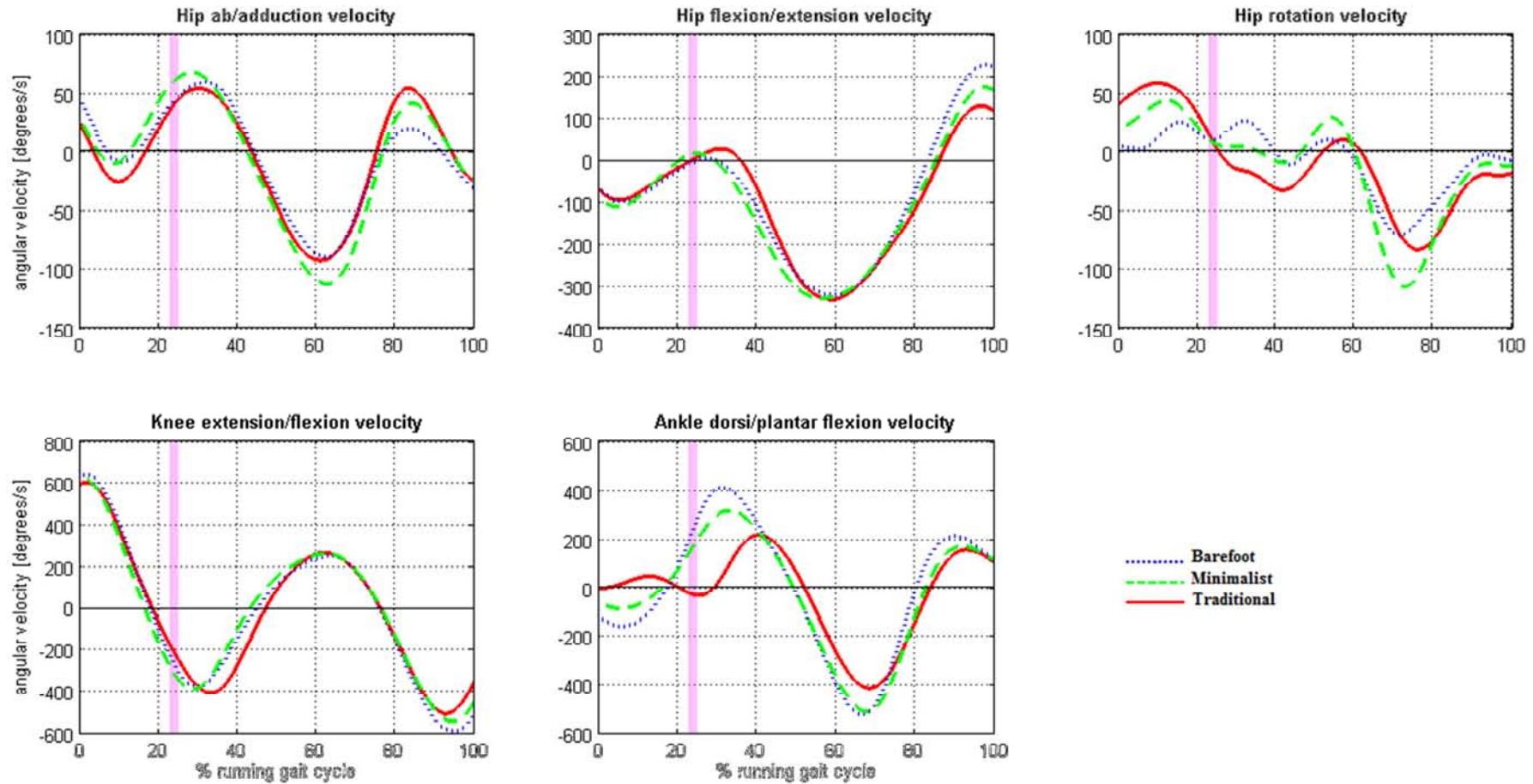


Figure 4.11. Hip, knee and ankle angular velocities in the three running styles. Barefoot running is represented as dotted blue line, Minimalist running as green dashed line while Traditional running as red solid line. Angular velocities are shown as a percentage of the considered running gait cycle (from left toe off to left heel strike). The pink band identifies initial contact instant (23-25% of the considered running gait cycle).

Hip, knee and ankle powers P were then computed as the product of the joint moment τ and the corresponding joint angular velocity ω :

$$P(t) = \tau \omega \quad (4.10)$$

where ω was expressed in rad/s. The hip net power was obtained by summing the hip powers that derived from each of the three degrees of freedom of the hip. Since the power corresponds to the rate of transferring energy, a positive power indicates that the body is generating energy through concentric muscle activity (the muscle shortens as it contracts), while a negative power indicates that the body is absorbing energy through eccentric muscle activity (the muscle lengthens as it contracts).

Both minimalist and barefoot running displayed a sharp reduction in peak knee extensor power (395.5W and 454.7W for barefoot and minimalist respectively) compared to traditional running (790.5W). A shift in power absorption from the knee to the ankle is clearly visible in barefoot and minimalist running (Figure 4.12). Moreover barefoot running, being characterized by a forefoot strike pattern, showed a greater increase in ankle power absorption than minimalist running. In fact the load on the plantarflexors is reduced while adopting a midfoot strike pattern (Blaise Williams et al., 2012). Furthermore, a considerable delay in power absorption occurred while running with traditional shoes, due to the delay in the appearance of the plantarflexion moment. However, a larger increase in ankle power generation in barefoot running may be potentially injurious (Blaise Williams et al., 2012).

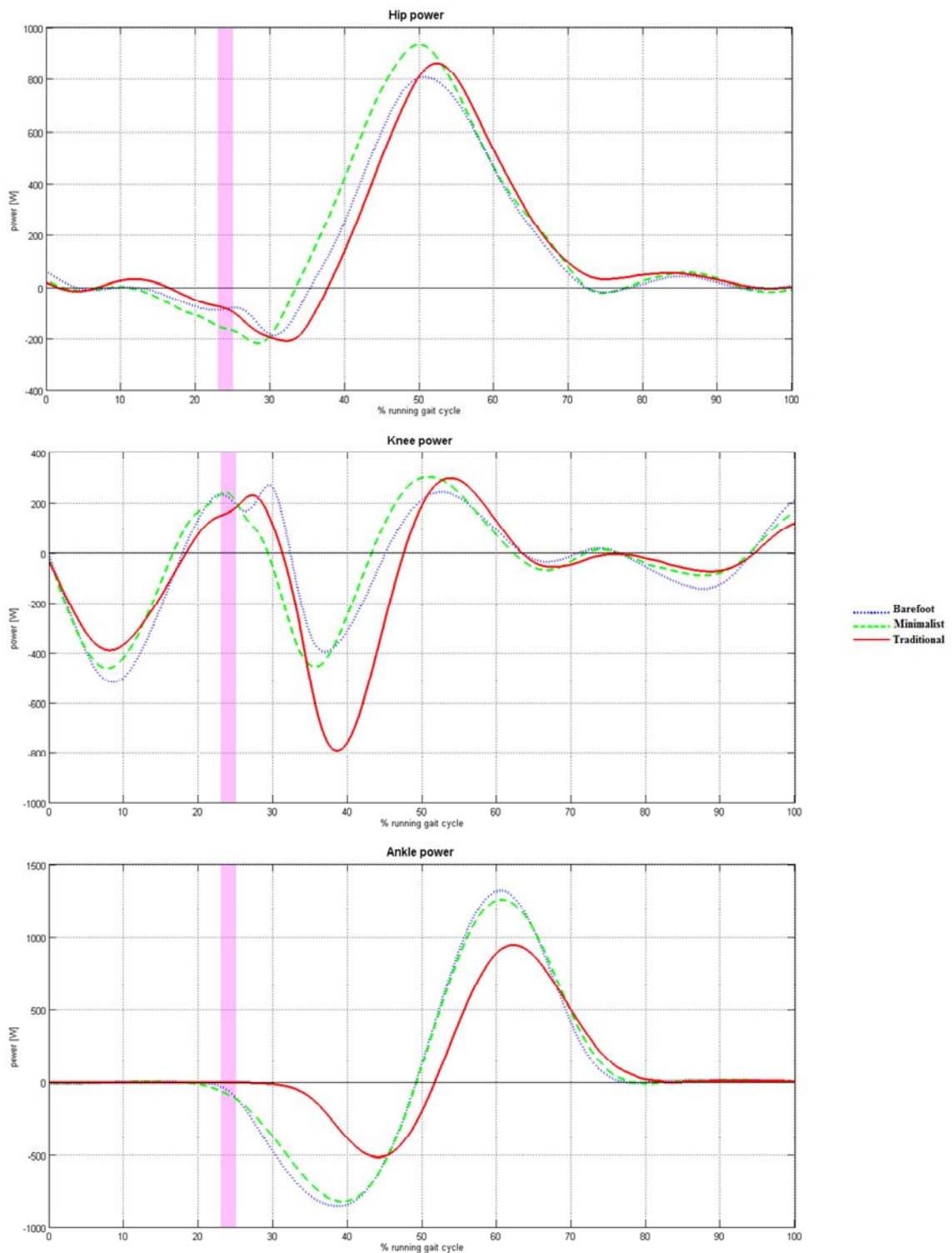


Figure 4.12. Hip, knee and ankle powers in the three running styles. Barefoot running is represented as dotted blue line, Minimalist running as green dashed line while Traditional running as red solid line. Powers are shown as a percentage of the considered running gait cycle (from left toe off to left heel strike). The pink band identifies initial contact instant (23-25% of the considered running gait cycle).

Overall, barefoot running highlighted a reduction of the total lower limb power absorption (1422.3 W) compared to minimalist (1482.3 W) and traditional running (1505.8 W) (Figure 4.13).

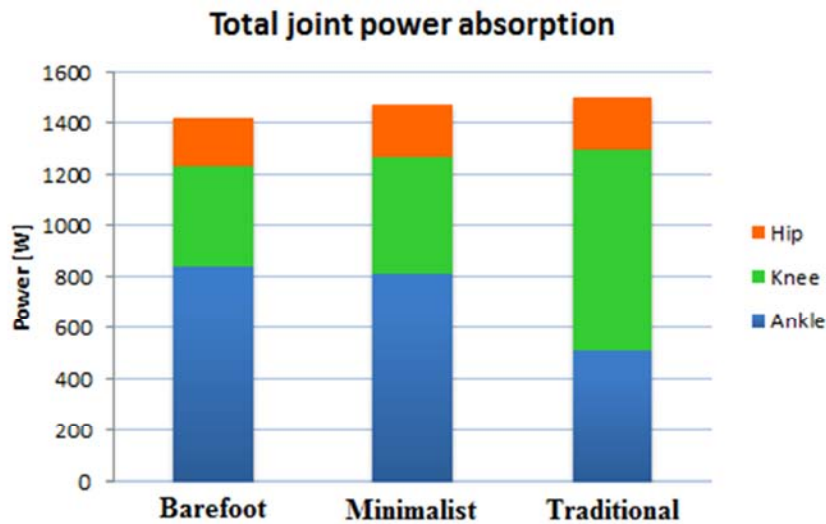


Figure 4.13. Total lower limb joint power absorption in barefoot, minimalist and traditional running.

Even if the lower total power absorption in barefoot and minimalist conditions may be beneficial in isolation, the increase in power absorption at the ankle while running barefoot may contribute to increase the risk of foot and ankle injuries (Blaise Williams et al., 2012). In conclusion, based on these considerations, it does not seem necessary to run barefoot or with minimalist shoes to gain potential benefits.

CHAPTER 5

Muscle action and its effects on the mechanics of running

5.1 Introduction

Biomechanical aspects of running injuries are often attributed to external loads measurements. However, previous investigations (Miller and Hamill, 2009) revealed the complex and often non-intuitive relationship between external loads and injury-inducing internal loads. Therefore, it is important to combine external and internal loads considerations when assessing skeletal loading with respect to injury. Joint contact forces have been shown to represent a more direct measure of the loads responsible for bone stress injuries during running (Rooney and Derrick, 2013, Scott and Winter, 1990). Joint contact forces can be measured by using instrumented prosthesis implants, but this method is quite invasive. On the other hand, static optimization (SO) tool in OpenSim enables to estimate muscle activations, muscle forces and joint contact forces in a non-invasive way.

The SO tool and some adjustments adopted in the current study will be introduced in the following chapter, followed by an analysis of muscle activations and joint contact forces in the three different running styles.

5.2 Load sharing problem

The load sharing problem consists on the calculation of the forces within the anatomical structures. It can be seen as the distribution of the intersegmental resultant force and moment into muscles, ligaments and articular surfaces. Since the number of the individual anatomic structures involved in the transmission of the force across a joint often exceeds the minimum number needed to obtain a determinate solution, the load

sharing problem represents a statically indeterminate problem (Crowninshield and Brand, 1981).

Physiologically speaking, the statistical indeterminacy is solved by the central nervous system, which is able to choose a set of muscles which executes a particular motion (Rasmussen et al., 2001). Nevertheless, practically speaking, the following approaches to achieve a unique solution are required (Modenese, 2010):

- I. To reduce the number of unknown variables, grouping the muscle forces based on physiological criteria;
- II. to use physiological relationships to increase the number of constraints of the problems, making it consequently equal to the number of the unknown variables;
- III. to seek an optimum solution that maximizes or minimizes an objective function, defining the unknown variables as design variables.

5.3 Static optimization method

The commonly adopted procedure to determine the unknown muscle forces is a constrained optimization problem generically defined as follows:

$$\text{minimize} \quad f(x) \quad (5.1)$$

$$\text{subject to} \quad h_i(x) = 0 \quad i = 1, \dots, n \quad (5.2)$$

$$g_j(x) \leq 0 \quad j = 1, \dots, m \quad (5.3)$$

$$lb < x_k < ub \quad k = 1, \dots, p \quad (5.4)$$

The optimization task strictly related to the load sharing problem can be proposed as follows:

$$\text{minimize} \quad J(F_i) \quad (5.5)$$

$$\text{subject to} \quad \sum_{i=1}^n \mathbf{r}_{ij} \times \mathbf{F}_i = \mathbf{M}_j \quad i = 1, \dots, n; \quad (5.6)$$

$$j = 1, \dots, d$$

$$0 \leq F_k \leq F_{max,k} \quad k = 1, \dots, m \quad (5.7)$$

Where J represents the objective function, \mathbf{F}_i is the force magnitude of the i -th muscle, n is the number of muscles involved in the system, d represents the number of degrees of freedom of the system, \mathbf{r}_{ij} is the moment arm of the i -th muscle with respect to the j -th joint and \mathbf{M}_j is the net moment acting on the j -th joint.

This approach is called static optimization (SO) because it solves each frame of the motion independently from the previous and the following ones. The first imposed constraint (Eq. 5.6) dictates the respect of the moment equilibrium equation with respect to the joints for the obtained optimized forces. The second imposed constraint (Eq. 5.7) highlights the fact that muscles can only pull (muscular stress can only be tensile) and that the muscular forces have an upper physiological limit related to the muscle force-length-velocity properties.

Physiological features like the muscular synergism (Dul et al., 1984) need to be taken into account in the choice of the cost function. As according to the specific task or condition, the central nervous system chooses a different muscular recruitment, aiming to optimize a different performance. It is likely that a unique sharing load criterion does not exist.

5.4 Static optimization tool in OpenSim

The SO tool in OpenSim adopts a nonlinear polynomial cost function which was shown (Dul et al., 1984) to accurately depict synergism between the recruited muscles. The general form of the cost function can be written as follows:

$$J = \sum_{i=1}^n (a_i)^p \quad p \geq 1 \quad (5.8)$$

where n is the number of muscles involved in the model, a_i is the activation level of the muscle i at a discrete time step and p is a constant defined by the user. The muscle force outputs were constrained to produce the joint moments predicted in the dynamic analysis (Eq. 5.6). To evaluate the importance of including muscle physiology, SO was solved both neglecting and incorporating muscle force-length-velocity properties. When discarding physiological muscle properties each muscle was assumed to be an ideal force generator:

$$\mathbf{F}_i = a_i F_i^0 \quad (5.9)$$

where F_i^0 is the maximum isometric force of the i -th muscle. On the other hand, in the “physiological case”, the force generated by a muscle was constrained by its force-length-velocity (FLV) properties (Anderson and Pandy, 2001):

$$\mathbf{F}_i = a_i f(F_i^0, l_i, v_i) \quad (5.10)$$

where $f(F_i^0, l_i, v_i)$ is the function of the force-length-velocity surface for the muscle, l_i is the length and v_i the shortening velocity of the i -th muscle (Zajac, 1989). This

function computes the active fiber force along the tendon assuming an inextensible tendon and does not take into account contribution from muscle's parallel elastic element (simtk-confluence.stanford.edu).

The required inputs and outputs for the SO tool are shown in Figure 5.1. Both experimental data, OpenSim and setting files are necessary. All the mentioned files were generated either using the OpenSim GUI, Notepad++ or Matlab.

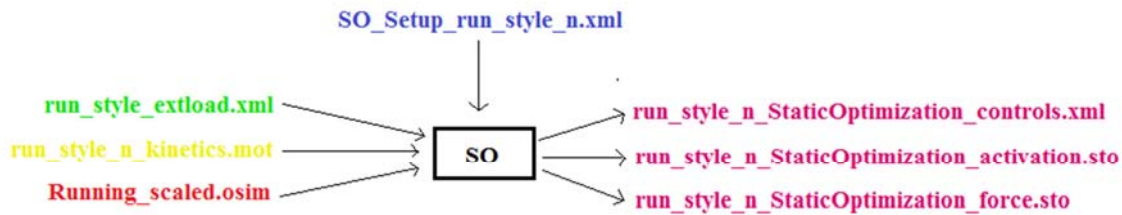


Figure 5.1. Inputs and Outputs of the SO tool. Experimental data are shown in green, OpenSim files in red and settings files in blue. Files generated by the workflow are shown in yellow (input) and fuchsia (outputs).

The SO_Setup_run_style_n.xml specifies the power p to which the muscle activations should be raised in the cost function. It has been shown (Rasmussen et al., 2001) that the choice of the exponent p strongly influence the muscle activation profile and the muscle synergism. In the current study a value of $p = 2$ was chosen to simultaneously obtain reliable estimations of muscle activations and joint contact forces (Modenese et al., 2011). The two storage output files contain the time histories of muscle activations and forces.

Some adjustments were necessary to make the scaled model suitable for static optimization. Firstly, to enable the simulations to run, reserve actuators were included at each joint to increase the force of the actuators. Reserve actuators are recruited through the same optimization as normal muscle actuators and provide additional moment if necessary. Secondly, being the subject considered in Delp's model a 99-year-old man, the muscle maximum isometric force was not adequate to the 24-year-old well-trained subject involved in the current study. Therefore, it was considered necessary to find an appropriate factor to adjust the muscle maximum isometric force. A recent study (Handsfield et al., 2014) showed that total lower limb muscle volume scales with the height-mass product ($R^2 = 0.92$). According to this study the regression equation can be stated as follows:

$$V_m = 47mh + 1285 \quad (5.11)$$

where V_m is the lower limb muscle volume, m and h the subject mass (expressed in kg) and height (expressed in meters). Being mass and height of Delp's model 75.16 kg and 1.67 m respectively, whereas 87.23 kg and 1.73 m those of the adopted model, the obtained muscle volumes resulted in:

$$V_{m_{Delp}} = 7184.31 \text{ cm}^3 \quad (5.12)$$

$$V_{m_{curr_model}} = 8377.51 \text{ cm}^3 \quad (5.13)$$

Computing the ratio between the lower limb muscle volume of the current model and Delp's model, a factor equals to 1.16 was found. Assuming that muscle volume would be proportional to the maximum isometric force through the physiological cross sectional area (see section 3.3.1), each muscle maximum isometric force was increased by 16%. Since some of the muscles (e.g. gastrocnemius, soleus) showed a plateau corresponding to the maximum activation, this value was considered underestimated (probably also the tetanic stress should be increased) and another adjustment factor calculated. Lee et al. (2000) introduced two predictive models (regression equations) to estimate the whole-body muscle volume. Since the first model takes into account the circumference of the upper arm, thigh and calf, it would have been useful to indicate the level of training of the involved subject. Being anthropometric measurements not available, the second model was adopted. This model takes into consideration subject age, sex and race beyond mass and height. The regression equation that describes this model is:

$$SM = 0.244 * mass_{body} + 7.8 * height + 6.6 * sex - 0.098 * age + race - 3.3 \quad (5.14)$$

where SM is the skeletal muscle mass (expressed in kg), $sex = 1$ for male and 0 for female, $race = -1.6$ for Asian, 1.2 for African American and 0 for white or Hispanic. Being both of the subjects white, the obtained skeletal muscle mass for the two models resulted in:

$$SM_{Delp} = 24.96 \text{ kg} \quad (33\% \text{ of the total body mass}) \quad (5.15)$$

$$SM_{curr_model} = 35.73 \text{ kg} \quad (41\% \text{ of the total body mass}) \quad (5.16)$$

By computing the ratio between the skeletal muscle mass of the current model and Delp's model, a factor equals to 1.43 was found. Therefore, each muscle maximum isometric force was multiplied by this factor.

5.5 Muscle activations

The evaluation of muscle activation and its relationship with kinematic and kinetic data during the running cycle plays a fundamental role in the complete understanding of running biomechanics. Simulated activations of mainly involved lower limb muscles are shown in Figure 5.2. Being subject-specific experimental EMG data not available, experimental EMG averaged from eight subjects during shod running at a similar speed (3.3 m/s) to the current study (Cappellini et al., 2006) were used as reference values. However, differences deriving from the worn running shoes, the involved subjects and the slightly changes in running velocity need to be taken into account while comparing the different activations. For example, it has been shown that speed changes are responsible of the increase in the intensity of muscle activation and are less related to their relative timings (Cappellini et al., 2006). Overall, rectus femoris, semitendinosus and tibialis anterior were highly active during the phase preceding foot contact and at foot contact. During midstance gluteus maximus, gluteus medius, tensor fascia latae, biceps femoris long head, vastii lateralis and medialis were active, while the major activation of lateral and medial gastrocnemii and soleus was found in mid-to late stance, providing body propulsion (Figure 5.2).

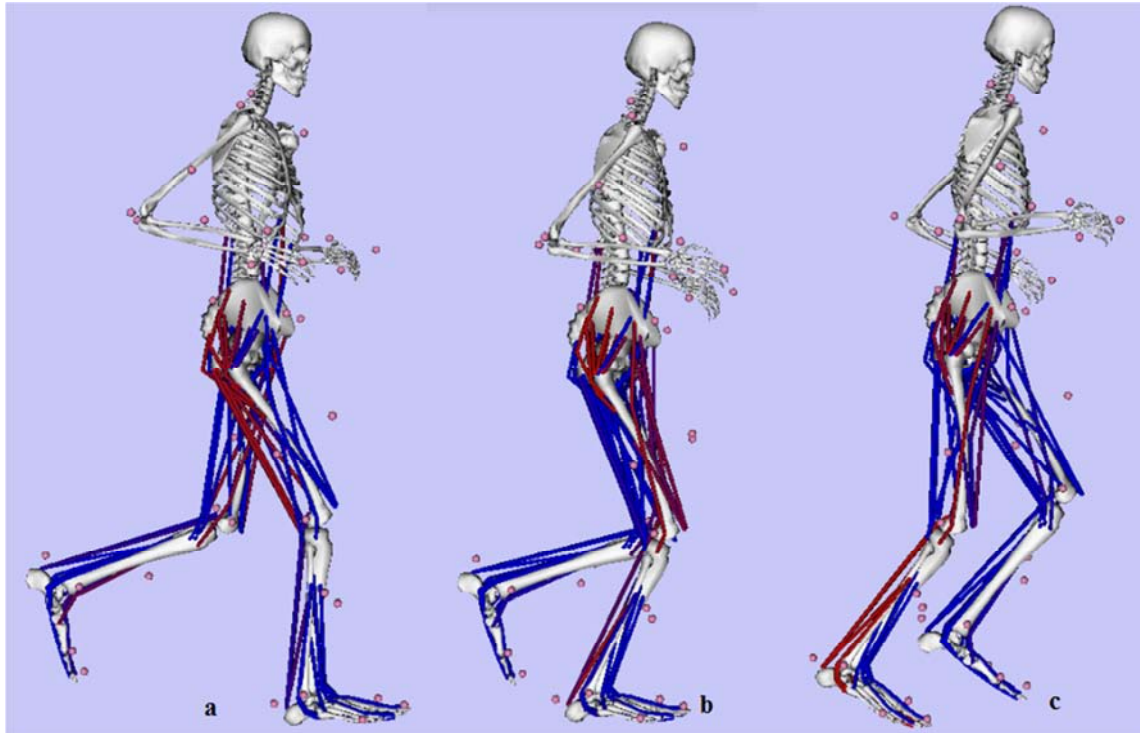


Figure 5.2. Muscle activations at foot strike (a), midstance (b) and toe-off (c) in a barefoot trial. Active muscles are shown in red while non-active muscles are shown in blue.

Generally, comparing the muscle activations in the three running styles (Figure 5.3), traditional running displayed a more or less pronounced delay in muscle activations compared to barefoot and minimalist running. However, in most cases this delay did not correspond to a shift in time of the total activation, since the deactivation timing matched those of the other styles (apart for tibialis anterior where the activation is considerably longer while wearing traditional shoes in comparison to the other styles). This evidence resulted in a general minor timing activation during traditional running compared to barefoot and minimalist running. An increased activity of knee extensor muscles (vastii lateralis and medialis) after impact during minimalist running (activation peaks equal to 0.49 and 0.70 in vastus medialis and lateralis respectively) supports the concept of a more upright posture while wearing minimalist shoes (De Wit et al., 2000). According to Komi et al. (1987), the major leg extensor muscles were expected to change their activation patterns with the different impact conditions. In fact, before foot strike muscle activity is pre-programmed based on the expected impact shock. The major goal of muscles in this phase is to prepare the locomotor system for landing (Divert et al., 2005). Plantar flexors (medial and lateral gastrocnemius and soleus)

amplitudes showed higher activity in pre-activation in barefoot and minimalist conditions compared to traditional running. This finding supports the lack of heel impact during minimalist and barefoot running (Divert et al., 2005). The lower tibialis anterior activity at foot impact during barefoot and minimalist conditions (0.07 in barefoot and minimalist against 0.16 in traditional running) was consistent with the less foot dorsiflexion at foot strike compared to traditional running (Standifird et al., 2013, Stockton and Dyson, 1998).

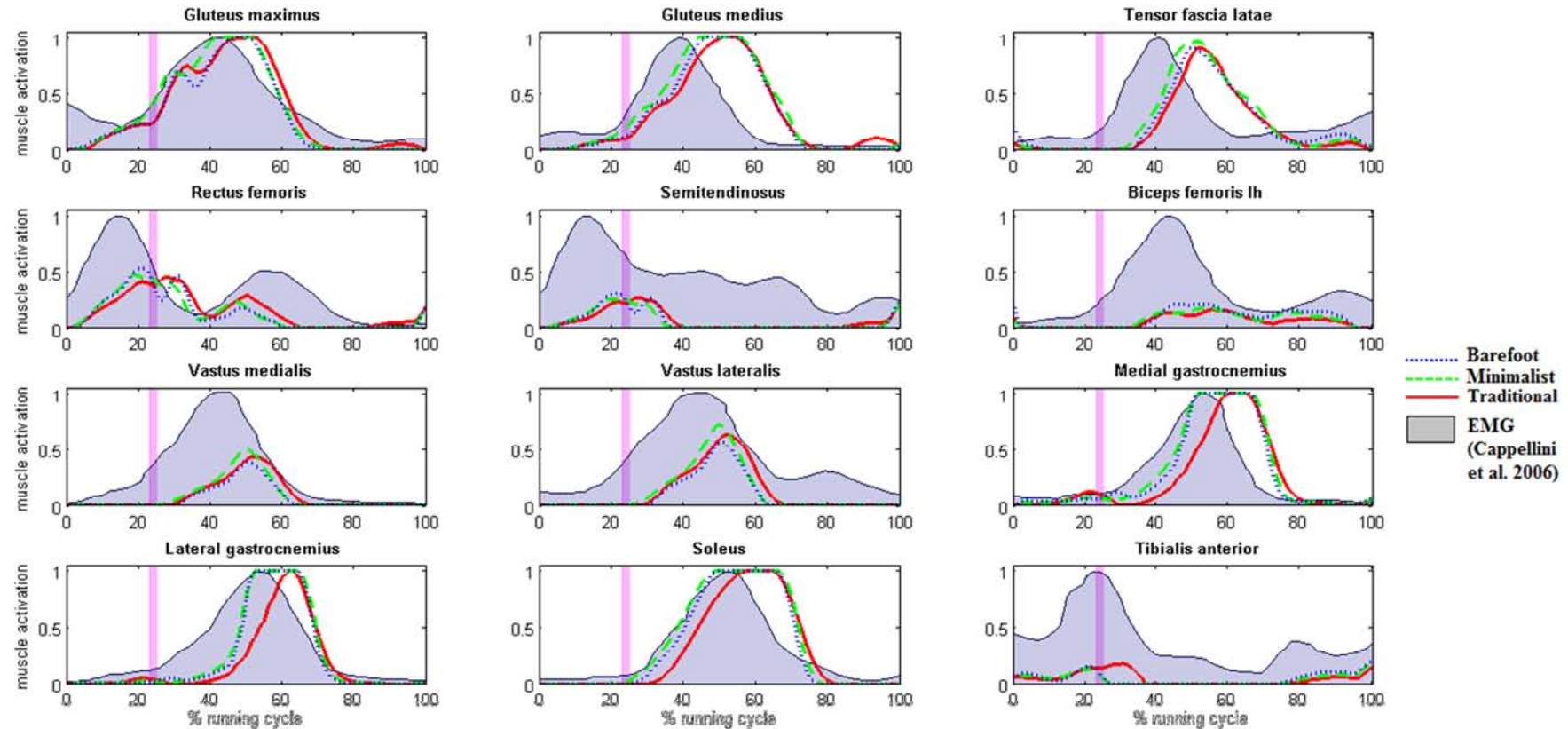


Figure 5.3. Comparison of average simulated muscle activations from SO for barefoot (dotted blue line), minimalist (dashed green line) and traditional (solid red line) running. Speed-matched experimental EMG data (Cappellini et al., 2006) are shown in the gray area. The pink band identifies initial contact instant (23-25% of the considered running gait cycle).

Being experimental EMG data collected during shod running (Cappellini et al., 2006), a comparison between these data and traditional running will be done. To quantitatively understand how accurately simulations matched experimental data, two index were introduced: an intensity index (II) and a phase index (PI). For each muscle the II was computed as follows:

$$II = \frac{A_{nT}}{A_{eT}} 100 \quad (5.18)$$

where A_{nT} is the area under the activation curve during traditional running while A_{eT} is the area under the experimental activation curve (Figure 5.4). This index, expressed as a percentage, was aimed to provide a measurement of the similarity between the muscle activation amplitudes.

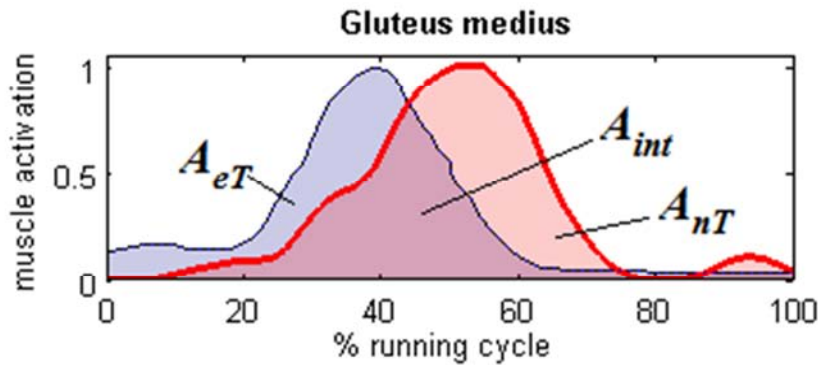


Figure 5.4. Visualization of the area under the numerical activation curve (A_{nT}) and under the experimental activation curve (A_{eT}) of gluteus medius for traditional running. The intersection between A_{nT} and A_{eT} is indicated as A_{int} .

On the other hand, the PI was computed for each muscle as follows:

$$PI = \frac{A_{int}}{A_{eT}} 100 \quad (5.19)$$

where A_{int} is the area corresponding to the intersection between A_{nT} and A_{eT} (Figure 5.4). This index offered a measurement of the shift displacement between the two different activations. To make data comparable and therefore to obtain these indexes, muscle activation has been normalized by the maximum force reached by each muscle while executing the movement. The closer these indexes were to 100, the better the simulated data matched experimental data. These concepts can be easily visualized in Figure 5.5 where the two index are combined in the same graph. The red star in the graph represents the ideal value, being both PI and II equals to 100. Therefore, this condition would be achieved when both A_T and A_{int} are equals to A_{exp} and the

simulated data would correspond exactly to the experimental data. Four regions that aimed to provide a measurement of the accuracy of the numerical activations were defined in the plane identified by the two indexes. Both the axes were divided into four parts, with the only difference that the range of the II was defined between 0 and 110, since A_{nT} could be higher than A_{eT} . Based on where each muscle is located in the plane, results corresponding to its activation might be very accurate ($PI > 75$, $II > 82.5$), accurate ($50 < PI < 75$, $55 < II < 82.5$), inaccurate ($25 < PI < 50$, $27.5 < II < 55$) or very inaccurate ($0 < PI < 25$, $0 < II < 27.5$). In the current study muscle activations that showed the best accuracy with experimental activations were gluteus maximus, soleus, gluteus medius, medial gastrocnemius, biceps femoris long head, rectus femoris and tibialis anterior as they fell in the “accurate” region. On the other hand, the least accurate muscle activations was found in vastus medialis, tensor fascia latae, semitendinosus, vastus lateralis and lateral gastrocnemius.

However, while making these considerations it has to be kept in mind that results would have been more reliable if EMG were collected directly on the subject involved in the study while wearing traditional shoes.

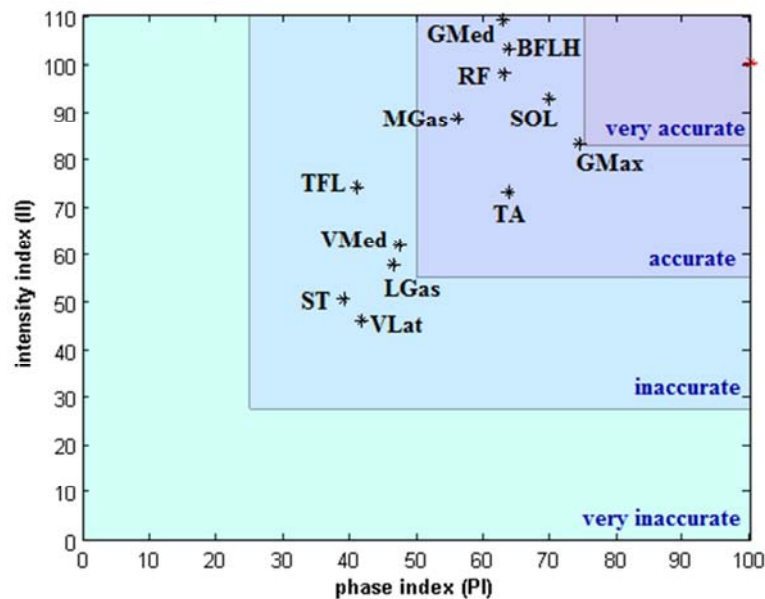


Figure 5.5. Representation of muscle activation in terms of phase index (PI) and intensity index (II). Gluteus maximus (GMax), gluteus medius (GMed), Tensor fascia latae (TFL), Rectus femoris (RF), Semitendinosus (ST), Biceps femoris long head (BFLH), Vastus medialis (VMed), Vastus lateralis (VLat), Medial gastrocnemius (MGas), Lateral gastrocnemius (LGas), Soleus (SOL) and Tibialis anterior (TA) are represented. The red star represents the ideal value, where both PI and II are equals to 100. The blue boxes represent the accuracy level, from very accurate (dark blue, top right) to very inaccurate (light blue, bottom left) simulations.

5.6 Muscle forces and joint contact forces

Scott and Winter (1990) were among the first researchers to highlight the necessity of looking beyond GRFs when evaluating the importance of skeletal loading to injuries (Joshua McDowell, 2008). Therefore, to gain a complete understanding of running injury mechanisms, analysis of joint contact forces (JCFs) at the hip, knee and ankle was undertaken. JCFs are forces acting across the articulating surfaces and they include the effect of muscle activity. These forces correspond to the active compression forces due to muscles plus the intersegmental loads carried by the joint structure (Winter, 2009).

As anticipated, in this study JCFs were computed both considering and discarding force-length-velocity muscle properties. The obtained values for the three joints and for the different running styles are shown in Figure 5.6. While hip contact forces resulted almost the same in the two analyses, the major differences can be noticed in the knee contact forces. In fact, peak knee contact forces displayed an increase of 31%, 34% and 23% in barefoot, minimalist and traditional running respectively when including FLV muscle properties than when discarding them. Furthermore, a delay in the occurrence of peak knee contact forces (2% of the running gait cycle) when considering FLV properties with respect to the “non-physiological” case can be appreciated. Knee extensors and flexors forces are shown in Figure 5.7 for minimalist running, since this running style displayed the major knee contact force differences. When including FLV muscle properties, muscles activated at midstance, which is the region where the maximum peak knee contact force occurred, generally displayed an increase in force magnitude (189% in lateral gastrocnemius, 44% in medial gastrocnemius, 456% in sartorius, 24% in vastus intermedius and lateralis, 27% in vastus medialis) in comparison to the “non-physiological” case, except for rectus femoris that showed a decrease of 59%. These higher values in muscle forces explain the higher values in peak knee contact forces.

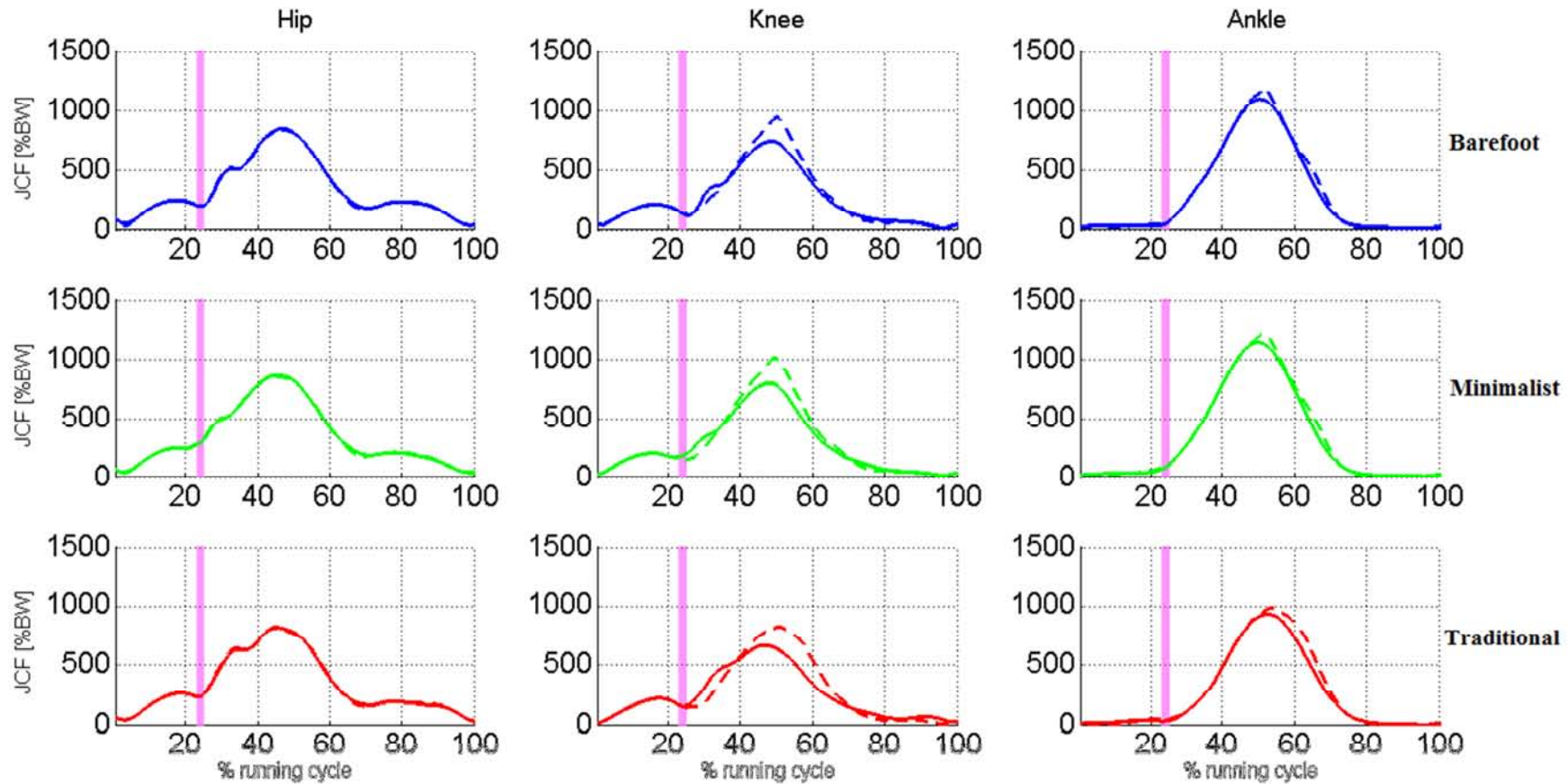


Figure 5.6. Average hip, knee and ankle contact forces for the three running styles. Forces are expressed as percentage of the body weight. The dotted line represents results from SO including FLV muscle properties while the solid line refers to SO without FLV muscle properties. The pink band identifies foot strike region.

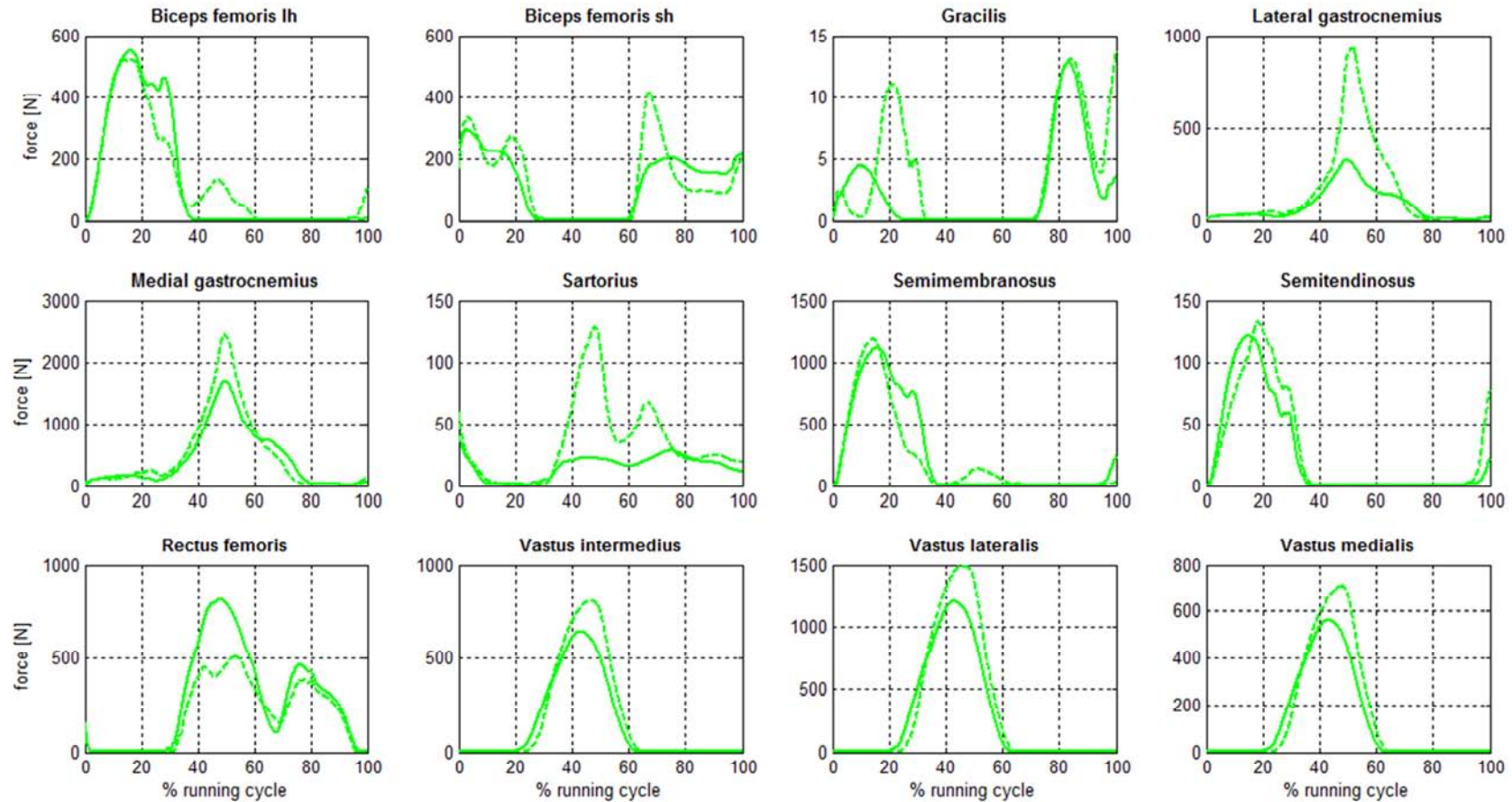


Figure 5.7. Knee extensors and flexors force for minimalist running. The dashed line represents results obtained including FLV muscle properties, while the solid line represents results obtained discarding FLV muscle properties.

Even if the difference was less pronounced, also peak ankle contact forces showed a larger amplitude in the “physiological” case, with an increase of 10%, 9% and 5% in barefoot, minimalist and traditional running respectively in comparison to the “non-physiological” case. It has been shown (Anderson and Pandy, 2001) that FLV muscle properties have little impact on the static optimization solution during gait. On the other hand, based on the above mentioned results, it is possible to affirm that FLV properties considerably influence internal loads estimation during running. In fact, the activation dynamics plays an important role in running since this activity requires fast contraction-relaxation cycles, therefore physiological properties cannot be neglected.

According to Scott and Winter (1990), all peak loads occurred in correspondence to midstance (44-48% of the considered gait cycle). Considering all the three joints, minimalist running displayed the greatest peak contact forces (851.1±42.5%BW, 1019.7±86.3%BW, 1275.0±75.0%BW at the hip, knee and ankle respectively), while traditional running showed the lowest peak contact forces (829.8±31.9%BW, 840.4±95.7%BW, 998.5±105.7 at the hip, knee and ankle respectively) (Figure 5.8). This finding was consistent with the generally higher and longer muscle activations during minimalist running compared to barefoot and traditional conditions. Since high joint contact force values are usually related to an increased articular pain (Besier et al., 2009) and to an increased risk of bone stress injuries to runners (Miller and Hamill, 2009), minimalist running resulted the most disadvantageous way of running for the analyzed subject. Furthermore, these evidence may justify the occurrence of the fibula stress fracture reported by the subject after moving to minimalist running.

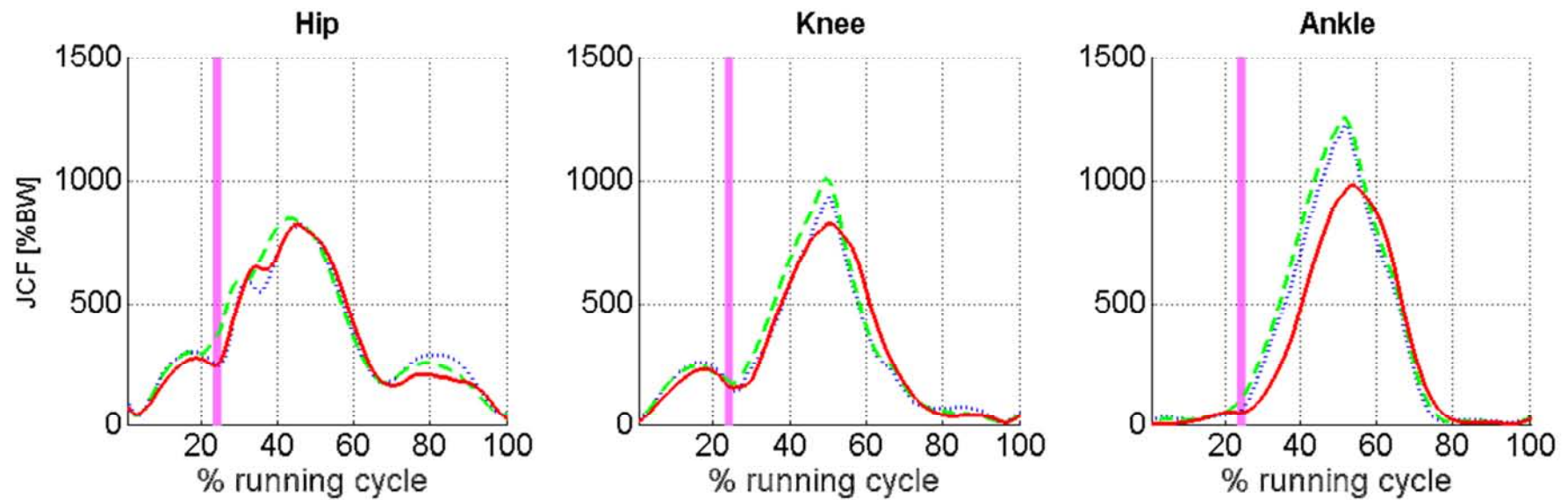


Figure 5.8. Comparison of average hip, knee and ankle contact forces for barefoot (dotted blue line), minimalist (dashed green line) and traditional (solid red line) running. The pink band represents foot strike region.

Nevertheless, differences in methodology and in running velocity and the lack of experimental data for all the three joints during running make the comparison of the obtained joint contact forces to those in literature difficult. Considering traditional running, peak hip contact forces (HCFs) are less than Edwards et al. (2008) (1190%BW at 4.4m/s) but greater than those estimated by Van Den Bogert et al. (1999) (520%BW at 3.5m/s) and by Rooney and Derrick (2013) (790%BW at 4.25m/s) which predicted only axial contact forces. Being experimental hip contact forces available in literature both for walking (Bergmann et al., 2001) and for running (Bergmann et al., 1993), a comparison including the simulated data deriving from this study can be done (Figure 5.9). By comparing the mean peak HCFs, it is possible to affirm that peak HCFs increased with the raise of the velocity.

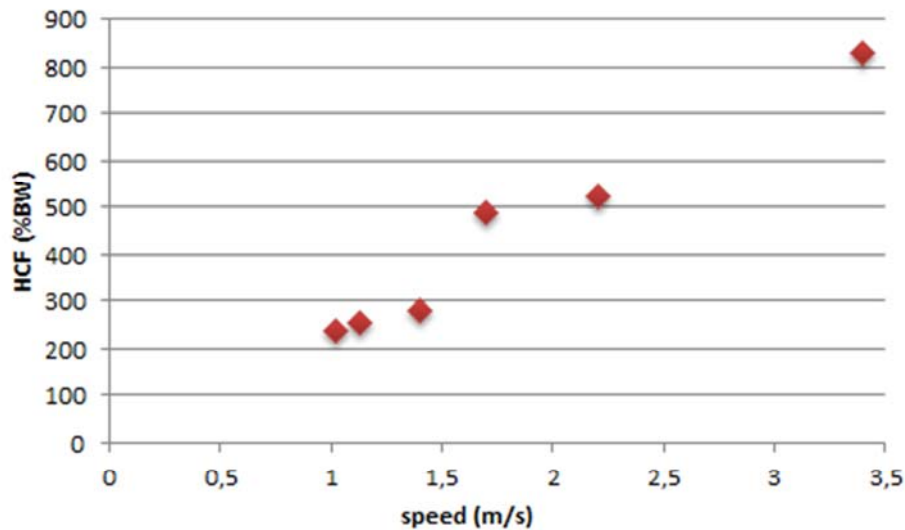


Figure 5.9. Mean experimental peak HCFs while slow walking (1.02m/s), normal walking (1.13m/s) and fast walking (1.4m/s) (Bergmann et al., 2001), running at 1.7m/s and 2.2m/s (Bergmann et al. 1993) and simulated peak HCF while running with traditional shoes at 3.4m/s. HCFs are expressed as a percentage of the body weight.

Peak knee contact forces (KCFs) ($840.4 \pm 97.7\%BW$) were considerably lower than those estimated by Edwards et al. (2008) (1510%BW at 4.4m/s), Glitsch and Baumann (1997) (1500%BW at 4.4m/s) and Rooney and Derrick (2013) (1190%BW at 4.25m/s). Apart from slightly different running conditions, the lower values obtained in the current study likely derived from a lower running speed in comparison with literature (Table 5.1).

Table 5.1. Comparison of peak hip, knee and ankle contact forces predicted in different studies at different velocities during shod running (* = only axial contact forces).

	Peak HCF (%BW)	Peak KCF (%BW)	Peak ACF (%BW)	Running speed (m/s)
Scott et al. (1990)			1110-1410	4.3-5.3
Glitsch et al. (1997)		1500	1200	4.4 (KCF) – 5 (ACF)
Van Den Bogert et al. (1999)	520			3.5
Edwards et al. (2008)	1190	1510		4.4
Rooney et al.* (2013)	790	1190	1110	4.25
Present study	829.8	840.4	998.5	3.4

Peak ankle contact forces (ACFs) ($998.5 \pm 105.7\%BW$) were slightly lower than those of Scott and Winter (1990) (1110-1410%BW at 4.3-5.3m/s), Glitsch and Baumann (1997) (1200%BW at 5m/s) and Rooney and Derrick (2013) (1110%BW at 4.25m/s). Also in this case, the difference in peak magnitudes in the current study and in literature may derived from a different running speed.

Conclusions

An understanding of the running injuries mechanisms is fundamental to suggest the most advantageous running style that the subject should adopt and footwear that he should wear to prevent injuries.

According to previous investigations, this study reveals differences in kinetics, kinematics and internal loads between barefoot and traditional running. These findings resulted in the increase of step length, running speed (Squadrone and Gallozzi, 2009a, De Wit et al., 2000), impact peak magnitude (Cavanagh and LaFortune, 1980, Richards, 2008, Novacheck, 1998), knee flexion (Lieberman et al., 2010b, Schütte et al., 2011) and plantarflexion (Schütte et al., 2011, Altman and Davis, 2012, Squadrone and Gallozzi, 2009a) at impact from barefoot to traditional conditions. Furthermore, the current study highlights the fact that minimalist running for the subject under investigation did not exactly mimic barefoot conditions and it often displayed unusual values of biomechanical variables with respect to in the available literature. In detail, minimalist running reported the highest vertical loading rate which is related to a poor shock absorption. In addition, the lowest impact peak magnitude, the shortest time to impact peak, the poorest repeatability in maintaining the same strike pattern, the largest posterior impact peak and the greatest lateral impact force were detected while wearing minimalist shoes. At initial contact, minimalist running showed the largest external pelvic rotation, the highest hip abduction and the highest knee flexion which may reduce the risk of Achilles tendinopathy (Tam et al., 2014). Moreover, peak knee extension moment in minimalist running resulted lower than traditional running. Muscle activation in minimalist conditions was generally the highest and the longest between the three running styles. Finally, minimalist running displayed the greatest peak contact forces at the hip, knee and ankle, potentially increasing articular pain and risk of bone stress injuries. Based on all these considerations, minimalist running results the most disadvantageous way of running for the athlete involved in the study. This statement may derive either from inappropriate structural characteristics of minimalist shoe or more likely from the subject's inability of running properly with this kind of shoes.

Therefore, these results may justify the occurrence of the fibula stress fracture reported by the subject while moving from traditional to minimalist running. This evidence leads to the conclusion that musculoskeletal modelling can be a valid support in investigating and preventing the occurrence of running related injuries.

However, some limitations need to be kept in mind while evaluating the results of this study. First of all, this investigation has been performed examining just one subject, therefore no statistic among a wide population is available. In addition, the lack of experimental EMG data belonging to the subject while performing the trials prevents a direct and more reliable comparison between numerical and experimental muscle activations. Moreover, the lack of anthropometric measurements does not allow the computation of a more subject-specific factor to adjust the estimation of the muscle maximum isometric force. These parameters would have been useful to take into account the remarkable level of training of the involved subject. Finally, some of the muscles (gluteus maximus, gluteus medius, medial gastrocnemius, lateral gastrocnemius and soleus) reach a saturation level in their activation which lasts over time. This is not physiologically correct and it depends on the weakness of the model.

It would be useful to extend this study to a larger number of subjects, both healthy and reporting injuries to investigate how results from numerical simulation differ and to yield into running injury mechanism. Moreover, it would be fundamental to collect EMG measurements to validate numerical results. Finally, it would be interesting to execute mechanical tests on the worn shoes to analyze some shoes mechanical properties (e.g. cushioning, rigidity) and to identify their possible influence on kinematics, kinetics and internal loads.

References

- ALTMAN, A. R. & DAVIS, I. S. 2012. Barefoot Running: Biomechanics and Implications for Running Injuries. *American College of Sports Medicine.*, 11.
- ANDERSON, F. C. & PANDY, M. G. 1999. A Dynamic Optimization Solution for Vertical Jumping in Three Dimensions. *Computer Methods in Biomechanics and Biomedical Engineering*, 2:3, 201 - 231.
- ANDERSON, F. C. & PANDY, M. G. 2001. Static and dynamic optimization solutions for gait are practically equivalent. *J Biomech*, 34, 153-61.
- ARNOLD, A. S., LIU, M. Q., SCHWARTZ, M. H., ÖUNPUU, S., DIAS, L. S. & DELP, S. L. 2006. Do the hamstrings operate at increased muscle–tendon lengths and velocities after surgical lengthening? *Journal of Biomechanics*, 39, 1498-1506.
- BARRE, A. & ARMAND, S. 2014. Biomechanical ToolKit: Open-source framework to visualize and process biomechanical data. *Comput Methods Programs Biomed*, 114, 80-7.
- BERGMANN, G., DEURETZBACHER, G., HELLER, M., GRAICHEN, F., ROHLMANN, A., STRAUSS, J. & DUDA, G. N. 2001. Hip contact forces and gait patterns from routine activities. *J Biomech*, 34, 859-71.
- BERGMANN, G., GRAICHEN, F. & ROHLMANN, A. 1993. Hip joint loading during walking and running, measured in two patients. *Journal of Biomechanics*, 26, 969-990.
- BESIER, T. F., FREDERICSON, M., GOLD, G. E., BEAUPRÉ, G. S. & DELP, S. 2009. Knee Muscle Forces during Walking and Running in Patellofemoral Pain Patients and Pain-Free Controls. *J Biomech*, 427.
- BLAISE WILLIAMS, D. S., GREEN, D. H. & WURZINGER, B. 2012. Changes in lower extremity movement and power absorption during forefoot striking and barefoot running. *The International Journal of Sports Physical Therapy*, 7.
- BONACCI, J., SAUNDERS, P. U., HICKS, A., RANTALAINEN, T., VICENZINO, B. G. T. & SPRATFORD, W. 2013. Running in a minimalist and lightweight shoe is not the same as running barefoot: a biomechanical study. *Br J Sports Med*.
- BURNET, E. N., ARENA, R. A., PIDCOE, P. E., ESTIVALET, M. & BRISSON, P. 2009. Relationship between pelvic motion, torque and metabolic energy in running. *Reaserach Gate*.
- CAPPELLINI, C., IVANENKO, Y. P., POPPELE, R. E. & LACQUANITI, F. 2006. Motor Patterns in Human Walking and Running. *Journal of Neurophysiology*, 95, 3426-3437.
- CAPPOZZO, A., CATANI, F., LEARDINI, A., BENEDETTI, M. G. & DELLA CROCE, U. 1996. Position and orientation in space of bones during movement: experimental artefacts. *Clinical Biomechanics*, 11, 90-100.
- CAVANAGH, P. R. & LAFORTUNE, M. A. 1980. Ground reaction forces in distance running. *Journal of Biomechanics*, 13, 397-406.
- CROWNINSHIELD, R. D. & BRAND, R. A. 1981. The prediction of forces in joint structures; distribution of intersegmental resultants. *Exerc Sport Sci Rev*, 9, 159-81.
- DE WIT, B., DE CLERCQ, D. & AERTS, P. 2000. Biomechanical analysis of the stance phase during barefoot and shod running. *J Biomech*, 33, 269-78.
- DELP, S. L., ANDERSON, F. C., ARNOLD, A. S., LOAN, P., HABIB, A., JOHN, C. T., GUENDELMAN, E. & THELEN, D. G. 2007. OpenSim: Opens-Source Software to Create and Analyze Dynamic Simulations of Movement. *IEEE Transactions on Biomedical Engineering*, 54, 1940-1946.

- DELP, S. L. & LOAN, J. P. 1995. A graphics-based software system to develop and analyze models of musculoskeletal structures. *Comput Biol Med*, 25, 21-34.
- DELP, S. L., LOAN, J. P., HOY, M. G., ZAJAC, F. E., TOPP, E. L. & ROSEN, J. M. 1990. An interactive graphics-based model of the lower extremity to study orthopaedic surgical procedures. *IEEE Transactions on Biomedical Engineering*
- 37.
- DIVERT, C., MORNIEUX, G., BAUR, H., MAYER, F. & BELLI, A. 2005. Mechanical Comparison of Barefoot and Shod Running. *Int J Sports Med*, 593–598.
- DORN, T. W. 2011. *Computational modelling of lower-limb muscle function in human running*. The University of Melbourne.
- DUDA, G. N., BRAND, D., FREITAG, S., LIERSE, W. & SCHNEIDER, E. 1996. Variability of femoral muscle attachments. *Journal of Biomechanics*, 29, 1185-1190.
- DUL, J., TOWNSEND, M. A., SHIAMI, R. & JOHNSON, G. E. 1984. Muscular synergism--I. On criteria for load sharing between synergistic muscles. *J Biomech*, 17, 663-73.
- EDWARDS, W. B., GILLETTE, J. C., THOMAS, J. M. & DERRICK, T. R. 2008. Internal femoral forces and moments during running: implications for stress fracture development. *Clin Biomech (Bristol, Avon)*, 23, 1269-78.
- FRIEDERICH, J. A. & BRAND, R. A. 1990. Muscle fiber architecture in the human lower limb. *Journal of Biomechanics*, 23, 91-95.
- FUKUNAGA, T., ROY, R. R., SHELLOCK, F. G., HODGSON, J. A. & EDGERTON, V. R. 1996. Specific tension of human plantar flexors and dorsiflexors. *J Appl Physiol (1985)*, 80, 158-65.
- GAGE, J. 1990. An overview of normal walking. *AAOS Instructional Course Lectures*, 39, 291-303.
- GLITSCH, U. & BAUMANN, W. 1997. The three-dimensional determination of internal loads in the lower extremity. *J Biomech*, 30, 1123-31.
- HAMNER, S. R., SETH, A. & DELP, S. L. 2010. Muscle contributions to propulsion and support during running. *Journal of biomechanics*, 43, 2709-2716.
- HANDSFIELD, G. G., MEYER, C. H., HART, J. M., ABEL, M. F. & BLEMKER, S. S. 2014. Relationships of 35 lower limb muscles to height and body mass quantified using MRI. *J Biomech*, 47, 631-8.
- HEIDENFELDER, J., STERZING, T., BULLMANN, M. & MILANI, T. L. 2008. Heel strike angle and foot angular velocity in the sagittal plane during running in different shoe conditions. *Journal of Foot and Ankle Research*.
- HICKS, J. & DEMBIA, C. 2013. *How Inverse Kinematics Works* [Online]. <http://simtk-confluence.stanford.edu:8080/display/OpenSim/How+Inverse+Kinematics+Works>. Available: <http://simtk-confluence.stanford.edu:8080/display/OpenSim/How+Inverse+Kinematics+Works>.
- HOLZBAUR, K. R., MURRAY, W. M. & DELP, S. L. 2005. A model of the upper extremity for simulating musculoskeletal surgery and analyzing neuromuscular control. *Ann Biomed Eng*, 33, 829-40.
- JOSHUA MCDOWELL, T. 2008. *Factors Affecting Lower Extremity Loading During Running*. PhD Thesis, Iowa State University.
- KERRIGAN, D. C., FRANZ, J. R., KEENAN, G. S., DICHARRY, J., DELLA CROCE, U. & WILDER, R. P. 2009. The Effect of Running Shoes on Lower Extremity Joint Torques. *American Academy of Physical Medicine and Rehabilitation*, 1, 1058-1062.
- KIRTLEY, C. 2006. *Clinical Gait Analysis: Theory and Practice*, Elsevier.

- KLEIN HORSMAN, M. D., KOOPMAN, H. F. J. M., VAN DER HELM, F. C. T., PROSE, L. P. & VEEGER, H. E. J. 2007. Morphological muscle and joint parameters for musculoskeletal modelling of the lower extremity. *Clinical Biomechanics*, 22, 239-247.
- KOMI, P. V. 2000. Stretch-shortening cycle: a powerful model to study normal and fatigued muscle. *Journal of Biomechanics*, 33, 1197-1206.
- KOMI, P. V., GOLLHOFER, A., SCHMIDTBLEICHER, D. & FRICK, U. 1987. Interaction Between Man and Shoe in Running: Considerations for a More Comprehensive Measurement Approach. *Int J Sports Med*, 8, 196-202.
- KWON, Y.-H. 1998. *Ground Reaction Force* [Online].
<http://www.kwon3d.com/theory/grf/grf.html>. Available:
<http://www.kwon3d.com/theory/grf/grf.html>.
- LEE, R. C., WANG, Z., HEO, M., ROSS, R., JANSSEN, I. & HEYMSFIELD, S. B. 2000. Total-body skeletal muscle mass: development and cross-validation of anthropometric prediction models. *American Society for Clinical Nutrition*, 72, 796-803.
- LIEBERMAN, D. E. 2010. *Running Barefoot or in Minimal Footwear* [Online].
<http://barefootrunning.fas.harvard.edu/2FootStrikes&RunningShoes.html>. Available:
<http://barefootrunning.fas.harvard.edu/2FootStrikes&RunningShoes.html>.
- LIEBERMAN, D. E., VENKADESAN, M., DAOUD, A. I. & WERBEL, W. A. 2010a. *Biomechanics of Foot Strikes & Applications to Running Barefoot or in Minimal Footwear* [Online].
<http://www.barefootrunning.fas.harvard.edu/6FAQ.html>. Available:
<http://www.barefootrunning.fas.harvard.edu/6FAQ.html>.
- LIEBERMAN, D. E., VENKADESAN, M., WERBEL, W. A., DAOUD, A. I., D'ANDREA, S., DAVIS, I. S., MANG'ENI, R. O. & PITSILADIS, Y. 2010b. Foot strike patterns and collision forces in habitually barefoot versus shod runners. *Nature*, 463, 531-5.
- LIEBERMAN, D. E., VENKADESAN, M., WERBEL, W. A., DAOUD, A. I., D'ANDREA, S., DAVIS, I. S., OJIAMBO MANG'ENI, R. & PITSILADIS, Y. 2010c. Foot strike patterns and collision forces in habitually barefoot versus shod runners. *Nature*, 463.
- LIVINGSTONE, S. R. 2008. *Macquarie Motion Capture Manual. Understanding Vicon Nexus*. [Online]. http://www.psy.mq.edu.au/me2/mocap_v1/clean_gaps.html. Available:
http://www.psy.mq.edu.au/me2/mocap_v1/clean_gaps.html.
- LU, T. W. & O'CONNOR, J. J. 1999. Bone position estimation from skin marker co-ordinates using global optimisation with joint constraints. *J Biomech*, 32, 129-34.
- LUND, K. & HICKS, J. 2014. *Getting Started with Inverse Kinematics* [Online]. <http://simtk-confluence.stanford.edu:8080/display/OpenSim/Getting+Started+with+Inverse+Kinematics>. Available: <http://simtk-confluence.stanford.edu:8080/display/OpenSim/Getting+Started+with+Inverse+Kinematics>.
- MACERA, C. A., PATE, R. R., POWELL, K. E., JACKSON, K. L., KENDRICK, J. S. & CRAVEN, T. E. 1989. Predicting lower-extremity injuries among habitual runners. *Arch Intern Med*, 149, 2565-8.
- MERCER, J. A., BLACK, D., BRANKS, D. & HRELJAC, A. 2001. Stride length effects on ground reaction forces during running.
- MILLER, R. H. & HAMILL, J. 2009. Computer simulation of the effects of shoe cushioning on internal and external loading during running impacts. *Computer Methods in Biomechanics and Biomedical Engineering*, 12, 481-490.
- MODENESE, L. 2010. *A state of the art lower limb model: application to muscle forces estimation*. PhD Transfer Report, Imperial College London.
- MODENESE, L., PHILLIPS, A. T. M. & BULL, A. M. J. 2011. An open source lower limb model: Hip joint validation. *Journal of Biomechanics*, 44, 2185-2193.

- MOSBY 2009. Mosby's Medical Dictionary. 8th ed.: Elsevier.
- MOTION LAB SYSTEMS. 2008. *The C3D file format. User guide*. [Online].
http://www.c3d.org/pdf/c3dformat_ug.pdf. Available:
http://www.c3d.org/pdf/c3dformat_ug.pdf.
- NOVACHECK, T. F. 1998. The biomechanics of running. *Gait and Posture*, 7, 77-95.
- PAGE, A., DE ROSARIO, H., MATA, V., HOYOS, J. V. & PORCAR, R. 2006. Effect of marker cluster design on the accuracy of human movement analysis using stereophotogrammetry. *Med Biol Eng Comput*, 44, 1113-9.
- PERL, D. P., DAOUD, A. I. & LIEBERMAN, D. E. 2012. Effects of footwear and strike type on running economy. *Med Sci Sports Exerc*, 44, 1335-43.
- PERRY, J. 1992. *Gait analysis, normal and pathological function*, SLACK Incorporated.
- PETRONE, N. 2013. Motion capture system: instrumentation and analysis. Slides from lectures.
- PIZZUTOLO, F. 2012. Misura del movimento e della postura: stereofotogrammetria. Slides from lectures.
- RASMUSSEN, J., DAMSGAARD, M. & VOIGT, M. 2001. Muscle recruitment by the min/max criterion -- a comparative numerical study. *J Biomech*, 34, 409-15.
- REINSCHMIDT, C. & NIGG, B. M. 1995. Influence of heel height on ankle joint moments in running. *Med Sci Sports Exerc*, 27, 410-6.
- RICHARDS, J. 2008. *Biomechanics in clinic and research*, Churchill Livingstone Elsevier
- ROONEY, B. D. & DERRICK, T. R. 2013. Joint contact loading in forefoot and rearfoot strike patterns during running. *J Biomech*, 46, 2201-6.
- ROOT, M. L., ORIEN, W. P., WEED, J. H. & HUGHES, R. J. 1999. *Valutazione biomeccanica del piede*, PICCIN.
- RUNNINGUSA. 2013. *State of the Sport - Part III: U.S. Race Trends* [Online].
<http://www.runningusa.org/state-of-sport-2013-part-III?returnTo=annual-reports>. Available: <http://www.runningusa.org/state-of-sport-2013-part-III?returnTo=annual-reports>.
- SATTERTHWAITE, P., NORTON, R., LARMER, P. & ROBINSON, E. 1999. Risk factors for injuries and other health problems sustained in a marathon. *Br J Sports Med*, 33, 22-26.
- SAUNDERS, P. *Barefoot Running* [Online]. <http://www.runforyourlife.com.au/articles-news-races/training/12-barefoot-running.html>. Available:
<http://www.runforyourlife.com.au/articles-news-races/training/12-barefoot-running.html>.
- SAXBY, L. 2011. *PROPRIOCEPTION, Making Sense Of Barefoot Running* [Online].
<http://www.shoes.com/content/2011/brandshops/vivobarefoot/propricioception.pdf>. Available:
<http://www.shoes.com/content/2011/brandshops/vivobarefoot/propricioception.pdf>.
- SCHACHE, A. G., BLANCH, P., RATH, D., WRIGLEY, T. & BENNELL, K. 2002. Three-dimensional angular kinematics of the lumbar spine and pelvis during running. *Hum Mov Sci*, 21, 273-93.
- SCHACHE, A. G., BLANCH, P. D. & MURPHY, A. T. 2000. Relation of anterior pelvic tilt during running to clinical and kinematic measures of hip extension. *Br J Sports Med*, 34, 279-283.
- SCHEYS, L., DESLOOVERE, K., SPAEPEN, A., SUETENS, P. & JONKERS, I. 2011. Calculating gait kinematics using MR-based kinematic models. *Gait Posture*, 33, 158-64.
- SCHEYS, L., SPAEPEN, A., SUETENS, P. & JONKERS, I. 2008. Calculated moment-arm and muscle-tendon lengths during gait differ substantially using MR based versus rescaled generic lower-limb musculoskeletal models. *Gait Posture*, 28, 640-8.

- SCHUBERT, A. G., KEMPF, J. & HEIDERSCHEIT, B. C. 2013. Influence of stride frequency and length on running mechanics. A systematic review. *Sports Health*.
- SCHÜTTE, K., MILES, K., VENTER, R. & VAN NIEKERK, S. M. 2011. Acute differences in sagittal plane lower limb kinematics between barefoot, minimalistic shoes and shod running in male athletes.
- SCOTT, S. H. & WINTER, D. A. 1990. Internal forces of chronic running injury sites. *Med Sci Sports Exerc*, 22, 357-69.
- SETH, A., SHERMAN, M., EASTMAN, P. & DELP, S. 2010. Minimal formulation of joint motion for biomechanisms. *Nonlinear Dyn*, 62, 291–303.
- SETH, A., SHERMAN, M., REINBOLT, J. A. & DELP, S. L. 2011. OpenSim: a musculoskeletal modeling and simulation framework for in silico investigations and exchange. *Procedia IUTAM*, 2, 212-232.
- SHEIKH-WARAK, A. 2012. *Comparing strains in the tibia induced by different running styles*. Imperial College London.
- SIMTK-CONFLUENCE.STANFORD.EDU. *OpenSim Support* [Online]. <http://simtk-confluence.stanford.edu:8080/display/OpenSim/OpenSim+Support>. Available: <http://simtk-confluence.stanford.edu:8080/display/OpenSim/OpenSim+Support>.
- SIMTK. 2011. *Neuromuscular Models Library* [Online]. https://simtk.org/project/xml/downloads.xml?group_id=95. Available: https://simtk.org/project/xml/downloads.xml?group_id=95.
- SLOCUM, D. B. & JAMES, S. L. 1968. Biomechanics of running. *Jama*, 205, 721-8.
- SQUADRONE, R. & GALLOZZI, C. 2009a. Biomechanical and physiological comparison of barefoot and two shod conditions in experienced barefoot runners. *The Journal of Sports Medicine and Physical Fitness*, 6-13.
- SQUADRONE, R. & GALLOZZI, C. 2009b. Biomechanical and physiological comparison of barefoot and two shod conditions in experienced barefoot runners. *J Sports Med Phys Fitness*, 49, 6-13.
- STANDIFIRD, T., MITCHELL, U., HUNTER, I., JOHNSON, W. & RIDGE, S. 2013. Lower extremity muscle activation during barefoot, minimalist and shod running.
- STMARY'SUNIVERSITY. 2013. *St Mary's University* [Online]. <http://www.smuc.ac.uk/clinic/>. Available: <http://www.smuc.ac.uk/clinic/>.
- STOCKTON, M. & DYSON, R. 1998. A comparison of lower extremity forces, joint angles and muscle activity during shod and barefoot running. *16 International Symposium on Biomechanics in Sports*. Konstanz, Germany.
- SWARTZ, M. H. 2010. *Textbook of physical diagnosis: history and examination*, Saunders/Elsevier.
- TAM, N., WILSON, J. L. A. & NOAKES, T. D. 2014. Barefoot running: an evaluation of current hypothesis, future research and clinical applications. *Br J Sports Med*.
- TONGEN, A. & WUNDERLICH, R. E. 2010. Biomechanics of Running and Walking. Mathematics Awareness Month.
- VAN DEN BOGERT, A. J., READ, L. & NIGG, B. M. 1999. An analysis of hip joint loading during walking, running, and skiing. 31, 131-142.
- VAN GENT, R. N., SIEM, D., VAN MIDDELKOOP, M., VAN OS, A. G., BIERMA-ZEINSTRAS, S. M. & KOES, B. W. 2007. Incidence and determinants of lower extremity running injuries in long distance runners: a systematic review. *Br J Sports Med*, 41, 469-80; discussion 480.
- VICONMOTIONSYSTEMS. *Essentials of motion capture* [Online]. http://www.udel.edu/PT/Research/MAL/essentials_of_motion_capture_v1_2.pdf.

Available:

http://www.udel.edu/PT/Research/MAL/essentials_of_motion_capture_v1_2.pdf.

- WICKIEWICZ, T. L., ROY, R. R., POWELL, P. L. & EDGERTON, V. R. 1983. Muscle architecture of the human lower limb. *Clin. Orthop.*, 179, 275-283.
- WINTER, D. A. 2009. *Biomechanics and Motor Control of Human Movement*, WILEY.
- WINTER, D. A. & BISHOP, P. 1992. Lower extremity injury - biomechanical factors associated with chronic injury to the lower extremity. *Sports Med*, 14, 149-156.
- WINTER, D. A., SIDWALL, H. G. & HOBSON, D. A. 1974. Measurement and reduction of noise in kinematics of locomotion. *J Biomech*, 7, 157-9.
- WU, G. & CAVANAGH, P. R. 1995. ISB recommendations for standardization in the reporting of kinematic data. *Journal of Biomechanics*, 28, 1257-1261.
- YAMAGUCHI, G. T. & ZAJAC, F. E. 1989. A planar model of the knee joint to characterize the knee extensor mechanism. *J Biomech*, 22, 1-10.
- ZAJAC, F. E. 1989. Muscle and tendon: properties, models, scaling, and application to biomechanics and motor control. *Crit Rev Biomed Eng*, 17, 359-411.

Aknowledgments

At the end of this study I would like to express my gratitude towards all the people who made this experience possible and special. First of all I would like to thank my supervisor, Prof. Nicola Petrone, for increasing my interest in the biomechanics field, for believing in me and for giving me the chance to undertake this extraordinary experience. Secondly I would like to express my sincere gratitude to my co-supervisor Dr Luca Modenese for his constant guidance and willingness. His enthusiasm and his passion for research always motivated me and his precise advice was invaluable. I would like to thank him also for his patience and his support. Special thanks go to Dr Andrew T.M. Phillips for his constant support and for giving me the opportunity to work in an extremely qualified environment. I would like to thank also Dr Anantharaman Gopalakrishnan for his help, patience and for strongly believing in me. Heartfelt thanks to Claire, Luis, Nivea and Eleni, my office mates at Imperial College London. It has been a pleasure to spend my time with them and to share both scientific and personal thoughts. I consider myself lucky because I had the extraordinary chance to develop this project at Imperial College London. During my stay over there I've learnt a lot of things, both from the academic and personal point of view.

I would like to sincerely thank my family for going along with my choices, for making this experience possible and for constantly supporting me during these academic years. Finally, I would like to express my gratitude to all my friends for encouraging me and for being always close to me. I would not have never reached such an important goal without them.